



**HAL**  
open science

## Les avalanches dans les systèmes vitreux

Stefano Spigler

► **To cite this version:**

Stefano Spigler. Les avalanches dans les systèmes vitreux. Physique [physics]. Université Paris sciences et lettres, 2017. Français. NNT : 2017PSLET021 . tel-02313838

**HAL Id: tel-02313838**

**<https://theses.hal.science/tel-02313838>**

Submitted on 11 Oct 2019

**HAL** is a multi-disciplinary open access archive for the deposit and dissemination of scientific research documents, whether they are published or not. The documents may come from teaching and research institutions in France or abroad, or from public or private research centers.

L'archive ouverte pluridisciplinaire **HAL**, est destinée au dépôt et à la diffusion de documents scientifiques de niveau recherche, publiés ou non, émanant des établissements d'enseignement et de recherche français ou étrangers, des laboratoires publics ou privés.

# THÈSE DE DOCTORAT

de l'Université de recherche Paris Sciences et Lettres  
PSL Research University

**Laboratoire de Physique Théorique et Modèles Statistique**  
Université Paris Sud, Université Paris Saclay

Avalanches in glassy system

**Ecole doctorale n°564**

Ecole Doctorale Physique en Île de France

**Spécialité Physique**

**Soutenu par Stefano SPIGLER**  
**le 25 septembre 2017**

Dirigée par Silvio FRANZ

## COMPOSITION DU JURY :

M. BARRAT Jean-Louis  
Université Joseph Fourier Grenoble,  
Rapporteur

M. RIZZO Tommaso  
Istituto dei Sistemi Complessi Roma,  
Rapporteur

M. BIROLI Giulio  
CEA,  
Membre du jury

Mme. CAMMAROTA Chiara  
King's Kollege,  
Membre du jury

M. FOFFI Giuseppe  
Université Paris Sud,  
Membre du jury

M. WYART Matthieu  
École Polytechnique Fédérale de  
Lausanne,  
Membre du jury







# Avalanches in glassy systems

A DISSERTATION PRESENTED

BY

**Stefano Spigler**

LABORATOIRE DE PHYSIQUE THÉORIQUE ET MODÈLES STATISTIQUE,  
UNIVERSITÉ PARIS SUD, UNIVERSITÉ PARIS SACLAY

PHYSIQUE

PARIS SCIENCES ET LETTRES, ÉCOLE DOCTORALE PHYSIQUE EN ÎLE DE  
FRANCE, 564

SEPTEMBER 2017

PARIS, FRANCE

*Directeur de thèse:*

Silvio Franz, Université Paris Sud

*Rapporteurs:*

Jean-Louis Barrat, Université Joseph Fourier Grenoble

Tommaso Rizzo, Istituto dei Sistemi Complessi Roma

*Jury:*

Giulio Biroli, CEA Paris Saclay

Chiara Cammarota, King's College London

Giuseppe Foffi, Université Paris Sud

Matthieu Wyart, École Polytechnique Fédérale de Lausanne



*To all the important people close to me.*





# Abstract

Many systems that are somehow characterized by a degree of disorder share a similar structure: the energy landscape has many sample-dependent local energy minima. When a small external perturbation is applied to the system at low temperature, it is reasonable to expect that the dynamics will lead the system from a minimum to another, thus displaying a random and jerky response. The discontinuous jumps that one observes are called avalanches, and the focus of this work is the computation of their distribution. One of the results is indeed the development of a framework that allows the computation of this distribution in infinite-dimensional systems that can be described within a replica symmetry breaking ansatz. We apply the results to one of the simplest models of structural glasses, namely dense packings of (harmonic) soft spheres, either at jamming or at larger densities, subject to a shear transformation that induces jumps both in the total energy and in the shear stress of the system. We argue that, when the shear strain is small enough, the avalanche distribution develops a power-law behavior, whose exponent can be directly related to the functional order parameter of the replica symmetry breaking solution. This exponent is also related to the distribution of contact forces (or at least of the contact forces between some of the spheres), whose asymptotic behavior is known not to depend strongly on the spatial dimension; for this reason, we compare the infinite-dimensional prediction with three-dimensional simulations of the same systems and, remarkably, we find a good agreement. In the rest of the thesis we compare our results with previous works, and we also discuss some of the consequences that the avalanche distribution leads to, concerning the statistical elastic properties of dense granular media.



## Abstract (french)

Beaucoup de systèmes qui ont un certain degré de désordre ont des similarités dans leur structure: le paysage énergétique est aléatoire et il a plusieurs minima locaux de l'énergie. Quand on ajoute une petite perturbation externe au système à basse température, il est raisonnable d'attendre que la dynamique conduira le système d'un minimum à l'autre, et ça donne lieu à une réponse aléatoire et saccadée. Les sautes discontinues que l'on observe sont appelés avalanches, et l'intérêt de ce travail est le calcul de leur distribution. Un des résultats est en effet le développement d'un cadre pour calculer cette distribution dans des systèmes en dimension infinie qui peuvent être décrits avec le replica symmetry breaking. Nous appliquons les résultats à l'un des modèles les plus simples des verres structuraux, c'est à dire les empilements denses de sphères molles avec répulsion harmonique, avec une déformation (shear strain) du volume comme perturbation. Nous soutenons que, quand la déformation est suffisamment petite, une portion de la distribution des avalanches devient une loi de puissance, dont l'exposant peut être directement lié au paramètre d'ordre de la brisure de symétrie de replica. Cet exposant est également lié à la distribution des forces de contact (au moins entre certaines sphères), dont le comportement asymptotique on sait que ne dépend pas fortement de la dimension spatiale; pour cette raison nous comparons les prédictions de champ moyen en dimension infinie avec des simulation du même système en dimension trois et, remarquablement, on trouve un bon accord. Dans le reste de la thèse nous discutons aussi les similarités avec des travaux précédents et quelques conséquences que la distribution des avalanches donne sur les propriétés élastiques de la matière granulaire dense.



<b>Acknowledgements</b>	<b>3</b>
<b>1 Disordered systems</b>	<b>5</b>
1.1 Replica symmetry breaking . . . . .	10
1.2 Systems of spheres and jamming . . . . .	15
<b>2 Athermal response to perturbations</b>	<b>23</b>
2.1 Avalanches . . . . .	23
2.2 Spheres and shear-strain . . . . .	26
2.3 Asymptotic behavior . . . . .	31
2.4 Numerical simulations . . . . .	37
<b>3 Consequences on elastic moduli</b>	<b>47</b>
3.1 Stress-strain curves . . . . .	48
3.2 Quenched elastic moduli . . . . .	50
3.3 Elastic moduli under different scalings . . . . .	55
<b>4 Reconstruction of the order parameter</b>	<b>59</b>
4.1 Mean-field framework . . . . .	60
4.2 Numerical simulations . . . . .	63
<b>Conclusions</b>	<b>71</b>
<b>Appendices</b>	
a Derrida-Ruelle cascades . . . . .	75
b Distribution of athermal avalanches . . . . .	83
<b>Bibliography</b>	<b>105</b>



# List of figures

1.1	Angell plot . . . . .	6
1.2	Supercooled liquid . . . . .	9
1.3	Energy landscape and pure states . . . . .	12
1.4	Hierarchy of states . . . . .	14
1.5	Glasses and jamming . . . . .	16
1.6	Fractal energy landscape . . . . .	17
1.7	Average coordination number . . . . .	18
1.8	Rattler in a cage . . . . .	19
2.1	Energy landscape with a small perturbation . . . . .	25
2.2	Shear strain . . . . .	26
2.3	Level crossing . . . . .	30
2.4	Distribution of avalanches in infinite dimensions (jamming) . . . . .	33
2.5	Distribution of avalanches in infinite dimensions (UNSAT) . . . . .	33
2.6	Lees-Edwards boundary conditions . . . . .	40
2.7	Particle images . . . . .	40
2.8	Random jumps in energy and stress . . . . .	41
2.9	Distribution of avalanches in 3D (numerical) . . . . .	42
2.10	Cumulative distribution of jumps . . . . .	43
3.1	Excess low-energy modes in jammed systems . . . . .	48
3.2	Average stress-strain curve and yielding . . . . .	49
3.3	Mean and variance of the shear modulus . . . . .	54

4.1	Repulsion from the ground state . . . . .	61
4.2	First results . . . . .	64
4.3	Repulsion in 1d . . . . .	66
4.4	Repulsion in 2d . . . . .	67
4.5	Repulsion in 3d . . . . .	68
a.1	Cascade of Poisson point processes for a $k = 2$ RSB system . .	79
b.1	Ultrametric tree for a $k$ -RSB system . . . . .	85
b.2	Factor graph for the joint distribution of the clusters' minima	87
b.3	Derivation of the distribution of a cluster's minimum . . . . .	88





# Acknowledgements

This thesis represents the work that I have done during the past three years at the Laboratoire de Physique Théorique et Modèles Statistiques (LPTMS), in Orsay, France. I would like to express my sincere gratitude to my supervisor Silvio Franz, without whom this would not have been possible, for carefully and continuously helping me with my work and teaching me how to do research. Beside my advisor, I want to thank the institution that hosted me, the LPTMS, for its support and for the opportunity it gave me to get to know the academic world; in particular, I thank the director Emmanuel Trizac, Giacomo Gradenigo, Haggai Landa, Alberto Rosso, Raoul Santachiara and all the PhD students.

Then I want to express my special appreciation to the Simons Collaboration on cracking the glass problem, funded by the Simons Foundation, for the stimulating environment where I had the chance to interact with and to learn from the professionals of the field: special acknowledgement goes to Francesco Zamponi and Pierfrancesco Urbani for the helpful discussions, and to all the postdocs whom I shared the office with.

I offer my sincere thanks to all the members of the committee appointed to examine and evaluate my work: Jean-Louis Barrat, Tommaso Rizzo, Giulio Biroli, Chiara Cammarota, Giuseppe Foffi and Matthieu Wyart. I would also like to show my appreciation to the *École Normale Supérieure*, to the *École Doctorale Paris Sciences et Lettres* and to the *École Doctoral Physique en Île-de-France* for the scholarship and the chance to live in one of the most beautiful cities in the world, Paris, whose only flaw is not being the residence of the people closest to me.

Paris,  
September 2017





## Disordered systems

The object of our interest are disordered systems with *glassy behavior*. Glassiness is a collection of phenomenological behaviors that characterize many different systems endowed with some form of disorder. The most prominent property is dynamical in nature, and it is an extreme slowing down of the dynamics at low temperature. An important timescale is the relaxation time, that is the time taken for a system to reach thermal equilibrium, or, equivalently, a measure of the time taken by the system to explore the whole phase space in an ergodic fashion; the relaxation time of glassy systems increases several orders of magnitude as the temperature is lowered (see for instance Figure 1.1), and it soon becomes so large that it exceeds the experimental times. By definition, a system observed within a timescale smaller than its relaxation time appears out of equilibrium — this can be verified, for example, probing the fluctuation-dissipation theorem — and therefore, when the temperature is lowered below some empirically defined *glass transition temperature*  $T_g$  at which the relaxation time becomes too large to be actually reached experimentally, the system appears to be gradually “freezing”. Below this point the system is no longer able to sample the phase space (at least not within reasonable times), and it is therefore no longer ergodic.

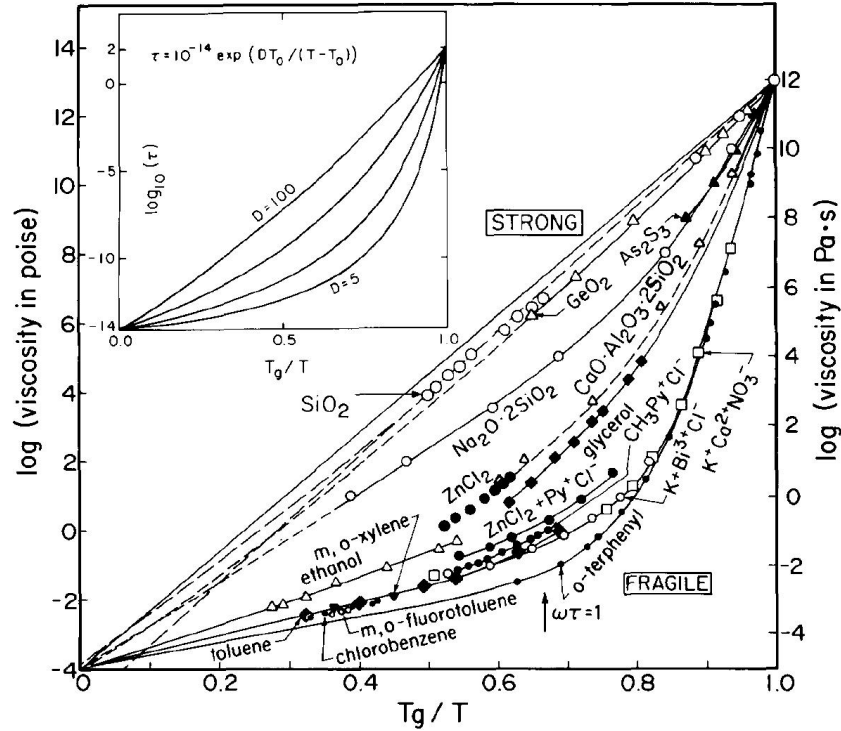


Figure 1.1: This plot shows the extreme increase of the viscosity (several orders of magnitude) as the temperature is lowered towards the glass transition temperature  $T_g$ , for various supercooled liquids that are typical “glassformers”. The viscosity  $\eta$  is related to the relaxation time  $\tau$  via Maxwell’s relation  $\eta = G_\infty \tau$ , where  $G_\infty$  is the instantaneous shear modulus specific to the liquid [Cavagna, 2009]; although  $G_\infty$  changes with the temperature, its variation can be neglected in comparison to the variation of the relaxation time. Notice that the temperature has been rescaled by the temperature  $T_g$ , defined as the temperature at which the liquid has viscosity  $\eta = 10^{13}$  Poise; this rescaled plot is called Angell plot [Angell et al., 1995].

Disordered systems are intimately related to some form of *frustration*; a system is frustrated if some of its parts (whether they are particles, spins or larger structures) feel conflicting forces or conflicting geometrical constraints. In some systems the frustration results from a quenched disorder, that is, each sample of the system has an intrinsic structure that is random and different from the other samples; this is the case of spin glasses, that are disordered magnets where some magnetic spins are quenched at random, fixed locations in space but are free to rotate and align in different directions. The simplest model that has been used to analytically study these magnets is the

Edwards-Anderson model, that is a disordered Ising model in  $d$  dimensions, with Hamiltonian

$$\mathcal{H}(\underline{s}; J) = - \sum_{\langle i, j \rangle} J_{ij} s_i s_j, \quad (1.1)$$

where the sum is over the bonds  $\langle i, j \rangle$  on a  $d$ -dimensional lattice, the spins  $\{s_i\}$  are Ising spins that can be either  $+1$  or  $-1$ , and  $\{J_{ij}\}$  are Gaussian random variables that mimic the disordered interaction between magnetic dipoles in these magnetic systems. Since it is hard to solve the thermodynamics of this model, the corresponding mean-field version, called the Sherrington-Kirkpatrick model, has been introduced. In this model the couplings, rather than belonging to a finite dimensional lattice, couple all possible pairs of spins  $i$ - $j$  via a random interaction  $J_{ij}$  — whose variance, now, has to scale as  $N^{-\frac{1}{2}}$  in order for the system to have an extensive free energy. All these models are frustrated because there is a finite probability that any set of spins has conflicting couplings. For instance, a triangle in the Sherrington-Kirkpatrick model made by the spins  $i, j, k$  has, with finite probability, negative couplings  $J_{ij}, J_{jk}, J_{ki} < 0$ ; these couplings tend to align each spin in the opposite directions with respect to its neighbors, but in a triangle this is not possible — two spins have to be parallel!

A generalization of this model to higher order interactions is the mean-field  $p$ -spin model, where the interactions involve all possible groups of  $p$  spins, with random couplings  $\{J_{i_1 \dots i_p}\}$ :

$$\mathcal{H}(\underline{s}; J) = - \sum_{i_1, \dots, i_p} J_{i_1 \dots i_p} s_{i_1} \cdots s_{i_p}. \quad (1.2)$$

It turns out that a slightly different version of the  $p$ -spin model (with  $p \geq 3$ ), namely with *spherical* spins (not only  $\pm 1$ ) such that  $\sum_{i=1}^N s_i^2 = N$ , is easier to study and is deeply connected with the physics of another class of systems: the *structural glasses* [Kirkpatrick and Wolynes, 1987; Kirkpatrick and Thirumalai, 1987a,b; Kirkpatrick et al., 1989]. Structural glasses are systems of particles (atoms, molecules, ...) that interact through a pair potential. Such systems usually display a liquid-crystal transition at some *melting temperature*  $T_m$ , but in some cases it is possible to avoid the crystallization by carefully lowering the temperature fast enough: when this happens, the system is a *metastable supercooled liquid* [Debenedetti and Stillinger, 2001; Cavagna, 2009]; it is metastable because there is always the crystal state lying at a lower energy, but even though the crystal is somehow excluded from the explored phase space (thus making the dynamics strictly speaking not ergodic), the system nonetheless behaves as if it were at equilibrium

(e.g. the fluctuation-dissipation theorem holds true). When the temperature is further lowered the relaxation time increases, and at some temperature  $T_g$  it becomes so large that the supercooled liquid falls out of equilibrium within the experimental timescale (Figure 1.1 and Figure 1.2), and it becomes a glass. Of course, other glasses can be made with more complex liquids, composed for example of colloidal particles or polymers. The simplest models for structural glasses that have been studied are systems of spherical particles interacting via Lennard-Jones forces (the pair potential between two particles at distance  $r$  being of the form  $V(r) = 4\epsilon \left[ \left(\frac{\sigma}{r}\right)^{12} - \left(\frac{\sigma}{r}\right)^6 \right]$ ), or via short range purely repulsive interactions as for hard spheres and soft spheres (these systems will be introduced in *Systems of spheres and jamming* later in this chapter. It is interesting to notice that these structural glasses have no intrinsic, quenched disorders, but nonetheless their configurations appear disordered and amorphous (one says that the disorder is self generated [Charbonneau et al., 2014b]): the reason lies in the fact that such systems are still (geometrically) frustrated, even without explicit disorder in the Hamiltonian.

The thermodynamics of the Sherrington-Kirkpatrick model, of the p-spin model and of systems of hard and soft spheres in infinite dimensions have been solved analytically. The solution of all these systems involves a phase transition; in the low temperature phase (or high density, for the systems of spheres) the solution can be interestingly described in the framework of the so-called *replica symmetry breaking* and results in a very complex energy landscape, with the existence of a multitude of equilibrium states (more details will be provided in the next section, *Replica symmetry breaking*). Such a landscape justifies many of the phenomenological properties of glasses, but nonetheless, the actual existence of a true thermodynamic glass transition in finite dimensional systems is still not entirely clear. In finite dimensions, there are two main points of view [Berthier and Biroli, 2011]: one is the *landscape scenario*, or Random First-Order Transition theory [Kirkpatrick and Thirumalai, 2012, 2014], that, inspired by the mean-field analysis, tries to explain the glassy phenomenology as a true thermodynamic phase transition, with a non-trivial energy landscape and an abundance of metastable states that slow down the dynamics (although many concepts that are introduced in mean-field models become meaningless in finite dimensions). The other is the idea of *dynamic facilitation*, that does not regard the thermodynamics as the principal reason for the glassy behavior, but rather ascribes the cause of the slowdown to the frustration in the system, for which at low temperature the particles' movement are inhibited by their neighbors. There is a class of

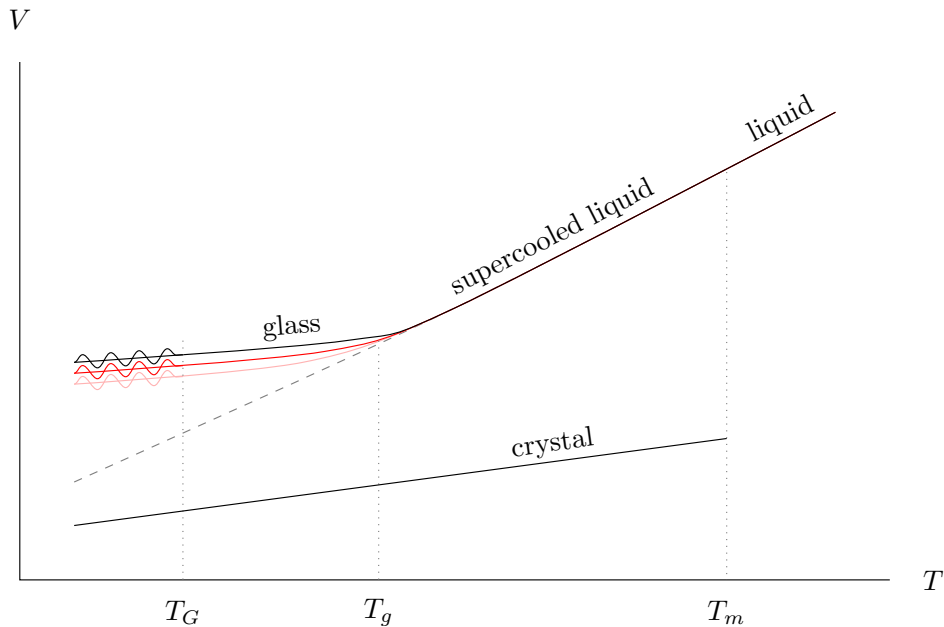


Figure 1.2: Volume of a glassformer liquid (similar plots hold for the entropy or the enthalpy). At the melting temperature  $T_m$  the system would crystallize, but such a transition in some cases can be avoided by cooling the liquid fast enough. The resulting supercooled liquid is metastable and falls out of equilibrium when the temperature is further lowered below some temperature  $T_g$ . The liquid might fall out of equilibrium at slightly different temperatures, depending on how the preparation protocol and on the choice of the criterion to determine  $T_g$ .  $T_G$  is the temperature of the *Gardner transition* that will be introduced in Chapter 1 - *Systems of spheres and jamming*; below  $T_G$  the system enters the *marginal glass phase*.

models, known as Kinetically Constrained Models, that try to explain the glassy behavior within the dynamic facilitation scenario: they are typically defined as particles on some lattice, subject to dynamical rules for the allowed moves. Of course, the two points of view are not mutually exclusive, and they might even be describing different aspects of these complex systems. Marginal models in between the two classes have also been studied. For instance the models in [Newman and Moore, 1999; Spigler, 2014; Franz et al., 2016] have a trivial thermodynamics and display glassy properties (without any transition) due to some dynamic facilitation, but, turning on a small perturbation a finite temperature glass transition appears, showing that the distinction between the two points of view is thinner than what it looks like.

## 1.1 Replica symmetry breaking

In this section we want to briefly introduce the concept of replica symmetry breaking and how it arises in physical problems. A thorough explanation can be found in [Nishimori, 2001; Castellani and Cavagna, 2005; De Dominicis and Giardinà, 2006; Mézard et al., 2008; Zamponi, 2010]. Let us consider a spin system with a generic Hamiltonian  $\mathcal{H}(\underline{s}; J)$ , where  $\underline{s}$  is a configuration; this Hamiltonian depends on some quenched disorder  $J$  — e.g. like in the Sherrington-Kirkpatrick model — that is expressed as a random variable with a given probability distribution. The disorder has been introduced because different samples of this system have different structural, intrinsic properties. In the case of a spin glass, the disorder is due to the fact that different samples have the spins quenched in random locations, and this is modeled with random couplings  $J$ . Then, the thermodynamics of a specific sample, and thus of a specific realization of the random variable  $J$ , is given by the usual free energy

$$f_J \equiv - \lim_{N \rightarrow \infty} \frac{1}{\beta N} \log Z_J \equiv - \lim_{N \rightarrow \infty} \frac{1}{\beta N} \log \sum_{\underline{s}} e^{-\beta \mathcal{H}(\underline{s}; J)}, \quad (1.3)$$

$Z_J$  being the partition function of the sample. Of course  $\log Z_J$  is in general a random variable, and the statistical properties of the system are given by the statistical properties of  $f_J$  (say, mean and variance). Unfortunately, even for the simplest distribution of the disorder  $J$ , we are not able to compute easily the sample-to-sample average of  $\log Z_J$ , namely

$$f = - \lim_{N \rightarrow \infty} \frac{1}{\beta N} \overline{\log Z_J} = - \lim_{N \rightarrow \infty} \frac{1}{\beta N} \overline{\log \sum_{\underline{s}} e^{-\beta \mathcal{H}(\underline{s}; J)}}, \quad (1.4)$$

where the overline denotes averages over the disorder  $J$ . The way this problem has been overcome is the so-called *replica trick*, that is the limit

$$\log Z = \lim_{n \rightarrow 0} \frac{Z^n - 1}{n} = \lim_{n \rightarrow 0} \frac{\log Z^n}{n}. \quad (1.5)$$

This trick is used as follows: we are usually able to compute  $\overline{Z_J^n}$  for integer  $n$ , since this is actually the partition function of  $n$  non-interacting copies (“replicas”) of the same original system,  $\mathcal{H}(\underline{s}^1; J) + \dots + \mathcal{H}(\underline{s}^n; J)$  — the disorder  $J$  is the same in all the copies; then, performing some suitable analytic continuation on  $n$  we can try to compute

$$f = - \lim_{N \rightarrow \infty} \lim_{n \rightarrow 0} \frac{1}{\beta N n} (\overline{Z_J^n} - 1) = - \lim_{N \rightarrow \infty} \lim_{n \rightarrow 0} \frac{1}{\beta N n} \log \overline{Z_J^n}. \quad (1.6)$$

In general, this method can effectively be used for fully connected (mean-field) models; in these cases we might be able to cast  $\overline{Z_J^n}$  as

$$\begin{aligned} \overline{Z_J^n} &= \sum_{\underline{s}^1, \dots, \underline{s}^n} \overline{e^{-\beta\mathcal{H}(\underline{s}^1) - \dots - \beta\mathcal{H}(\underline{s}^n)}} = \\ &= \sum_{\underline{s}^1, \dots, \underline{s}^n} \left[ \int \prod_{a,b=1}^n dQ_{ab} \delta \left( Q_{ab} - \frac{1}{N} \underline{s}^a \cdot \underline{s}^b \right) \right] \overline{e^{-\beta\mathcal{H}(\underline{s}^1) - \dots - \beta\mathcal{H}(\underline{s}^n)}} \equiv \\ &\equiv \int \prod_{ab} dQ_{ab} e^{-NA[Q;\beta]}. \end{aligned} \quad (1.7)$$

where  $A[Q;\beta]$  is some functional of the matrix  $Q_{ab}$ , whose elements are the *overlaps* between replica  $a$  and replica  $b$ :  $q_{ab} = \frac{1}{N} \underline{s}^a \cdot \underline{s}^b$ . Therefore,

$$f \equiv - \lim_{N \rightarrow \infty} \lim_{n \rightarrow 0} \frac{1}{\beta N n} \log \int \prod_{ab} dQ_{ab} e^{-NA[Q;\beta]}. \quad (1.8)$$

Of course the detailed form of the functional  $A[Q;\beta]$  changes from system to system, but here we are only interested in the general approach. The integral in (1.8) for large  $N$  is dominated by the maximum of  $-NA[Q;\beta]$ , and thus it can be computed via a saddle-point approximation (or Laplace method):

$$f \equiv - \lim_{n \rightarrow 0} \frac{1}{\beta n} \min_Q A[Q;\beta]. \quad (1.9)$$

The minimization is performed with respect to all  $n \times n$  matrices  $Q$ , in the limit  $n \rightarrow 0$ ! This is, in general, a very difficult task. What we can do, instead, is to minimize the functional  $A[Q;\beta]$  with respect to matrices belonging to a restricted subset of matrices that can be easily parametrized. This is nothing more than a variational method to estimate the true free energy, and in order to solve the problem exactly we “just” have to guess the (simplest) correct form of the matrix that minimizes the functional. Parisi [Parisi, 1979, 1980, 1983; Mézard et al., 1984a] came up with what turned out to be the correct idea (as it would have been later proved by Talagrand for the Sherrington-Kirkpatrick model and other systems [Talagrand, 2003]). For many different systems (Sherrington-Kirkpatrick model, dense soft spheres, ...), in the “glassy phase” (i.e. the low temperature phase or high density) the solution predicts that the matrix  $Q$  has a very complex, hierarchical structure, and the system is said to display replica symmetry breaking.

The following interpretation can be derived from the solution with replica symmetry breaking. At sufficiently low temperature the Gibbs measure of any sample is split into sample-dependent ergodic components, known as

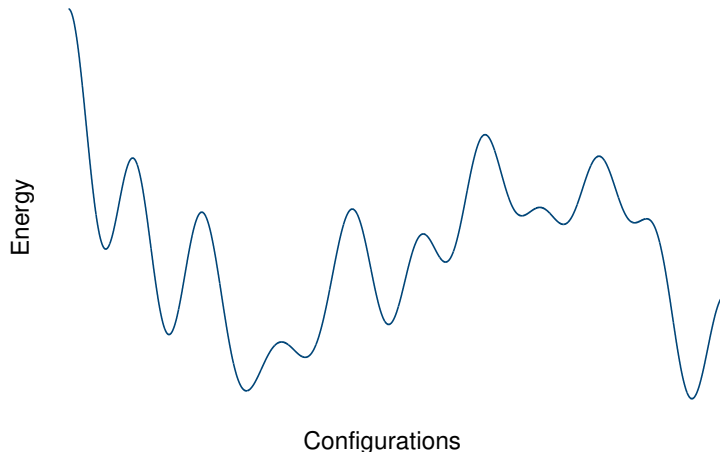


Figure 1.3: The free energy (1.9) has many local minima, in the phase with replica symmetry breaking. The relative Gibbs measure has many pure states that roughly correspond to these minima.

*pure states* (Figure 1.3), that can be thought of as the basins surrounding the local minima of the free energy. Their statistical properties are contained in the matrix  $Q$  that satisfies the saddle-point minimization in (1.9). To describe the organization of the states in the phase-space we first introduce the notion of *overlap*  $q(\underline{s}^1, \underline{s}^2)$  between two configurations  $\underline{s}^1, \underline{s}^2$ : this is a co-distance that measures the similarity between two configurations; its absolute value is normalized between 1 and 0 (for identical and maximally different configurations, respectively). Different definitions are used for different systems: for instance, for a spin glass with  $N$  spins (e.g. the Sherrington-Kirkpatrick model) it can be defined as  $q(\underline{s}^1, \underline{s}^2) = N^{-1} \underline{s}^1 \cdot \underline{s}^2$ ; for  $N$  spheres,  $q(\underline{s}^1, \underline{s}^2) = N^{-1} \sum_{i,j=1}^N W(|\underline{s}_i^1 - \underline{s}_j^2|)$ , where  $\underline{s}_i^{1,2}$  is the position of the  $i$ -th particle in the two configurations and  $W(r)$  is a window function that vanishes when  $r$  is larger than some threshold and such that  $W(0) = 1$ . The specific choice is irrelevant for what follows, since proper definitions are equivalent [Parisi, 1998; Franz et al., 1999; Parisi and Ricci-Tersenghi, 2000; Parisi, 2002]. Then, after defining the overlap between configurations, we define the overlap between two states  $\alpha, \beta$  as the average of the overlap between configurations belonging to the two states,  $q_{\alpha\beta} = \sum_{\underline{s}^1 \in \alpha, \underline{s}^2 \in \beta} w(\underline{s}^1; \beta) w(\underline{s}^2; \alpha) q(\underline{s}^1, \underline{s}^2)$ ; here  $w(\underline{s}; \beta)$  is the Boltzmann weight  $Z_J^{-1} \exp(-\beta \mathcal{H}(\underline{s}; J))$ , and we consider a configuration  $\underline{s}$  belonging to a state  $\alpha$  if it lies in its basin (or, operatively, if a steepest descent dynamics brings the configuration to the

minimum of the basin, called the state's inherent structure). Since replica symmetry breaking corresponds to the appearance of many disjoint states, we can use as order parameter of such a symmetry breaking the sample-averaged probability distribution of the overlap between pairs of states, namely  $\mathcal{P}(q, \beta) = \overline{\sum_{\alpha\gamma} w_\alpha(\beta)w_\gamma(\beta)\delta(q - q_{\alpha\gamma})}$  [Mézard et al., 2008], where  $w_\alpha(\beta) = \frac{e^{-\beta F_\alpha}}{\sum_\gamma e^{-\beta F_\gamma}}$  is the Boltzmann weight of the state  $\alpha$ , and  $\{F_\alpha\}$  are the states' free energies, defined as  $\exp(-\beta F_\alpha) = \sum_{\underline{s} \in \alpha} w(\underline{s}; \beta)$ . Equivalently, we can consider as order parameter the so-called *Parisi function*  $\beta x(q, \beta) = \beta \int_0^q d\bar{q} \mathcal{P}(\bar{q}, \beta)$  (in the literature of replica symmetry breaking the function  $x(q, \beta)$  is called the *functional order parameter*).

Loosely speaking, we can group the states in Figure 1.3 into clusters such that any two states in a cluster have a mutual overlap larger than some threshold  $q_{\text{th}}$ , that plays the role of a coarse-graining scale; when  $q_{\text{th}}$  is large enough then each cluster is formed by a single state (that has maximum overlap with itself). As the threshold is decreased, different clusters merge together, until there is only one cluster. A simple way to view how different clusters merge is to draw a tree with all the states as leaves (see Figure 1.4); moving upwards along the tree corresponds to lowering  $q_{\text{th}}$ , and when some states are joined into the same cluster we draw a new node, until we reach the root of the tree, that is associated with a maximal cluster containing all the states — this cluster is found at a scale  $q_{\text{th}} = q_{\text{min}}$ , that is the minimum possible overlap between any two states. In the figure we have drawn an example of such a process, where every state starts in the smallest possible clusters at an overlap  $q_3$  that is defined as the self overlap  $q_{\alpha\alpha}$  — this quantity does not depend on the state  $\alpha$ , and it is called the Edwards-Anderson order parameter  $q_{\text{EA}}$ . Then, we assume that at a scale  $q_2$  some states can be grouped into distinct clusters, that eventually join at a scale  $q_1$ .

The fact that we can draw such a tree implies that the clusters at each scale  $q_{\text{th}}$  are disjoint. This property is called *ultrametricity* and follows from the properties of the matrix  $Q$  that satisfies the saddle-point condition (1.9); an equivalent way to state it is to say that for any three states  $\alpha, \beta, \gamma$ , the mutual overlaps satisfy  $q_{\alpha\beta} \geq \min\{q_{\alpha\gamma}, q_{\beta\gamma}\}$ ; moreover, if we assume without loss of generality that  $q_{\alpha\beta} \leq q_{\beta\gamma} \leq q_{\gamma\alpha}$ , then applying the inequality to all possible permutations of the indices yields  $q_{\alpha\beta} = q_{\beta\gamma} \leq q_{\gamma\alpha}$ . This property is manifest in Figure 1.4 if we relate the mutual overlap  $q_{\alpha\beta}$  to the overlap scale  $q_1$  at which the two states  $\alpha, \beta$  merge into a unique cluster.

The tree built in this way is a random structure, since it depends on the states

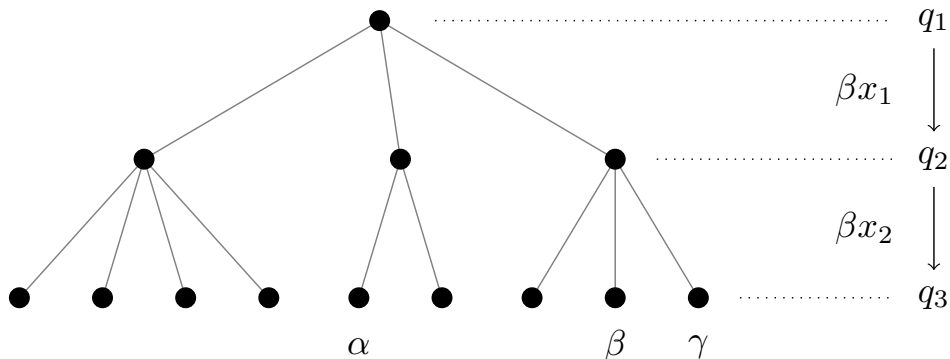


Figure 1.4: The states can be arranged in a hierarchical structure, where ultrametricity is manifest.

in a specific sample, and its distribution is related to the functional order parameter  $\beta x(q, \beta)$ , that in turn can be computed from the saddle-point matrix  $Q$  in (1.9). In principle the Parisi function could be any increasing function; in particular, if the states can be organized in an ultrametric structure as in Figure 1.4, we might expect it to be a step function with a number  $k$  of steps. It turns out that in practice the models that have been studied either have a continuous  $\beta x(q, \beta)$  ( $k = \infty$ , known as “full replica symmetry breaking”) or  $k = 1$  (called “1-step replica symmetry breaking”). (There is the exception of the Derrida’s Generalized Random Energy Model [Derrida, 1980, 1981], that can have any number  $k$  of steps, but it is somewhat artificial). In the following we will nonetheless regard  $\beta x(q, \beta)$  as a step function that takes discrete values  $0 \leq \beta x_1 < \dots < \beta x_k \leq \beta$  on intervals separated by the points  $0 \leq q_1 < \dots < q_{k+1} = 1$ . The number  $k$  is the number of *levels of replica symmetry breaking*, that is the “depth” of the tree of clusters shown in Figure 1.4 (in the example  $k = 2$ ). The numbers  $\{q_i\}$  are a discretization of the possible values that the mutual overlap between two states  $\alpha, \beta$  can take; for instance, when  $k = 1$  there are only two possible values: either  $q_{\alpha\alpha} = q_2 \equiv q_{\text{EA}}$  for the self overlap, or  $q_{\alpha\beta} = q_1 < q_{\text{EA}}$  for  $\alpha \neq \beta$ . The numbers  $\{\beta x_i\} \equiv \{\beta x(q_i, \beta)\}$  instead characterize the structure of the tree. The details of this distribution can be found in Appendix a. The stochastic process that describes the distribution of the tree is a branching process: this means that, starting from a root node (the top of the tree), the process generates a first layer of child nodes, that we identify as the clusters at the scale  $q_1$  in Figure 1.4; the distribution according to which are extracted the child nodes depends on a single parameter, that is  $\beta x_1$ .

Then, the branching process is iterated starting from each child node, thus generating a second layer of child nodes, this time using  $\beta x_2$  as the only parameter of the distribution. In the example shown in the figure (where  $k = 2$ ), we stop after reaching this second level, and the last nodes that have been generated at the bottom of the tree are identified as the states of the sample; for a generic  $k$  we would continue iterating the branching process until we reach the  $k$ -th level. For a continuous Parisi function, a suitable limit has to be taken in the end. This process allows us to compute the distribution of the free energies of the states in a sample, and it will be essential for computing the distribution of static avalanches in mean field systems (see Chapter 2). Normalizing the free energies one finds the associated Boltzmann weights,  $w_\alpha(\beta)$ ; their distribution, induced by that of the free energies, is known as *Derrida-Ruelle cascade*.

## 1.2 Systems of spheres and jamming

Granular materials are complex systems with a rich phenomenology. Varying the external control parameters or the internal properties, these systems can display characteristics that are typical of either liquids or solids. Among the simplest models that can be studied, either numerically or analytically, are those of spherical particles with short range, repulsive interaction: these are systems made by  $N$   $d$ -dimensional frictionless spheres of radius  $R$ <sup>1</sup> that interact via a pair potential

$$\mathcal{V}(r) = \epsilon \left(1 - \frac{r}{2R}\right)^\alpha \theta\left(1 - \frac{r}{2R}\right), \quad (1.10)$$

where  $r$  is the distance between two particles' centers,  $\epsilon > 0$  is the intensity of the repulsion and  $\alpha$  can be tuned to different values (typically one studies harmonic spheres with  $\alpha = 2$  or Hertzian spheres with  $\alpha = \frac{5}{2}$ ). This interaction is identically zero when the two particles are not overlapping ( $r > 2R$ ), and increases with the compenetration (for this reason we talk about “soft spheres”); it is of course possible to take the limit  $\epsilon \rightarrow \infty$ , known as the hard sphere limit: in this case the potential is  $\mathcal{V}(r) = \infty$  if the particles overlap ( $r < 2R$ ) and 0 otherwise — that is, particles cannot overlap. Notice that hard spheres behave similarly to soft spheres at zero temperature, and are athermal systems, in the sense that their thermodynamics is the same at any temperature:  $\beta\mathcal{V}$  is independent of  $\beta$ ,

---

<sup>1</sup>In  $d = 2$  the system tends to crystalize very easily at high densities, and it is thus not useful for studying disordered packings. Nonetheless, as one introduces some polydispersity (i.e. particles with different radii) the crystallization can be avoided.

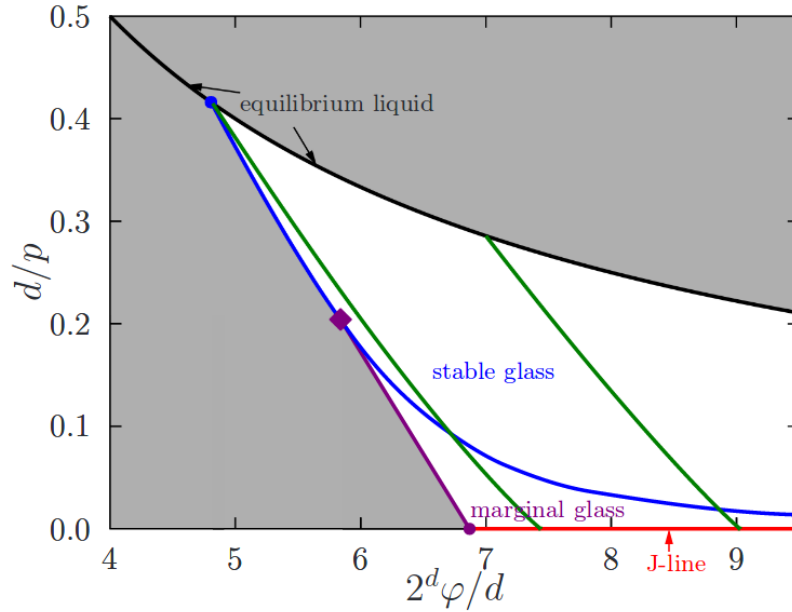


Figure 1.5: Phase diagram showing the liquid, stable glass, marginal glass and jamming phases of systems of hard spheres. Picture taken from [Charbonneau et al., 2014b].

since the energy only takes the values 0 or  $\infty$ ; the suitable control parameter is then the pressure. The thermodynamics of systems of hard spheres has been solved analytically in the limit of infinite spatial dimensions [Kurchan et al., 2012, 2013; Charbonneau et al., 2014a], where they become mean field and can be solved within the replica symmetry breaking framework. The solution predicts the following behavior (see also Figure 1.5): at low pressure the system is first in the equilibrium liquid phase; increasing the pressure — and avoiding the crystallization — one reaches the metastable supercooled liquid and the dynamics slows down, and eventually the system falls out of equilibrium and gets stuck in the basin of one state, thus forming a glass (in the following we will refer to this as a *simple glass* or *stable glass*). The stable glass is described by a 1-step replica symmetry breaking ansatz, that predicts the existence of many states (each corresponding to a different glass) separated by large barriers. Then, it was discovered, first by Gardner in the spherical  $p$ -spin model [Gardner, 1985], then by [Charbonneau et al., 2014b] for hard spheres, that at an even larger pressure the glass becomes unstable and there is another transition (the Gardner transition) (see Figure 1.2), after which the system is described by a full (continuous) replica symmetry

breaking ansatz. The physical meaning is that in this phase, that we will refer to as the *marginal glass*, while each state’s basin remains well separated from the others, its “bottom” breaks into a very rough, “fractal” energy landscape with many smaller valleys separated by small energy barriers (see Figure 1.6 for a pictorial representation). Finally, in the limit of infinite pressure the system reaches a critical phase called *jamming*.

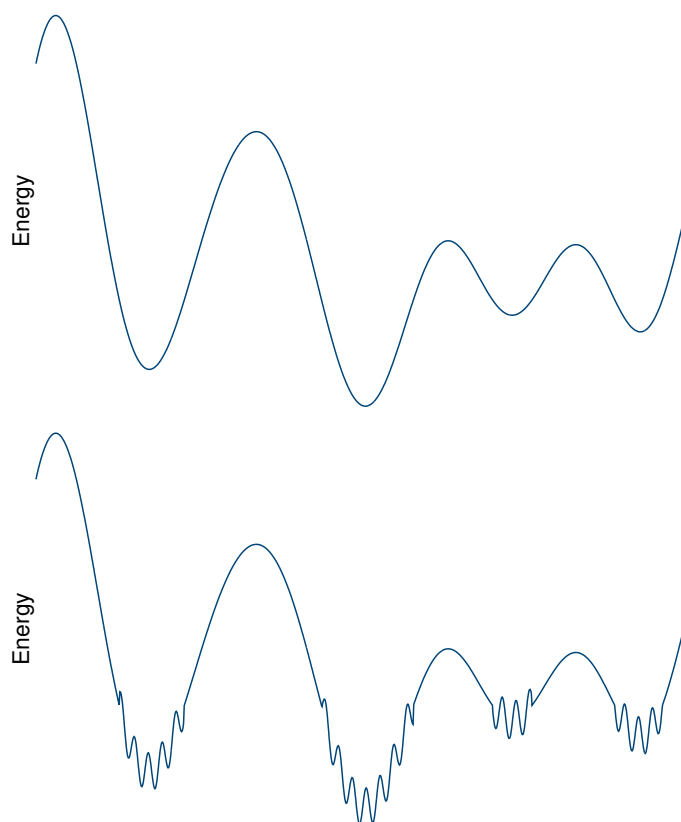


Figure 1.6: Representation of the free energy landscape of a glass: the picture on the top is for a stable glass, while the one on the bottom is for the marginal glass, after the Gardner transition. See also [Charbonneau et al., 2014b].

The concept of jamming as a unified concept in the physics of disordered media had been introduced in [Liu and Nagel, 1998] noticing that many different granular systems achieve mechanical stability as the density is increased. A  $d$ -dimensional system of hard spheres jams when an infinite pressure is applied; this point is *marginally mechanically stable* because it

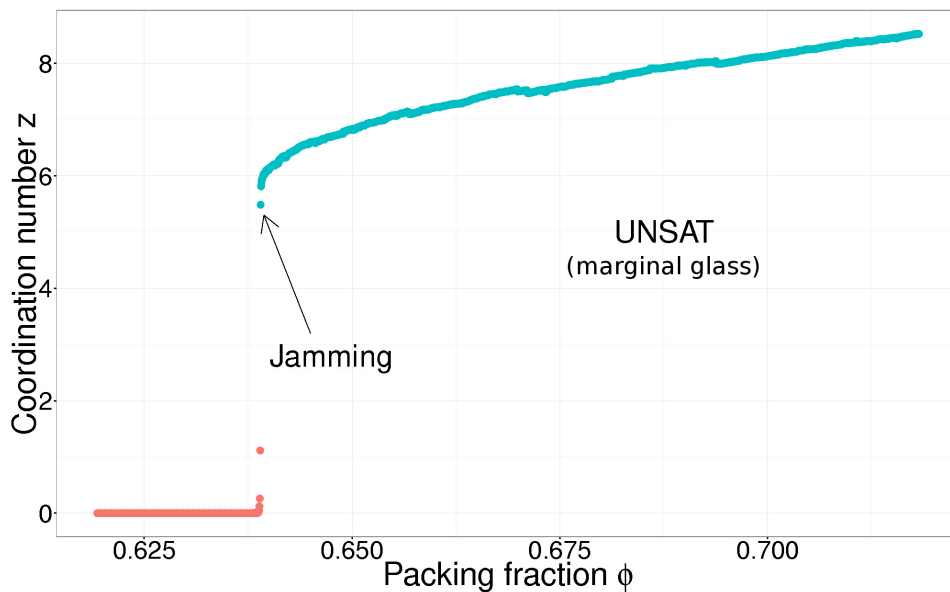


Figure 1.7: Average coordination number as a function of the packing fraction, for one specific three-dimensional sample of 1000 soft spheres with harmonic repulsion.

barely satisfies the so-called *Maxwell's condition* [Van Hecke, 2009], namely the fact that a system can be mechanically stable — no net force on any particle — only if the number of forces (that is the number  $Z$  of pairs of particles in contact in the systems) is larger than the number of degrees of freedom (namely, the  $dN$  particles' coordinates). Since the number  $Z$  can be written as a function of the average coordination number  $z$  per particle (that is, its average number of contacts) as  $Z = \frac{1}{2}zN$ , we have that a system is mechanically stable only if  $z \geq 2d$ ; the factor  $\frac{1}{2}$  avoids counting twice the contacts. At jamming  $z = 2d$ , and the system is said to be *isostatic* [Liu et al., 2011]. We can also study the jamming problem in systems of soft spheres, where it is then possible to further increase the density of the packing. Of course in these systems the jamming point is not found at infinite pressure, but rather when the condition for marginal mechanical stability  $z = 2d$  is met — the pressure is in fact zero for soft spheres at jamming; in Figure 1.7 we plot the average number of contacts per particle  $z$  as a function of the packing fraction  $\phi$ , defined as the total volume occupied by the particles contained in a unit volume. For small packing fractions there are no particles in contact and the energy is 0. As the density is increased (always allowing the system to relax to a minimum of the energy landscape), at some point the system jams with a sharp transition, where the coordination number  $z$

jumps to a finite value, approximately equal to  $2d$ . The packing fraction at which the system jams fluctuates (in  $d = 3$  it is about  $\phi_J \approx 0.64$ ) and it depends on the specific sample; in the thermodynamic limit when the number of particles  $N$  tends to  $\infty$  all the samples jam at the same packing fraction. Upon further compression the number  $z$  increases, and close to the jamming point one finds the scaling

$$z - 2d \sim \sqrt{\phi - \phi_J}, \quad (1.11)$$

(this scaling does not change varying the dimension  $d$  or the exponent  $\alpha$  in the interaction (1.10)) [O’Hern et al., 2003]. Notice that the Maxwell’s condition is not strictly satisfied in finite dimensions, because there is a finite probability that in a jammed configuration there is a “cage” formed by jammed particles and such that on the inside there is enough space to accommodate another particle that does not interact with its surroundings (see Figure 1.8); these *rattlers* should not be counted in (1.11). In three-dimensional configurations at jamming, approximately 1-5% of the particles are rattlers [Atkinson et al., 2013; Charbonneau et al., 2016]; this percentage vanishes quickly as the dimension is increased [Charbonneau et al., 2012].

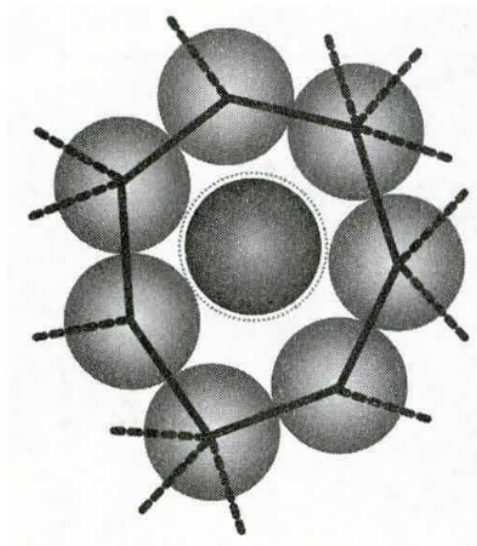


Figure 1.8: A rattler in a two-dimensional configuration at jamming. The surrounding cage is stable (jammed) and the rattler does not interact with it. The lines represent contacts between the particles. Picture taken from [Charbonneau et al., 2015].

It turns out that the jamming point has critical properties that control its neighborhood, in the sense that also other quantities show a critical scaling when approaching this point from the denser phase (sometimes called *jammed*, *marginal glass* or UNSAT phase), even though they might depend on the force exponent  $\alpha$  [O’Hern et al., 2002; Liu and Nagel, 2010]. For instance, the pressure above jamming scales as  $p \sim \phi - \phi_J$  for harmonic spheres ( $\alpha = 2$ ) and as  $p \sim (\phi - \phi_J)^{1.5}$  for Hertzian spheres ( $\alpha = \frac{5}{2}$ ), regardless of the dimension; in general the scaling is consistent with saying that  $p \sim (\phi - \phi_J)^\psi$  with  $\psi = \alpha - 1$ . A critical behavior is also found in the pair correlation function and in the distribution of the contact forces between neighboring particles. The “gap”  $h_{ij}$  between two particles at  $\underline{r}_i, \underline{r}_j$  is their distances minus the particles’ diameter,  $h_{ij} \equiv |\underline{r}_i - \underline{r}_j| - 2R$ . The distribution  $g(h)$  of the gaps is related to the pair correlation function  $\tilde{g}(r) = g(h + 2R)$ , and it behaves as a power law for small gaps:

$$g(h) \sim h^{-\gamma}. \quad (1.12)$$

Similarly, the force distribution has a pseudo-gap at small forces, that is

$$P(f) \sim f^\theta. \quad (1.13)$$

The two exponents  $\gamma$  and  $\theta$  are predicted by the mean-field theory (that is, in infinite dimensions), where their value is  $\gamma \approx 0.41269$  and  $\theta \approx 0.42311$ . The measured value for  $\gamma$  in finite dimensions ( $d \geq 2$ ) has been found to be compatible with this value [Charbonneau et al., 2012]. The distribution of forces on the other hand is a little trickier, because different exponents have been measured in finite dimensions. It turns out that there are two classes of contacts, according to whether the breaking/opening of the contact gives rise to an extended or localized rearrangement of particles; the distribution of forces restricted to forces belonging to any of the two groups also has a power-law behavior for small forces, and one finds different exponents in the two cases: “localized” forces have an exponent  $\theta_l \approx 0.17$  and “extended” forces have an exponent  $\theta_e \approx 0.42$  (regardless of the spatial dimension) [Charbonneau et al., 2015]. The particles that are involved in local rearrangements are called *bucklers*, and their number decreases with the spatial dimension; for this reason one finds that the exponent in the total distribution of the forces interpolates between the two exponents  $\theta_{l,e}$ , tending to  $\theta_e$  when  $d \rightarrow \infty$ . In [Wyart, 2012; Lerner et al., 2013; Müller and Wyart, 2015] it has been shown that mechanical stability, or rather the fact that the jammed system of hard spheres cannot be further compressed, implies two bounds on the exponents, namely that  $\gamma \geq \frac{1-\theta_l}{2}$  and  $\gamma \geq \frac{1}{2+\theta_e}$ ; quite remarkably the predicted and

measured data satisfy these bounds, but only marginally, in the sense that  $\gamma(\approx 0.413) \approx \frac{1-\theta_l}{2}(\approx 0.415) \approx \frac{1}{2+\theta_e}(\approx 0.413)$  assume almost the same value. In their analysis the authors also argue that the rearrangements found in these systems when some temperature is introduced or when the system is sheared will typically be extended, and thus the relevant exponent should be the force exponent  $\theta_e$ . In the following chapter we are going to study the response of systems of soft spheres under shear strain, and we are going to argue that the distribution of the *avalanches* induced by the rearrangements at jamming are indeed governed by a power law with an exponent strictly related to  $\theta_e$ .



# 2

## Athermal response to perturbations

In Chapter 1 we have described the qualitative structure of the phase space of disordered systems. This chapter is devoted to the description of the behavior of these systems, and in particular of their ground state, when an external perturbation is introduced. The chapter is organized as follows: in the next section (*Avalanches*) we define the quantities that we are interested in, namely the (static) *avalanches*. In the section *Spheres and shear-strain* we present the systems that we focus on, that are dense systems of harmonic soft spheres, whose confining box is subject to a small shear strain. Next we proceed with a discussion on the probability distribution of the avalanches, summarizing the mean-field framework that allows its computation in infinite-dimensional systems, shown in details in Appendix b. In the end we compare these analytic mean-field results (in *Asymptotic behavior*) with three-dimensional numerical simulations (in *Numerical simulations*).

### 2.1 Avalanches

Disordered systems have complex *rugged* free-energy landscapes, with many sample-dependent local minima, as shown schematically in Figure 2.1 — the

picture shows the free energy of the configurations, for instance through a “section” of the phase space. When we introduce a small perturbation, the energy of each configuration is shifted by some amount that depends on the configuration itself: for instance when a magnetic system is embedded into a magnetic field  $\underline{h}$ , the energy of any spin configuration  $\{\underline{s}_i\}$  is shifted by  $\underline{h} \cdot \sum_i \underline{s}_i$ . In general we may want to study the effects of some perturbation with different protocols or different evolution dynamics. For instance, the perturbation can be increased constantly at a finite rate, while the system undergoes some dynamics; as a limiting case we can study a perturbation with a vanishingly small rate, such that the system has time to equilibrate in an almost constant field. At zero temperature the latter is equivalent to saying that the system always lies in its instantaneous ground state, namely the configuration that reaches the global energy minimum. Of course, the response is in general sensitive to the details of the protocol, and for the moment we are going to focus on the limiting case at zero temperature, with a perturbation that is increased instantly and in a stepwise fashion: we will refer to this as the *athermal quasi-static protocol*.

When the perturbation is small enough, we might expect that no state (i.e. the valleys in Figure 2.1) disappears or is created, and that the only effect is a small, state-dependent shift of their energies (red arrows in the same picture). Of course, also the energy of the barriers in between valleys is modified, but in the framework of the athermal quasi-static protocol the barriers are irrelevant, since we are only looking for the true, absolute ground state of the system. If the intensity of the perturbation is increased step by step and always in a quasi-static fashion and at zero temperature, the system *jumps* from a state to another as soon as the latter has a lower *total energy* (namely the unperturbed energy plus the energy shift). The jumps happen at random times because the energy landscape is random and sample-dependent, and in general the new ground state can be in a configuration very different from the previous one. For these reasons, the response of many disordered systems (such as spin glasses, structural glasses, elastic interfaces. . . ) is random and usually proceeds by discontinuous jumps ([Young et al., 1984; Young and Kirkpatrick, 1982; Franz and Parisi, 2000; Combe and Roux, 2000; Sethna et al., 2001; Krzakala and Martin, 2002; Rizzo and Yoshino, 2006; Yoshino and Rizzo, 2008; Rosso et al., 2009; Yan et al., 2015; Müller and Wyart, 2015; Jesi, 2015]), called *static avalanches* (“static” refers to the fact that we are always in the instantaneous ground state).

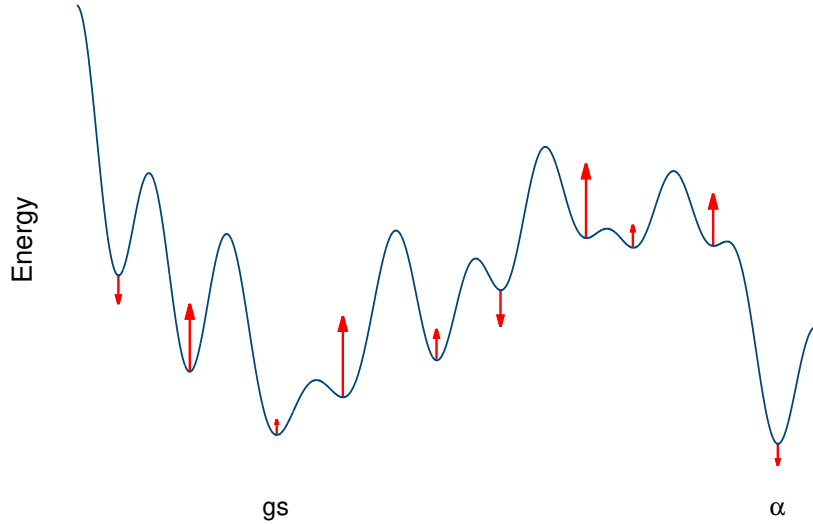


Figure 2.1: A simplified picture of the rugged free-energy landscape of a disordered system — along the horizontal axis there are the configurations. The valleys represent different phases of the system, and the ground state (gs) is the global minimum. When a small perturbation is turned on, the energy of the minima will be shifted by some configuration-dependent amount, and it might happen that the new global minimum ( $\alpha$ ) is no longer the previous ground state (gs).

Since avalanches are random objects, we want to know what is their distribution, averaged over several jumps and several samples. In some disordered systems one finds a *power-law* behavior for the distribution of jumps; for instance, in [Le Doussal et al., 2012] the authors find a power law in the density of magnetization jumps in spin glasses (with full replica symmetry breaking), in [Combe and Roux, 2000] a different power law is found for strain jumps in systems of hard spheres under shear-stress, and in [Liu et al., 2016] similar results are found for systems of spheres in the *elasto-plastic* phase (at a large shear strain), for different perturbation rates. Interestingly, often the same power-law exponent is found using different perturbation protocols ([Le Doussal and Wiese, 2009; Le Doussal et al., 2012; Liu et al., 2016]); indeed, it has been conjectured that the various responses in some of these disordered systems might lie in the same universality class, regardless of the dynamics [Liu and Dahmen, 2009].

## 2.2 Spheres and shear-strain

Our motivation to re-examine this problem in a general framework comes from the physics of soft spheres, in particular the jamming transition introduced in Chapter 1 [Liu and Nagel, 1998; O’Hern et al., 2003; Biroli, 2007; Parisi and Zamponi, 2010; Charbonneau et al., 2012; DeGiuli et al., 2014]. This type of system is among the simplest models for liquids (and glassformers): it is made of  $N$  identical spherical particles of radius  $R$ , in dimension  $d > 2$ ; two particles at a distance  $r$  (from center to center) interact via a pair potential

$$\mathcal{V}(r) = \left(1 - \frac{r}{2R}\right)^2 \theta\left(1 - \frac{r}{2R}\right), \quad (2.1)$$

that is, they repel elastically when in contact ( $r < 2R$ ) and do not interact when far away. The energy of the system is therefore  $\mathcal{H}(\{\underline{r}_i\}) = \sum_{i \neq j} \mathcal{V}(\|\underline{r}_i - \underline{r}_j\|)$ . The particles’ radius  $R$  is chosen in such a way that the total volume occupied by the particles in a unit box is a fixed value (the packing fraction)  $\phi$ :  $N \Omega_d R^d \equiv \phi$ , where  $\Omega_d$  is the volume of a sphere with unit radius in dimension  $d$ .

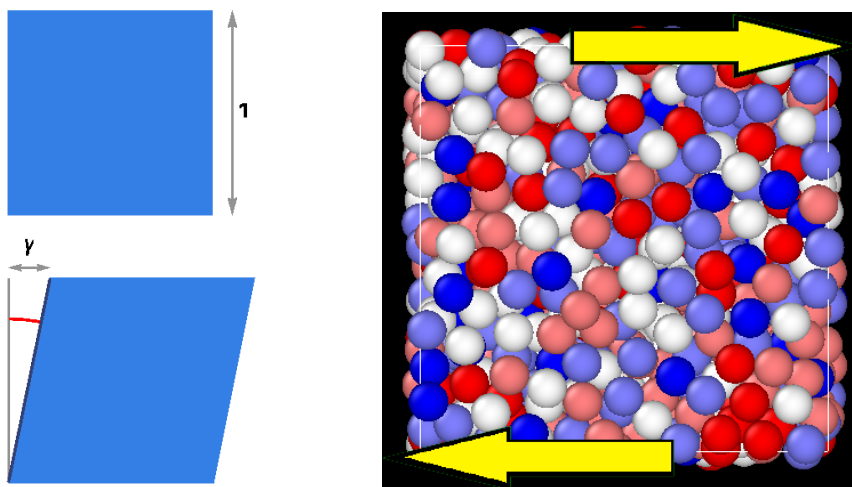


Figure 2.2: Shear transformation applied to a box of soft spheres. Each particle with coordinates  $(x_1, x_2, \dots)$  is translated to  $(x_1 + \gamma x_2, x_2, \dots)$ .

We want to study the static avalanches induced by a shear strain applied quasi-statically to the packing of spheres. A *shear strain* is a deformation of the system: in the quasi-static framework, applying a finite strain  $\gamma$  means that each particle, say with coordinates  $(x_1, x_2, \dots, x_d)$  — in arbitrary dimension  $d$  — is shifted to  $(x_1 + \gamma x_2, x_2, \dots, x_d)$ , i.e. the first coordinate is

translated by  $\gamma$  times the second coordinate, or equivalently the system is tilted in the  $x_1$ - $x_2$  plane as shown in Figure 2.2. Keep in mind that in the thermodynamic limit, the free-energy of these systems does not depend on the shape of the container, and thus it cannot depend on the shear, whatever are the boundary conditions [Yoshino and Mézard, 2010]. Nonetheless the response of the system is well defined even in that limit, and the reason is that the limits  $N \rightarrow \infty$  and  $\gamma \rightarrow 0$  do not commute — the same happens every time there is some symmetry breaking. For small shear strain  $\gamma$ , the energy  $\mathcal{H}(\{\underline{r}_i\}; \gamma)$  can be expanded in a Taylor series and it becomes  $\mathcal{H}(\{\underline{r}_i\}) - \gamma \Sigma(\{\underline{r}_i\})$ , where  $\mathcal{H}(\{\underline{r}_i\})$  is the unperturbed energy and  $\Sigma(\{\underline{r}_i\})$  is the *shear stress* of the configuration  $\{\underline{r}\}$ , that is equal to

$$\begin{aligned} \Sigma(\{\underline{r}_i\}) &\equiv -\frac{1}{2} \sum_{i \neq j} \mathcal{V}'(\|\underline{r}_i - \underline{r}_j\|) \|\underline{r}_i - \underline{r}_j\|^{-1} (\underline{r}_i - \underline{r}_j)_1 (\underline{r}_i - \underline{r}_j)_2 = \\ &= \frac{1}{2} \sum_{i \neq j} (\underline{r}_i - \underline{r}_j)_1 F_{ij,2}, \end{aligned} \quad (2.2)$$

The subscripts 1, 2 stand for the spatial directions along the axis  $x_1, x_2$ ,  $F_{ij,2}$  is the second component of the force between particles  $i$  and  $j$  and  $(\underline{r}_i - \underline{r}_j)_1 \equiv x_{i,1} - x_{j,1}$  is the first component of the displacement vector between the two particles. This shear stress is actually a part of the symmetric *stress tensor*, whose components  $\Sigma_{\alpha\beta}(\{\underline{r}_i\})$  ( $\alpha, \beta = 1, \dots, d$ ) are

$$\Sigma_{\alpha\beta}(\{\underline{r}_i\}) \equiv -\frac{1}{2} \sum_{i \neq j} \mathcal{V}'(\|\underline{r}_i - \underline{r}_j\|) \|\underline{r}_i - \underline{r}_j\|^{-1} (\underline{r}_i - \underline{r}_j)_\alpha (\underline{r}_i - \underline{r}_j)_\beta. \quad (2.3)$$

The stress tensor is a measure of the interactions between the particles in the system. In general, a shear strain in the plane  $x_\alpha$ - $x_\beta$  couples with the corresponding stress component  $\Sigma_{\alpha\beta}$ , while the other off-diagonal terms remain small; the diagonal terms on the other hand are related to the pressure of the system via

$$p = -\frac{1}{dV} \text{Tr} \Sigma = -\frac{1}{dV} (\Sigma_{11} + \dots + \Sigma_{dd}), \quad (2.4)$$

$\text{Tr} \Sigma$  being the trace of the tensor.

### Mean-field analytical computation

These systems of spheres have been recently analyzed and solved in the limit of infinite dimensions [Kurchan et al., 2012, 2013; Charbonneau et al., 2014a]. As explained in Chapter 1, athermal systems of soft spheres at

sufficiently large densities fall into the marginal glass phase, and are therefore characterized by a full replica symmetry breaking ansatz (RSB). Inside this phase, at a packing fraction  $\phi_J$ , we find the jamming point, that is the point where the system attains marginal mechanical stability and the particles barely touch each other (thus they have zero energy); at larger packing fractions the soft particles start to compenetrates and overlap with each other (increasing the energy), and if the density is not too large the system remains in the marginal glass phase: we call this portion of the phase space above the jamming point the UNSAT phase. The name stands for “unsatisfied”: the term is borrowed from the literature of *Constrained Satisfaction Problems*, and in particular from the non-convex perceptron introduced in [Franz and Parisi, 2016; Altieri et al., 2016; Franz et al., 2017]; the space occupied by a sphere can be interpreted as a constraint for the other particles, and the jamming point can then be viewed as the maximum density at which it is still possible to satisfy all the constraints. The portion of phase space below the jamming point, where the spheres can be accommodated without forming any contacts, is called the SAT phase and stands for “satisfied”; the jamming point is therefore a so-called SAT/UNSAT transition. It turns out that both the jamming point and the UNSAT phase are endowed with a hierarchy of states described by a full replica symmetry breaking ansatz, but the Parisi function  $\beta x(q, \beta, \phi)$  depends on the specific phase.

In Chapter 1 - *Replica symmetry breaking* and in Appendix a we explain that this functional order parameter plays an important role in the energy landscape, because it determines the branching process that defines the ultrametric tree of the states. At zero temperature the limit  $\lim_{\beta \rightarrow \infty} \beta x(q, \beta, \phi) \equiv y(q, \phi)$  is well defined. Since  $y'(q, \phi) \equiv \frac{dy(q, \phi)}{dq}$  is essentially the distribution of the overlap between any two states, its behavior near  $q = 1$  is directly linked to the density of states “close” to a reference state (that can be for example the ground state). It has been shown that the derivative of the Parisi function diverges near  $q = 1$  both at jamming and in the UNSAT phase; at jamming, the divergence is characterized by an exponent  $\mu_J \approx \frac{1}{1.41}$ :  $y'(q, \phi_J) \equiv y'_J(q) \sim (1 - q)^{-\mu_J - 1}$  (in the jamming literature this exponent is usually called  $\mu_J \equiv \frac{1}{\kappa}$  [Kurchan et al., 2012, 2013; Charbonneau et al., 2014a]); quite remarkably, in the whole UNSAT phase the Parisi function diverges with a constant exponent  $\mu_{\text{UNSAT}} = \frac{1}{2}$ :  $y'(q, \phi > \phi_J) \sim (1 - q)^{-\mu_{\text{UNSAT}}} \equiv y'_{\text{UNSAT}}(q)$  [Franz et al., 2017]. When a small perturbation is introduced, the distribution of the new ground state is related to a joint probability of finding a state at some overlap  $q$  with respect to the unperturbed ground state and that this new state is a global minimum of the energy: it is then reasonable to expect

the distribution of the new ground state to be heavily affected by the excess of states close to the unperturbed ground state ( $q \approx 1$ ). Indeed, we are going to show that, for sufficiently small external perturbations, the distribution of the energy difference between the new ground state and the unperturbed one develops power-law regime, whose exponent is strictly related to the exponents  $\mu_J, \mu_{\text{UNSAT}}$ .

In order to study athermal quasi-static avalanches we have to find the ground state of the unperturbed system and the ground state after that a small perturbation is applied. The former is the configuration that minimizes the unperturbed system's energy  $\mathcal{H}$ , while the latter is found, in the case of a shear strain  $\gamma$ , by minimizing the *total energy*  $\mathcal{H} - \gamma\Sigma$ , at a fixed value of  $\gamma$ . Then, we want to compute the distribution of the difference of the energies of the two ground states, and average them over several samples. In infinite dimensions the states of these systems are described by a mean-field RSB ansatz, that asserts the existence of infinitely many thermodynamic states  $\{\alpha\}$ , each characterized by an intrinsic free energy (that at zero temperature becomes the state's energy  $U_\alpha$ ) and an intrinsic stress  $\Sigma_\alpha$ . The states depend on the specific sample, and in Appendix a we review the joint distribution of all the energies  $\{U_\alpha\}$  and stresses  $\{\Sigma_\alpha\}$ ; in systems of soft spheres one expects the stresses and the energies to be independent one from the other [Yoshino and Mézard, 2010; Yoshino and Zamponi, 2014], and the distribution for the energies is given by the *branching process* introduced in Chapter 1 - *Replica symmetry breaking*, that defines the ultrametric structure of the phase space. This process is a cascade of Poisson point processes, and it depends on the specific RSB system only via its Parisi functional order parameter  $y(q, \phi)$  [Mézarid et al., 1985; Ruelle, 1987; Mézarid and Parisi, 2001; Panchenko and Talagrand, 2007; Mézarid et al., 2008]. The stresses on the other hand are sums of local variables (see (2.2)) that one expects to be “simply correlated”: their distribution is modeled as a *diffusion process* on the same tree, that starting from an initial value in the root node at the top of the tree (that was identified as the cluster containing all the states), reaches the leaves of the tree (identified with the states). Once we have the distribution of all the states' variables  $\{U_\alpha, \Sigma_\alpha\}$  we can find the probability distribution of the total energy difference between the unperturbed ground state and the perturbed one; the former is simply the minimum  $E_{\text{gs}} = U_{\text{gs}}$  among the states' energies  $\{U_\alpha\}$  (irrespective of the corresponding stress  $\Sigma_{\text{gs}}$  in that state, since  $\gamma = 0$ ), and the latter is the minimum  $E'_{\text{gs}} = U'_{\text{gs}} - \gamma\Sigma'_{\text{gs}}$  among the states' total energies  $\{U_\alpha - \gamma\Sigma_\alpha\}$ . Being the full derivation of such a distribution quite involved, for the sake of clarity we chose not to present it

here; it can be found in Appendix b.

In principle we would like to find the distribution of the difference between the total energy of the unperturbed ground state and that of the new ground state in an external field  $\gamma$ , that is  $E'_{\text{gs}} - E_{\text{gs}} \equiv (U'_{\text{gs}} - \gamma \Sigma'_{\text{gs}}) - U_{\text{gs}}$ . On the other hand, in the calculations it is clear that the relevant variable, whose distribution can be computed easily, is  $\Delta E \equiv \Delta U - \gamma \Delta \Sigma \equiv (U'_{\text{gs}} - U_{\text{gs}}) - \gamma(\Sigma'_{\text{gs}} - \Sigma_{\text{gs}}) = E'_{\text{gs}} - E_{\text{gs}} + \gamma \Sigma_{\text{gs}}$ . The quantity  $\Delta E$  is actually the difference between the total energy of the new ground state and that that the unperturbed one has under a shear  $\gamma$ :  $\Delta E = (U'_{\text{gs}} - \gamma \Sigma'_{\text{gs}}) - (U_{\text{gs}} - \gamma \Sigma_{\text{gs}})$ . The difference between  $\Delta E$  and  $E'_{\text{gs}} - E_{\text{gs}}$  is shown in Figure 2.3.

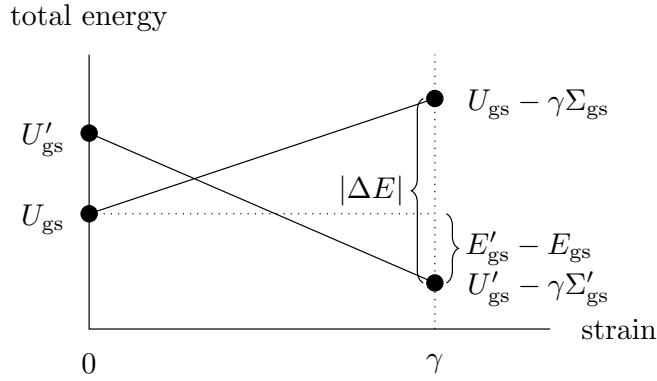


Figure 2.3: The level crossing between the unperturbed ground state (whose total energy is — by chance — increasing because of a negative shear stress  $\Sigma_{\text{gs}}$ ) and the state that is going to be the new ground state at shear strain  $\gamma$  (whose total energy is decreasing because of a positive shear stress  $\Sigma'_{\text{gs}}$ ). The difference between  $\Delta E$  and  $E'_{\text{gs}} - E_{\text{gs}}$  is also shown.

After performing all the calculations we arrive at the probability distribution of the jumps  $\Delta E$  in the total energy induced by a shear strain  $\sqrt{N}\gamma \ll 1$ :

$$\mathcal{P}(\Delta E|\gamma) \equiv \delta(\Delta E) \mathcal{R}(0|\gamma) - \theta(\Delta E < 0) \partial_{\Delta E} \mathcal{R}(\Delta E|\gamma), \quad (2.5)$$

$$\mathcal{R}(\Delta E|\gamma) = \exp \left\{ -\sqrt{N} |\gamma| \int dq y'(q) \sqrt{1-q} \rho \left( \frac{\Delta E}{\sqrt{N} |\gamma| \sqrt{1-q}} \right) \right\}, \quad (2.6)$$

$$\rho(x) \equiv 2(4\pi)^{-\frac{1}{2}} e^{-\frac{1}{4}x^2} + x \text{H} \left( \frac{x}{\sqrt{2}} \right). \quad (2.7)$$

where  $\text{H}(x) \equiv \int_{-\infty}^x \frac{dt}{\sqrt{2\pi}} e^{-\frac{t^2}{2}}$  is a complementary error function. Keep in mind that by definition  $\Delta E \leq 0$ , since the new ground state has to be at a lower total energy than the unperturbed one. Formula (2.5) shows manifestly that

the distribution is normalized and invariant under  $\gamma \rightarrow -\gamma$ ; this symmetry arises naturally from the computations and suggests the presence of a cusp in  $\gamma = 0$ , but in principle, it does not necessarily hold for different kinds of perturbations.

The validity of equations (2.5)-(2.6) is not restricted only to spheres, either at jamming or in the UNSAT phase. The approach that we have used is based on the distribution of the states' free energies, that depends only on a system's Parisi function. On the other hand the distribution of the states' variables that couple with the perturbation (that in our case is the shear strain) needs not be a diffusion on the ultrametric tree; furthermore, those variables might as well be correlated with the states' energies. Nonetheless, if

- a system is described by a (continuous) RSB ansatz, and thus by some functional order parameter  $y(q)$ ;
- the system is subject to any perturbation  $h$  that couples to some states' variables  $\{Y_\alpha\}$  (that is, when the field  $h$  is turned on the energy of each state  $Y_\alpha$  is shifted by  $hY_\alpha$ );
- the variables  $\{Y_\alpha\}$  are *independent* from the energies  $\{U_\alpha\}$ ;
- the variables  $\{Y_\alpha\}$  are distributed as a diffusion process on the ultrametric tree of the states (just like the stresses in the case of dense spheres);

then the equations (2.5)-(2.6) correctly describe the distribution of avalanches, apart from a rescaling of the field  $h$  that comes from the variance of the diffusion process. Of course not all perturbations satisfy these assumptions (in particular the one regarding the independence from the states' energies). Interestingly, the Sherrington-Kirkpatrick model for mean-field spin glasses, embedded in a magnetic field  $h$  that couples to the states' magnetizations  $M_\alpha$ , satisfies all the hypotheses.

### 2.3 Asymptotic behavior

In the previous section we have recalled that the increasing function  $y'(q)$  is related to the distribution of the overlap between pairs of states at zero temperature, and that in the models that we are interested in this function diverges near  $q = 1$ , signalling an abundance of states close to each other. It is clear that the integral in (2.6) depends heavily on the derivative of the Parisi function,  $y'(q)$ . In this section we are going to show that the

probability distribution of static avalanches develops a power-law behavior for sufficiently small jumps  $\Delta E$  when the applied perturbation  $\gamma$  is small, and the exponent of the power law is directly linked to the exponent  $\mu$  found in the functional order parameter  $y(q)$ .

In order to study the asymptotic behavior, let us introduce the function  $\mathcal{C}(\Delta E|\gamma) \equiv -\log \mathcal{R}(\Delta E|\gamma)$ , where  $\mathcal{R}$  is the function in (2.6). Then, neglecting the probability of *not jumping*, that is the term  $\mathcal{R}(0|\gamma)$ , the probability density of jumps is  $\mathcal{P}(\Delta E|\gamma) = \mathcal{R}(\Delta E|\gamma) \partial_{\Delta E} \mathcal{C}(\Delta E|\gamma)$ ; for  $|\Delta E| \ll \sqrt{N} |\gamma| \ll 1$  and assuming a generic scaling  $y(q) \sim (1-q)^{-\mu-1}$ , we have

$$\begin{aligned} \partial_{\Delta E} \mathcal{C}(\Delta E|\gamma) &= \int_0^1 dq y'(q) \rho' \left[ \frac{\Delta E}{\sqrt{N} |\gamma| \sqrt{1-q}} \right] = \\ &= \left| \frac{\Delta E}{\sqrt{N} \gamma} \right|^{-2\mu} \int_{\left| \frac{\Delta E}{\sqrt{N} |\gamma|} \right|^2}^{\infty} du u^{\mu-1} \mathbf{H} \left( -\sqrt{\frac{u}{2}} \right) \sim \left| \frac{\Delta E}{\sqrt{N} \gamma} \right|^{-2\mu}. \end{aligned} \quad (2.8)$$

The last scaling comes from  $\rho'(x) = \mathbf{H} \left( \frac{x}{\sqrt{2}} \right)$  and the fact that the integral is finite for  $\Delta E \left( \sqrt{N} |\gamma| \right)^{-1} \rightarrow 0$ .

Integrating and exponentiating we find also the behavior of  $\mathcal{R}(\Delta E|\gamma) = \exp -\mathcal{C}(\Delta E|\gamma)$ , and, in the end, the asymptotic behavior of  $\mathcal{P}(\Delta E|\gamma)$ :

$$\begin{aligned} \mathcal{P}(\Delta E|\gamma) &\sim \\ &\sim \begin{cases} \exp \left( -\text{const} \cdot \sqrt{N} |\gamma| \left| \frac{\Delta E}{\sqrt{N} \gamma} \right|^{-2\mu+1} \right) \left| \frac{\Delta E}{\sqrt{N} \gamma} \right|^{-2\mu}, & \text{for } \mu > \frac{1}{2}, \\ \left| \frac{\Delta E}{\sqrt{N} \gamma} \right|^{-1+\text{const} \times \sqrt{N} |\gamma|}, & \text{for } \mu = \frac{1}{2}. \end{cases} \end{aligned} \quad (2.9)$$

Notice how, for  $\mu > \frac{1}{2}$ ,  $\mathcal{P}(\Delta E|\gamma)$  is a power law if  $\left( \sqrt{N} |\gamma| \right)^{1+\frac{1}{2\mu-1}} \ll |\Delta E| \ll \sqrt{N} |\gamma| \ll 1$  — the lower cutoff is given by the exponential. Therefore in this range we have

$$\mathcal{P}(\Delta E|\gamma) \sim \left| \frac{\Delta E}{\sqrt{N} \gamma} \right|^{-\tau}, \quad (2.10)$$

where the *avalanche exponent* is  $\tau \equiv 2\mu$ . For  $\mu = \frac{1}{2}$  (and small field  $\sqrt{N} |\gamma|$ ) there is a small correction to the exponent, of order  $\sqrt{N} |\gamma|$ , due to the fact that the integration of  $|\Delta E|^{-1}$  in (2.8) gives rise to logarithmic corrections. In Figure 2.4 and in Figure 2.5 are shown the plots of the probability distribution related to two different functions  $y(q)$  (corresponding to jamming and the UNSAT phase), for some small values of the field.

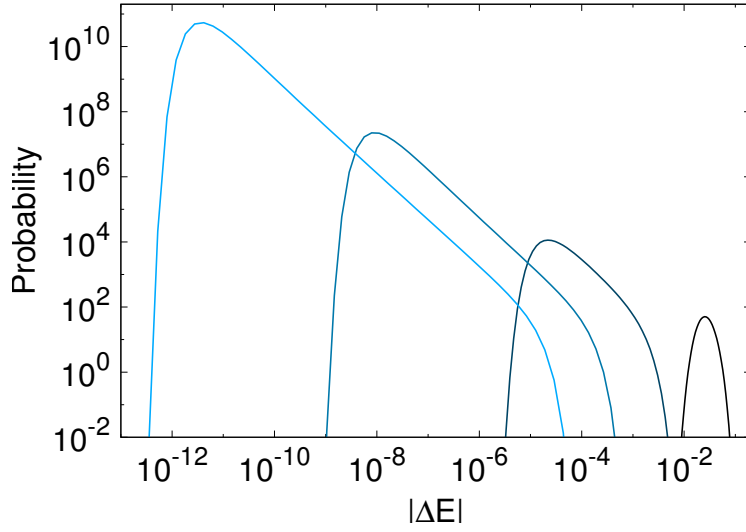


Figure 2.4: Plot of the distribution for a tentative function  $y(q)$  that diverges with an exponent  $\mu = \mu_J \approx \frac{1}{1.41}$ , for several values of the shear strain  $\gamma$  (from the left to the right, with values  $10^{-5}, 10^{-4}, 10^{-3}, 10^{-2}$ ): notice the development of the power-law region as the field is lowered.

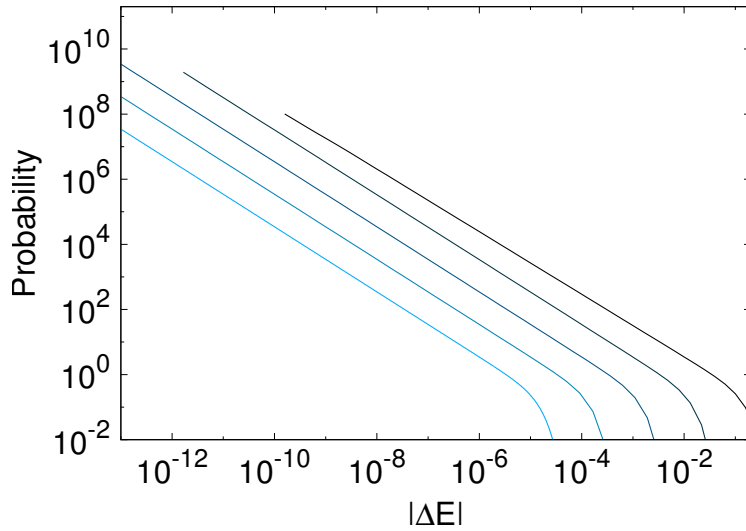


Figure 2.5: **b.** Plot for a function  $y(q)$  that diverges with  $\mu = \mu_{SK} = \mu_{UNSAT} = \frac{1}{2}$ , for several perturbations (from the left to the right, with  $\gamma = 10^{-5}, 10^{-4}, 10^{-3}, 10^{-2}, 10^{-1}$ ); here, the exponent of the power law displays minor corrections for larger field.

## Comparison with previous works

It turns out that the Sherrington-Kirkpatrick spin glass model has a Parisi function with the same zero temperature behavior as for soft spheres in the UNSAT phase: it diverges near  $q = 1$  as  $y(q) \sim (1 - q)^{-\mu_{\text{SK}}}$ ,  $\mu_{\text{SK}} = \mu_{\text{UNSAT}} = \frac{1}{2}$ . Furthermore, when the system is embedded in a magnetic field  $h$ , the variables that couple to the external field are the magnetizations: the total energy of a state is indeed  $U_\alpha - hM_\alpha$ ,  $U_\alpha$  being its intrinsic energy and  $M_\alpha$  its magnetization; the distribution of the magnetizations is independent from the states' energies and can be written as a diffusion process along the ultrametric tree [Mézard et al., 1985; Mézard and Virasoro, 1985; Mézard et al., 2008]. Therefore, as stated in *Mean-field analytical computation*, the distribution of avalanches in this system can be derived within the same framework that we used to study systems of soft spheres. We can compare then our result with [Le Doussal et al., 2012]: in that article the authors studied the static avalanches in the Sherrington-Kirkpatrick model in a magnetic field. They find via a differential equation approach based on replica symmetry breaking that the density of static avalanches  $\Delta M$  per unit  $\gamma$  in the magnetization is given by

$$\mathcal{P}(\Delta M) = \theta(\Delta M) \Delta M \int_0^1 dq y'(q) \frac{e^{-\frac{\Delta M^2}{4\pi(1-q)}}}{\sqrt{4\pi(1-q)}}. \quad (2.11)$$

If  $y(q)$  diverges, then the integral is dominated by  $q \approx 1$  and the probability of small jumps  $\Delta M$  displays a power-law behavior for small jumps, with an exponent  $\tau = 2\mu_{\text{SK}} = 1$  like for the jumps in the total energy:

$$\mathcal{P}(\Delta M) \sim \Delta M^{-1} \int_{\Delta M^2}^{\infty} dt e^{-t} \sim \Delta M^{-1}. \quad (2.12)$$

In our framework we can recover the same result starting from Equation (b.28); the detailed calculations can be found in Appendix b - *Distribution of other observables*, equations (b.44) to (b.46). In (b.28) we have computed the probability distribution  $\mathcal{P}(\Delta U, \Delta \Sigma, q|\gamma)$ , that is the joint distribution of the differences  $\Delta U, \Delta \Sigma$  in energy and stress between the unperturbed and perturbed ground states;  $q$  is their mutual overlap. If we keep only the first order in the Taylor expansion for small fields  $\gamma > 0$ , then integrate out the energy jump  $\Delta U$  and the overlap  $q$ , and divide by the field strength  $\gamma$ , we find the density of stress jumps per unit strain, a result identical to (2.11):

$$\mathcal{P}(\Delta \Sigma) \sim \Delta \Sigma^{-2\mu}. \quad (2.13)$$

Analogously, integrating out  $\Delta U$  and  $\Delta \Sigma$  and dividing by  $\gamma$  we can find the density  $\mathcal{P}(q)$  of jumps at a given overlap  $q$  (for a generic exponent  $\mu$ ):

$$\mathcal{P}(q) \sim \sqrt{\frac{1-q}{\pi}} y'(q) \sim (1-q)^{-\mu-\frac{1}{2}}. \quad (2.14)$$

In [Le Doussal et al., 2012] the authors found this result as well, that in the case of the Sherrington-Kirkpatrick model is expressed as  $\mathcal{P}(q) \sim (1-q)^{-1}$ . Since for small displacements we can link the overlap  $q$  between two configurations to their mutual mean square displacement  $\Delta^2$  via  $q \approx e^{-\Delta^2}$ , we find that the distribution of the mean square displacement found during a jump is (for small jumps and small fields)

$$\mathcal{P}(\Delta) = \mathcal{P}(q) \left| \frac{dq}{d\Delta} \right| \sim \Delta^{-2\mu}. \quad (2.15)$$

For completeness, with the same approach (expanding for small  $\gamma$ , integrating out  $\Delta \Sigma$  and  $q$ , and dividing by  $\gamma$ ), we find the density of jumps in internal energy per unit field,

$$\mathcal{P}(\Delta U) \sim \frac{1}{\gamma} \left( \frac{\Delta U}{\gamma} \right)^{-2\mu}. \quad (2.16)$$

Notice that we have to perform the Taylor expansion in order to compute these distributions, because they cannot be computed as easily as the one for the jumps in the total energy — their distribution cannot be written in a simple form as in (2.5)-(2.6). Performing the Taylor expansion we lose the lower cutoff of these probability densities, and without such cutoff, for any  $\mu \geq \frac{1}{2}$ , they would not be integrable ( $x^{-2\mu}$  is not integrable around  $x = 0$ ). The reason of this has to be ascribed to the fact that the cutoff is given by an essential singularity, which kills every power law and is not analytic; this, at least, is what happens in (2.9), where the cutoff is of the form  $e^{-Az^{-2\mu+1}}$ , for  $z = \left| \frac{\Delta E}{\sqrt{N}\gamma} \right| \ll 1$ .

## Frequency of jumps

It is interesting to discuss what is the behavior of the probability of not jumping, associated with the delta term in equation (2.5). Let us assume that the perturbing field  $\sqrt{N}|\gamma|$  scales as  $N^{-\alpha}$  for some exponent  $\alpha \geq 0$  (because we need  $\sqrt{N}|\gamma| \ll 1$  for our approach to be valid). If  $\alpha = 0$  (i.e.

$|\gamma| \sim N^{-\frac{1}{2}}$ ) then the probability of not jumping is (see (2.5)-(2.6))

$$\begin{aligned} \mathcal{P}(\Delta E = 0) = \mathcal{R}(0|\gamma) &\equiv \exp \left\{ -\sqrt{N} |\gamma| \rho(0) \int dq y'(q) \sqrt{1-q} \right\} \rightarrow \\ &\rightarrow \exp \left\{ -\text{const} \cdot \int dq y'(q) \sqrt{1-q} \right\} = 0. \end{aligned} \quad (2.17)$$

Therefore in the thermodynamic limit the system jumps with any perturbation, however small it might be. Moreover, the distribution of jumps  $\Delta E$  tends to a well defined limit, and the power-law behavior is suppressed beyond the finite region

$$(|\Delta E_{\min}|, |\Delta E_{\max}|) = \lim_{N \rightarrow \infty} \left( \left( \sqrt{N} |\gamma| \right)^{1 + \frac{1}{2\mu-1}}, \sqrt{N} |\gamma| \right). \quad (2.18)$$

In particular, in this case the typical jump is of order  $|\Delta E| \sim N^0$ .

There is, possibly, another interesting regime, that is the one that leads to a finite probability of not jumping when a small shear strain is applied, even in the thermodynamic limit  $N \rightarrow \infty$ . The zero-temperature maximum overlap between two states — the Edwards-Anderson order parameter  $q_{\text{EA}}$  — is 1 in the thermodynamic limit, and it might, in principle, scale as  $1 - \text{const} \cdot N^{-\beta}$ , with some exponent  $\beta$  (that is not known). In this case, all the diverging integrals in  $dq$  would have a cut-off at  $q_{\text{EA}}$ . If  $\sqrt{N} |\gamma|$  scales as  $N^{-\alpha}$  then the probability of not jumping becomes

$$\begin{aligned} \mathcal{P}(\Delta E = 0) = \mathcal{R}(0|\gamma) &\equiv \exp \left\{ -\sqrt{N} |\gamma| \rho(0) \int dq y'(q) \sqrt{1-q} \right\} \approx \\ &\approx \exp \left\{ -\rho(0) N^{-\alpha} \int_0^{1 - \text{const} \cdot N^{-\beta}} dq y'(q) \sqrt{1-q} \right\} \approx \\ &\approx \exp \left\{ -\text{const} \cdot N^{-\alpha} \cdot N^{\beta(\mu - \frac{1}{2})} \right\} \equiv e^{-\text{const} \cdot N^{\alpha_c - \alpha}}, \end{aligned} \quad (2.19)$$

where we have introduced the exponent  $\alpha_c \equiv \frac{1}{2}\beta(2\mu - 1)$ ; Therefore in the thermodynamic limit, if  $\sqrt{N} |\gamma| \sim N^{-\alpha}$  with  $\alpha < \alpha_c$  then  $\mathcal{P}(\Delta E = 0) \rightarrow 0$  and the systems always jumps, whereas if  $\alpha > \alpha_c$  then  $\mathcal{P}(\Delta E) \rightarrow 1$  and it never jumps. In the marginal case where  $\alpha = \alpha_c$  the probability of not jumping is finite (i.e. strictly between 0 and 1) even in the thermodynamic limit. Notice that with this scaling we find that the typical jump is naturally smaller and scales as  $|\Delta E| \sim N^{-\beta(2\mu-1)}$ . Notice that remarkably in the case of soft spheres in the UNSAT phase under shear, or in a Sherrington-Kirkpatrick model in a magnetic field,  $\alpha_c = 0$ , regardless of the value of the exponent  $\beta$ . In this case for  $\alpha > 0$  the perturbation is too small and the

system never jumps, while for  $\alpha = 0$  we find that  $\mathbb{P}(\Delta E = 0) \sim N^{-\text{const}}$  (i.e. the system always jumps, for  $N \rightarrow \infty$ ) due to logarithmic terms in the integral over  $dq$ ; in order to have a finite probability of not jumping in the UNSAT phase for  $N \rightarrow \infty$ ,  $\sqrt{N} |\gamma|$  must scale as  $(\log N)^{-1}$ .

## 2.4 Numerical simulations

In this section we are going to compare the mean-field predictions with numerical simulations in three dimensions. As stated in the previous sections, at zero temperature one finds that infinite-dimensional systems of soft spheres are characterized by different critical scalings at jamming and in the UNSAT regime. As described in [Charbonneau et al., 2014a] the jamming solution is characterized by a singular Parisi function  $y_J(q) \sim (1 - q)^{-\mu_J}$  for  $q \rightarrow 1$ . The exponent  $\mu_J$  is related to the pseudo-gap exponent  $\theta_e$  in the distribution of small contact forces at jamming (1.13), according to

$$\mu_J = \frac{3 + \theta_e}{2(2 + \theta_e)}, \quad (2.20)$$

In infinite dimensions one finds out that  $\theta_e \approx 0.42311$  and, consequently,  $\mu_J \approx 0.70634639$ . Accordingly, denoting  $\tau_J$  the value of the avalanche exponent  $\tau$  at jamming, we have  $\tau_J = 2\mu_J = \frac{3+\theta_e}{2+\theta_e} \approx 1.41269$ . On the other hand the UNSAT phase above jamming is characterized by another algebraic behavior of the Parisi function close to  $q = 1$  [Franz et al., 2017], that is  $y_{\text{UNSAT}}(q) \sim (1 - q)^{-\mu_{\text{UNSAT}}}$  with  $\mu_{\text{UNSAT}} = \frac{1}{2}$  regardless of the packing fraction. Therefore, the corresponding avalanche exponent  $\tau_{\text{UNSAT}}$  in this region is  $\tau_{\text{UNSAT}} = 2\mu_{\text{UNSAT}} = 1$ . Quite remarkably, the physics at jamming appears to be mean-field like also in low dimensions; for instance, the critical power-law distribution of small forces related to extended rearrangements does not seem to depend on the spatial dimension: numerically, one finds the same exponent  $\theta_e$  in dimensions from 2 to 12, and its value is the same as the mean-field prediction. Since  $\tau_J$  depends only on  $\theta_e$ , it is natural to wonder whether the avalanche distribution at jamming in low dimensions has also a power-law behavior, and whether the exponent (if any) coincides with the predicted value in the infinite-dimensional model.

We therefore study the distribution of quasi-static jumps in numerical simulations of systems of three-dimensional soft spheres under shear strain. We consider the standard frictionless harmonic soft sphere model with a potential

between spheres at distance  $r$

$$V(r) = \left(1 - \frac{r}{2R}\right)^2 \theta\left(1 - \frac{r}{2R}\right) \quad (2.21)$$

where  $R$  is the radius of the particles and  $\theta(x)$  is the step function. We prepare the samples either in the UNSAT phase at a specific packing fraction  $\phi$ , or at jamming, at a packing fraction  $\phi_J$  that is found numerically and varies slightly from sample to sample due to the finite size of the system (in three dimensions  $\phi_J \approx 0.64$ ). Of course in the former case we take  $\phi > \phi_J$ , in particular we simulate systems in the UNSAT phase at a packing fraction  $\phi \geq 0.75$ . The jamming configurations are found recurring to the fact that close to (above) jamming, the excess packing fraction  $\phi - \phi_J$  is proportional to the pressure  $p$  — see Chapter 1 - *Systems of spheres and jamming*. Thus, generating two UNSAT configurations at packing fractions  $\phi = 0.9, 1.0$  and minimizing their energies we find two points  $(\phi_1 = 1.0, p_1)$  and  $(\phi_2 = 0.9, p_2)$ ,  $p_{1,2}$  being the corresponding pressures. Performing a linear fit on these points we find an estimate  $(\phi_3, \tilde{p}_3 = 0)$  for the jamming point  $(\phi_J, p = 0)$ ; then, changing the radius in such a way that the system has a packing fraction  $\phi_3$ , we minimize the energy and find the pressure  $p_3$  — that in general is not exactly  $\tilde{p}_3 = 0$ . In practice we target a pressure range (usually we require that the pressure  $p \lesssim 10^{-5}$ ); if  $p_3$  is outside the target pressure range, we add it to the list of points  $(\phi_i, p_i)$  that is going to be used once again to find another estimate for the jamming point. In case  $p_i \equiv 0$  and  $\phi_i < \phi_J$ , we repeatedly replace  $\phi_i$  with  $\frac{1}{2}(\phi_i + \phi_{i-1})$  and minimize until we find a pressure  $p_i > 0$ . If the target pressure is low enough, in the end we reach configurations where the average number of contacts per particle is close to twice the space dimension  $d$  (as prescribed by the Maxwell’s isostatic condition) and  $\phi \approx 0.64$ . All the configurations (both UNSAT and at jamming) are generated via a quench from infinite temperature to zero temperature (that is, we start from random coordinates, drawn uniformly in the simulation box), and the minimizations end up all in different local minima. Every minimization is performed via a dissipative molecular dynamics, called the FIRE algorithm [Bitzek et al., 2006]; loosely speaking, we use the “Velocity Verlet” algorithm [Verlet, 1967] to discretize Newton’s equations of motion, and we add an inertial term that depends on the velocity and acceleration of the particles in the whole system; the minimization is stopped when the sum of all the forces squared is less than some threshold.

Each sample is then sheared according to the athermal quasi-static protocol, that is, the system is sheared with a small strain  $\delta\gamma$  and then a minimization is performed, letting the system relax to a local minimum; we repeat the

process until the sum of all the strain steps (called the *accumulated strain*) reaches a maximum value  $\gamma_{\max}$ . This is done because we expect the first jumps (at small shear strains) to be independent and identically distributed; finding the jamming point is usually computationally expensive and with this protocol we don't have to throw away a sample after a single step; on the other hand the accumulated strain cannot be too large, for a reason that will be explained in the next section (the so-called *yielding transition*). The simulation of a system under a shear strain in a simulation box is not entirely trivial, because we have to tilt the system's coordinates (e.g. Figure 2.2). Instead of tilting the axes and changing the coordinate system of the whole box, the shear strain can be introduced using the *Lees-Edwards boundary conditions* [Lees and Edwards, 1972; Kobayashi and Yamamoto, 2011]: to introduce such conditions, we can imagine that the whole system is divided into smaller cells, arranged on a regular cubic lattice (Figure 2.6, *left*). When a shear is imposed in the  $x_1$ - $x_2$  plane, rather than tilting each cell we can simply tilt the particles inside each cell, keeping the coordinate system orthogonal — the particles that exit a cell will enter the neighboring one. In practice we only simulate one elementary cell, endowed with suitable periodic boundary conditions: to do so we have to shift each “layer” of cells along the  $x_1$  direction (i.e. horizontally, in Figure 2.6, *right*), and the amount each cell is shifted by is proportional to the shear strain  $\delta\gamma$  and to the position of the cell along the  $x_2$  direction (say, with respect to a reference fixed cell). In order to enforce the shifting of the layers, when a particle exits the reference simulation box from the faces along the  $x_2$  direction (top and bottom faces in the figure), it has to be put back from the opposite face (as usual with periodic boundary conditions), but it has to be translated by  $\pm\delta\gamma$  along  $x_1$ ; the sign has to be different for particles crossing the top face or the bottom one, but it can be chosen freely within the simulation, because the two possible choices correspond to shearing the system towards the positive  $x_1$  direction or towards the negative one, and such a choice is physically irrelevant. The other faces are endowed with the usual periodic boundary conditions: when a particle crosses one of such faces, it is put back into the system from the opposite one. Of course, when some kind of periodic conditions are imposed on a system, the distance between two particles is not uniquely defined, because any particle has an infinite number of *images* through the periodic boundaries (Figure 2.7); we use the convention that the distance between two particles  $i, j$  is the smallest distance between  $i$  and any of the images of  $j$  (or vice-versa, equivalently).

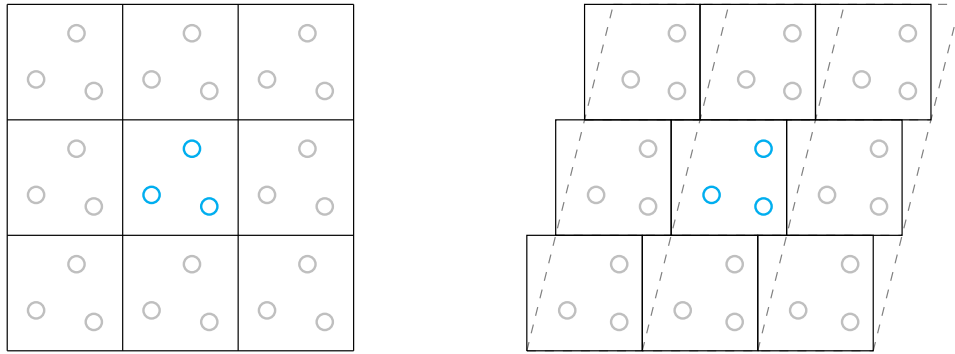


Figure 2.6: Pictorial representation of Lees-Edwards periodic boundary conditions. The red dots are all images of the same particle, in different repetitions of the periodic unit. The other colored particles are those that belonged to the same unit box before the perturbation is applied. On the right, the particles have been tilted, but the coordinate system remains orthogonal.

### Numerical results

To test our mean-field predictions in three dimensions, we simulate systems of soft spheres at various packing fractions — at jamming and in the UNSAT region ( $\phi = 0.64, 0.75, 0.8, 0.9$ ) — and for different system sizes —  $N = 500, 1000, 2000, 4000$  particles. We generate several hundreds of configurations (about 300 at jamming and 1000 at higher packing fractions) for each value of  $N$  and  $\phi$ ; then, every sample is sheared for 1000 steps with strain increment  $\delta\gamma = 10^{-5}$ , up to a maximum accumulated strain  $\gamma_{\max} = 0.01$ . We detect

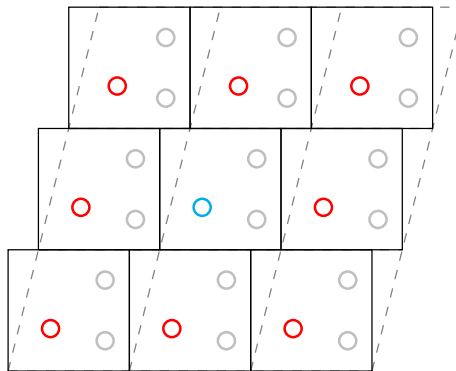


Figure 2.7: The blue particle is any particle belonging to the simulation box (that is the box in the center). The red particles are images of the blue one in different “periodic units”.

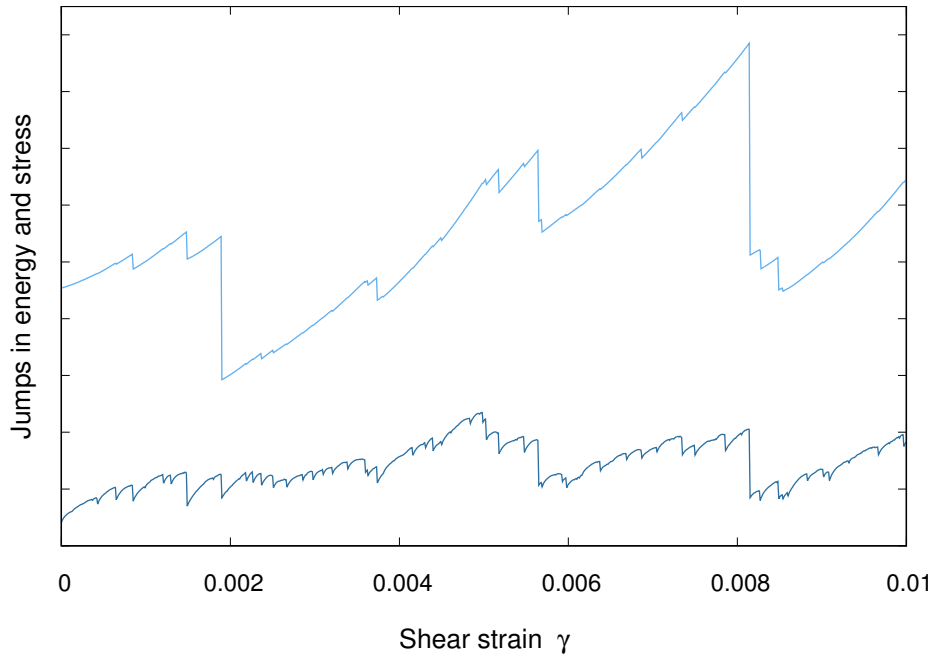


Figure 2.8: Total energy  $E$  (top, lighter curve) and stress  $\Sigma$  (bottom, darker curve) as a function of the accumulated shear strain for a system of  $N = 4000$  particles at jamming ( $\phi \approx 0.64$ ). Every step is made with  $\delta\gamma = 10^{-5}$ . We are interested in the distribution of jumps  $E_{\min}(\gamma + \delta\gamma) - E_{\min}(\gamma)$ ,  $E_{\min}(\gamma)$  being the instantaneous ground state when subject to a perturbation  $\gamma$ .

the avalanches in the systems by measuring the energy as a function of strain as in Figure 2.8; in our simulations the strain step is chosen to be  $\delta\gamma = 10^{-5}$ , and the accumulated strain at which we stop the simulation of the sample is  $\gamma_{\max} = 0.01$ ; every point in the figure corresponds to a shear strain step (after the minimization has been carried out). In order to measure the avalanche distribution we compute the energy jumps  $E_{i+1} - E_i$  from a step to the next one (adding the shear stress  $\delta\gamma\Sigma_i$  — which is always small in any case — as explained in *Spheres and shear-strain* and in Figure 2.3), and discard all the positive jumps that correspond to perturbations that did not lead to a change of state.

In Figure 2.9 we present the histogram of the energy jumps in a log-log plot, showing that a power law regime exists both at jamming and for the jammed configurations in the UNSAT phase. In Table 2.1 we compare the predicted exponents with the measured ones. The results show some agreement with the mean-field predictions; it is manifest that the exponent in the jammed

phase is smaller than the one at jamming, and that it does not depend strongly on the specific packing fraction  $\phi > \phi_J$ . Although some deviations from the theoretical, infinite-dimensional exponents (Figure 2.4-Figure 2.5) are clearly observed, we manage to somehow describe the distribution of avalanches. It is not clear whether these deviations are physical, and therefore the finite dimensional exponents are slightly different from the predicted values in infinite dimensions, or they are due to the numerics. The theoretical predictions are strictly valid for infinite dimensional systems, and even though we can argue that some properties do not vary with the dimension, there are features that surely do: for instance, in finite dimensions, there are localized excitations (the so-called bucklers) that are not captured by the mean-field description and might be responsible for the differences in the response (especially in small systems).

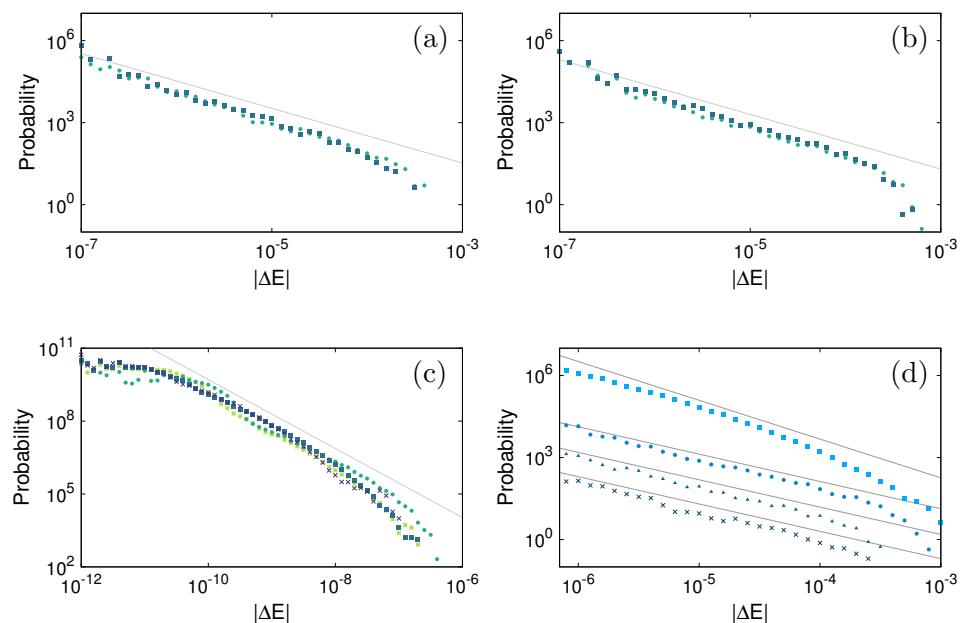


Figure 2.9: Avalanche distribution in systems of several sizes ( $N = 500, 1000, 2000, 4000$ ), with  $\delta\gamma = 10^{-5}$ . Histograms of the avalanches for systems in the UNSAT phase, prepared at packing fractions **(a)**  $\phi = 0.75$  and **(b)**  $\phi = 0.8$ . **(c)** Jamming, at  $\phi \approx 0.64$ . **(d)** Comparison of all the data: from top to bottom,  $\phi = \phi_J, 0.75, 0.8, 0.9$ . The distribution at jamming has been shifted by 4 orders of magnitude along the  $|\Delta E|$  axis, and all the histograms have been arranged vertically for a simpler comparison. The predicted power laws with  $\tau_J \approx \frac{2}{1.41} \approx 1.42$  and  $\tau_{\text{UNSAT}} = 1$  are also shown in all the plots.

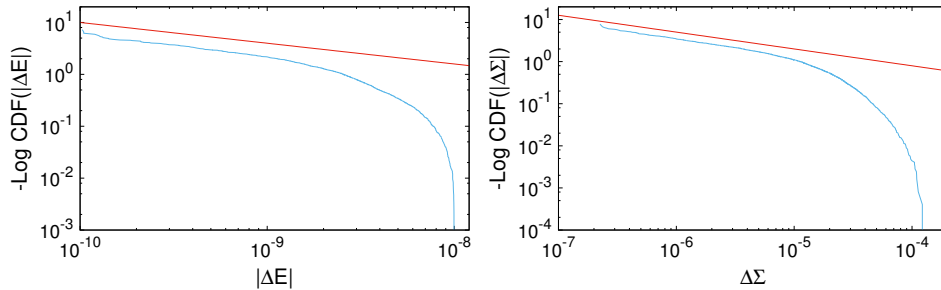


Figure 2.10: Cumulative distribution functions (CDF) for the avalanches in samples of  $N = 1024$  particles at jamming; the one on left is for the energy jumps  $\Delta E$  ( $\mathcal{P}_J^>(|\Delta E|)$ ), and the one on the right is for stress jumps  $\Delta\Sigma$  ( $\mathcal{P}_J^>(\Delta\Sigma)$ ). The predicted power laws are also shown, with an exponent  $-2\mu_J + 1 \approx -0.41269$ . These distributions have been found after removing the non power-law part for small jumps.

In Figure 2.10 we also show the cumulative distributions of jumps in the total energy  $|\Delta E|$  and stress  $\Delta\Sigma$  at jamming. Even though we only have an explicit formula for the former, we know from *Comparison with previous works* that the first term in the Taylor expansion (for small fields  $\gamma$ ) for the probability distribution function of the stress jumps has a power law behavior, and that if the exponent is smaller than  $-1$  there must be a lower cutoff (otherwise the distribution is not integrable in 0). It is plausible to assume that the cutoff is governed by a behavior similar to that found in the distribution of total energy jumps, where the cumulative distribution is  $\mathcal{P}_J^>(|\Delta E|) \equiv \text{Prob}[\text{jump} > \Delta E] \sim \exp(-\text{const} |\Delta E|^{-2\mu_J+1})$  (see equation (2.9)); therefore, we assume that the cumulative distribution of stress jumps also has a cutoff of the same form, and it behaves as  $\mathcal{P}_J^>(\Delta\Sigma) \sim \exp(-\Delta\Sigma^{-2\mu_J+1})$  — in particular, the derivative of this distribution gives the correct power law for the probability distribution function. For this reason in Figure 2.10 we plot  $-\log \mathcal{P}_J^>(|\Delta E|)$  and  $-\log \mathcal{P}_J^>(\Delta\Sigma)$

$\phi$	predicted	measured
0.64	1.42	$1.52 \pm 0.08$
0.75	1	$1.11 \pm 0.03$
0.8	1	$1.12 \pm 0.03$
0.9	1	$1.08 \pm 0.03$

Table 2.1: Comparison of predicted and measured exponents.

on a log-log scale, alongside with the predicted power laws with exponent  $-2\mu_J + 1$ .

In conclusion we have confirmed that the mean-field description is able to capture, at least with some approximation, the response of three-dimensional systems of spheres either at jamming or in the denser UNSAT phase. This is not surprising in the former phase, because we have already stated that it has been observed that, at jamming, some critical exponents do not vary with the spatial dimension, and hence are equal to the infinite-dimensional prediction. It is remarkable, on the other hand, that another critical behavior is found in the UNSAT phase, regardless of the packing fraction and characterized by an exponent close to the mean-field value. Of course it would be very interesting to study the response of similar systems also in higher dimensions, providing a stronger proof for this thesis.

There is another type of universality that arises from the comparison of the numerical study with the mean-field analytical result. In *Avalanches* we have said that, in principle, the response depends on the specific protocol with which the system is perturbed, but in the end we find a match between a static calculation (in infinite dimensions) and a quasi-static response (in three dimensions). The former assumes that the system always lies in its instantaneous ground state, at any value of the perturbation and whatever was the previous state. In the latter, instead, the system is perturbed slightly starting from a given configuration (a local minimum) and is then *locally* minimized (via a modified Newtonian dynamics): therefore, the state reached after a perturbation is not, in general, the new global instantaneous ground state, but it will reasonably be the closest local minimum found by the algorithm. As a minor remark, we have to keep in mind that the initial state found numerically, too, is *never* — for large systems — the true global ground state. This unexpected agreement had previously been observed in other systems [Le Doussal and Wiese, 2009; Le Doussal et al., 2012; Liu et al., 2016], and it has been ascribed to a universal response characterizing the slow response of some disordered systems [Liu and Dahmen, 2009]. A possible justification is found straightforwardly in our theoretical framework; the distribution of the states that defines the ultrametric tree Figure 1.4 enters into the probability density of the avalanches (2.5)-(2.6) through the derivative of the Parisi function  $y'(q)$ , that acts as a weight for the overlap  $q$  at which the new ground state is found. What allows us to compute the asymptotic power law for small external fields (2.9) is precisely the algebraic divergence of this function close to  $q = 1$ : without this divergence,

there would not be a power law. In *Replica symmetry breaking* we have introduced the Parisi function, and at zero temperature we have defined it as  $y'(q) = \frac{\partial}{\partial q} \lim_{\beta \rightarrow \infty} \beta \int_0^q d\bar{q} \mathcal{P}(\bar{q}, \beta)$ , where  $\mathcal{P}(q, \beta)$  is the distribution of the mutual overlap between any pair of states in the system. We can try and associate such a divergence near  $q = 1$  to an abundance of states close to each other (that is, at overlap  $q \approx 1$ ), that dominate the density  $\mathcal{P}(q, \beta)$  at zero temperature. With a hand-waving argument we might say that this divergence implies that it is sufficient to look at the states close to the initial one in order to capture the statistical properties of the response; moreover, we expect that the local energy landscape of a local energy minimum that is “deep enough” should not be distinguishable from the neighborhood of the “true” ground state (i.e. the deepest local minimum). Therefore, for these reasons, a local minimization should lead to a jump distribution that is not far from the true, “static” one.



# 3

## Consequences on elastic moduli

Systems compressed at or above jamming attain mechanical stability due to the extended network of contacts that form between particles (see Chapter 1, Figure 1.7). Consequently, they acquire some rigidity in the sense that above jamming they develop a finite resistance to deformations, namely finite *bulk* and *shear moduli*. The bulk modulus  $K$  is a measure of the resistance of the system to compressions and it is defined as  $K = -V \frac{dP}{dV}$ ,  $V$  being the volume and  $P$  the pressure; the shear modulus  $G$  is the susceptibility with respect to a shear strain,  $G = \frac{d\Sigma(\gamma)}{d\gamma}$ . A question that arises naturally is whether such dense amorphous systems display mechanical properties similar to those of crystalline solids. There are undoubtedly major differences between them; among the main ones is that in three dimensions the latter display a Debye distribution of soft (low energy) modes  $D(\omega) \sim \omega^2$  ( $\omega$  being the modes' frequency), whereas the former have an excess of low-energy excitations that gives rise to a so-called *boson peak* when the system is close to jamming [Wyart et al., 2005; Van Hecke, 2009; Liu and Nagel, 2010; Charbonneau et al., 2016] (see Figure 3.1). The excess soft modes are due to the marginal nature of the jamming point. This marginality is twofold: first, the mean-field theory predicts that in the whole surrounding Gardner phase there exists of

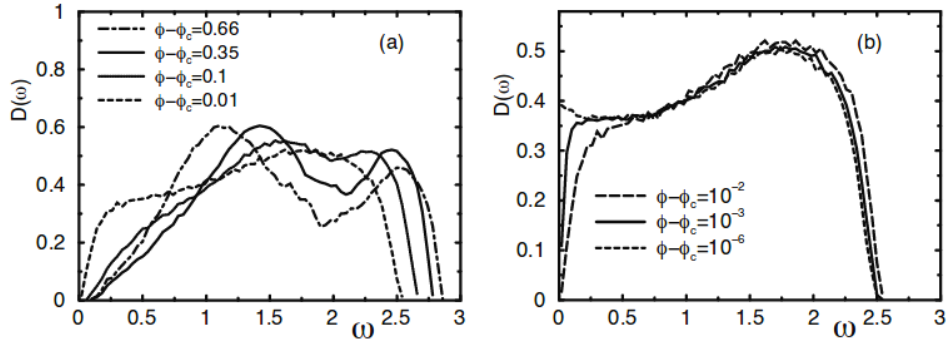


Figure 3.1: Density of states  $D(\omega)$  for systems at different packing fractions (far away from jamming on the left, and closer to jamming on the right). From [O’Hern et al., 2003].

a continuous hierarchy of states and energy levels separated by small energy barriers. Then, close to jamming there are even further soft modes due to the isostaticity of the packing [Franz et al., 2015], because tweaking a contact in the isostatic (and therefore *barely* stable) network leads to a very low-energy rearrangement.

### 3.1 Stress-strain curves

Nonetheless, the response of amorphous systems to an imposed quasi-static shear strain shares some characteristics with ordered matter. In Figure 3.2 we plot the *stress-strain curve* (dark blue curve), which shows the dependence of the shear stress  $\Sigma(\gamma)$  on the applied shear strain  $\gamma$ , increased quasi-statically; the curve has been computed averaging 200 different samples with 256 harmonic spheres, quasi-statically sheared up to an accumulated strain  $\gamma_{\max} = 0.5$  with steps  $\delta\gamma = 10^{-4}$ . This average response is qualitatively similar to that of crystals: initially they respond elastically and the shear stress  $\Sigma(\gamma)$  increases linearly with the applied strain, but at some point (called the *yielding point* or *yielding transition* [Lin et al., 2014; Dubey et al., 2016]), that for this system is found approximately at  $\gamma \approx 0.01$ , the response saturates and the shear stress becomes stationary. In ordered solids the phenomenology behind this behavior is due to the rearrangement of the dislocations in the medium, that after the yielding becomes “plastic” (i.e. irreversible) and cause the crystal to break. This, however, is not the complete description of the response of athermal amorphous systems; in Figure 3.2 the red curve is the stress-strain curve for a single sample: it has

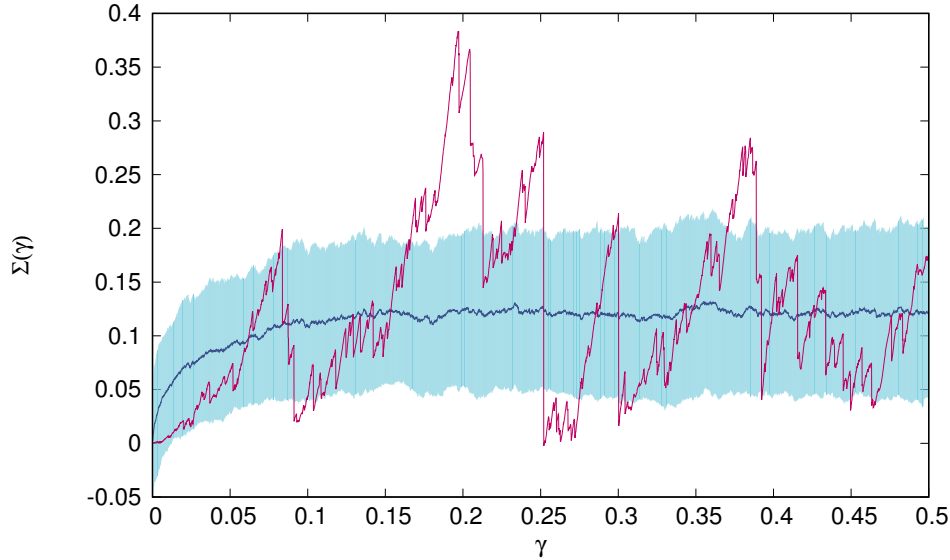


Figure 3.2: Average stress-strain curve for a system of 256 soft spheres (average over 200 samples); the shaded area shows the associated sample-to-sample variance, and superimposed is also shown the stress-strain curve of typical sample. After the yielding, the system is in the so-called *elasto-plastic* phase, because the continuous response is piecewise linear and punctuated with intermittent plastic drops in the shear stress that are, on average, larger than the avalanches found in the linear, elastic regime. Notice that the jumps shown in Figure 2.8 are computed up to an accumulated strain  $\gamma = 0.01$  and therefore correspond to the elastic region in this picture.

nothing to do with its average! It seems then that the average response of the system is not sufficient to characterize the properties of each curve, and previous works already studied whether it is even meaningful to apply the elastic theory to the average behavior of these singular systems ([Hentschel et al., 2011; Dubey et al., 2016; Biroli and Urbani, 2016]). Each point along the curve  $\Sigma(\gamma \equiv n\delta\gamma)$  corresponds to a different quasi-static step with a small strain  $\delta\gamma$ , and the discontinuities are the irreversible stress avalanches that we have been studying. If we consider a point at a specific shear strain  $\gamma$ , the point  $\Sigma(\gamma)$  along the random curve is a random variable whose statistics is given by the avalanche distribution  $\mathcal{P}(\Delta\Sigma = \Sigma(\gamma) - \Sigma(0)|\gamma)$ , with  $\Sigma(0)$  being the initial shear stress found at zero shear strain. Therefore, the expectation

value of the curve at that point  $\langle \Sigma(\gamma) \rangle$  can be written as

$$\langle \Sigma(\gamma) \rangle = \langle \Sigma(0) \rangle + \langle \Delta \Sigma | \gamma \rangle = \langle \Delta \Sigma | \gamma \rangle, \quad (3.1)$$

where we have kept into account the fact that the sample average of the initial stress  $\Sigma(0)$  is zero (as found numerically) and we have defined the average

$$\langle f(\Delta \Sigma) | \gamma \rangle \equiv \int d\Delta \Sigma \mathcal{P}(\Delta \Sigma | \gamma) f(\Delta \Sigma). \quad (3.2)$$

Strictly speaking (3.1) is valid only in the theoretical framework, where the state found at a given strain  $\gamma = n\delta\gamma$  is the true unique ground state and is thus independent of the number of steps  $n$  used to reach it. In the numerical quasi-static simulations we never find the true minimum of the total energy, and therefore we expect the state at  $\gamma = n\delta\gamma$  to depend on the number  $n$  and on the size  $\delta\gamma$  of the steps. However, in the following we assume that if  $\gamma$  and  $\delta\gamma$  are sufficiently small then we can neglect this dependence, at least in a statistical sense — i.e. in computing the average in (3.1).

The curve (3.1) is a perfectly regular functions, and as such it can be expanded in a power series with respect to the strain  $\gamma$  around zero:

$$\langle \Sigma(\gamma) \rangle \approx \gamma G_a + \frac{1}{2} \gamma^2 G_{a,2} + \frac{1}{3!} \gamma^3 G_{a,3} \cdots \quad (3.3)$$

The coefficient  $G_a$  is called the (linear) shear modulus, and all the higher order terms  $G_{a,2}$ ,  $G_{a,3}$  and so on are the nonlinear shear moduli. The “a” stands for “annealed”, since this expansion is for the sample-averaged stress-strain curve. These moduli are defined as

$$G_{a,m} = \partial_\gamma^m \langle \Sigma(\gamma) \rangle_{\gamma=0} = \partial_\gamma^m \langle \Delta \Sigma | \gamma \rangle_{\gamma=0}. \quad (3.4)$$

In particular, the linear elastic modulus  $G_a = \partial_\gamma \langle \Delta \Sigma | \gamma \rangle_{\gamma=0}$  is a finite positive quantity and it can be interpreted as the slope of the average stress-strain curve at zero strain.

## 3.2 Quenched elastic moduli

On the other hand we see that the average does not tell us all the information about the response of the system, that is actually extremely jerky and random. We have already stated in Chapter 2 - *Numerical simulations* that we expect the first jumps, those in the elastic regime at small shear strains (before yielding), to be almost independent and identically distributed — in

particular,  $\Sigma(\gamma) - \Sigma(0)$  and  $\Sigma(\gamma') - \Sigma(\gamma)$  are uncorrelated when  $\gamma' > \gamma$ . In Appendix b (equations (b.48)-(b.51)) we have computed the moments of their distribution and we have found that they scale with the strain step as

$$\langle \Delta \Sigma^k | \gamma \rangle \sim \gamma \quad (3.5)$$

for every  $k$ -th moment (with  $k \neq 0$ ). This behavior is reminiscent of a Brownian motion, where in particular the second moment scales linearly with the time interval (here represented by  $\gamma$ ); indeed, the assumption of independent jumps distributed according to the avalanche distribution is equivalent to stating that the elastic portion of the stress-strain curve is exactly a random walk with independent increments, whose distribution is slightly more complex than the Gaussian case of the Brownian motion. Keeping this analogy in mind, we can now try to study the “quenched” behavior of the stress-strain curve in a single sample. A way to do that is to define the linear and nonlinear shear moduli using limits of finite differences; for instance, we can define the quenched linear modulus as

$$G_q(\delta\gamma) \equiv \frac{\Sigma(\delta\gamma) - \Sigma(0)}{\delta\gamma}, \quad (3.6)$$

for a small strain step  $\delta\gamma$ . This is, of course, a random variable. To characterize its distribution we can compute the average and the second moment:

$$\langle G_q \rangle = \left\langle \frac{\Sigma(\delta\gamma) - \Sigma(0)}{\delta\gamma} \right\rangle, \quad (3.7)$$

$$\langle G_q^2 \rangle = \left\langle \left( \frac{\Sigma(\delta\gamma) - \Sigma(0)}{\delta\gamma} \right)^2 \right\rangle. \quad (3.8)$$

Using equation (3.5) we find the correct scaling for a small strain step  $\delta\gamma$ :

$$\langle G_q \rangle = \frac{\langle \Delta \Sigma | \delta\gamma \rangle}{\delta\gamma} \sim 1, \quad (3.9)$$

$$\langle G_q^2 \rangle = \frac{\langle \Delta \Sigma^2 | \delta\gamma \rangle}{\delta\gamma^2} \sim \delta\gamma^{-1}. \quad (3.10)$$

If we take the limit for  $\delta\gamma \rightarrow 0$  we see that the first equation tends to  $\lim \langle G_q \rangle = \partial_\gamma \langle \Sigma(\gamma) \rangle_{\gamma=0} = G_a$ , that is the annealed linear shear modulus, which is a finite quantity. The second equation, instead, tells us that the second moment diverges,  $\langle G_q^2 \rangle = \infty$ . If we recall the analogy with the Brownian motion, this result is not unexpected: it simply means that these random walks are not differentiable.

We can also study the statistics of the “quenched” nonlinear shear moduli  $G_{q,m}$ , with  $m > 1$ , that we can define as

$$G_{q,m} \equiv \delta\gamma^{-m} \sum_{n=0}^m \binom{m}{n} (-1)^{(m-n)} \Sigma(n\delta\gamma). \quad (3.11)$$

We define the quenched moduli as higher-order finite differences of the stress-strain curve, in such a way that the small  $\delta\gamma$  limit of their average can be easily calculated, yielding

$$\lim_{\delta\gamma \rightarrow 0} \langle G_{q,m} \rangle = \partial_\gamma^m \Sigma(\gamma) = G_{a,m}, \quad (3.12)$$

that is the corresponding annealed nonlinear shear modulus. Equation (3.12) comes from the fact that higher order finite differences tend to differential operators when the step is small [Milne-Thomson, 2000]. We can show that the second moment of all higher moduli diverges even faster than  $\langle G_q^2 \rangle$ ; for the purpose of proving it, let us call  $\mathcal{D}^m \Sigma(\gamma)$  the  $m$ -th order finite difference operator that appears in (3.11), namely

$$\mathcal{D}^m \Sigma(\gamma) = \sum_{n=0}^m \binom{m}{n} (-1)^{(m-n)} \Sigma(\gamma + n\delta\gamma); \quad (3.13)$$

notice that then  $G_{q,m} = \delta\gamma^{-m} \mathcal{D}^m \Sigma(0)$ . Just like for differential operators, this operator satisfies the relationship  $\mathcal{D}^{m+1} = \mathcal{D}^1 \mathcal{D}^m = \mathcal{D}^m \mathcal{D}^1$  and we can thus write

$$\begin{aligned} \langle G_{q,m}^2 \rangle &= \delta\gamma^{-2m} \langle (\mathcal{D}^m \Sigma(0))^2 \rangle = \delta\gamma^{-2m} \langle (\mathcal{D}^{m-1} \mathcal{D}^1 \Sigma(0))^2 \rangle = \\ &= \delta\gamma^{-2m} \left\langle \left[ \sum_{n=0}^{m-1} \binom{m-1}{n} (-1)^{(m-1-n)} \mathcal{D}^1 \Sigma(n\delta\gamma) \right]^2 \right\rangle. \end{aligned} \quad (3.14)$$

At this point we notice that  $\mathcal{D}^1 \Sigma(n\delta\gamma) = \Sigma((n+1)\delta\gamma) - \Sigma(n\delta\gamma) \equiv \Delta \Sigma_n$  is just an increment along the stress-strain curve; we put a subscript  $n$  to mark the fact that the differences  $\Sigma(\gamma + (n_1+1)\delta\gamma) - \Sigma(\gamma + n_1\delta\gamma)$  and  $\Sigma(\gamma + (n_2+1)\delta\gamma) - \Sigma(\gamma + n_2\delta\gamma)$  are uncorrelated when  $n_1 \neq n_2$ , because of the assumption of independence of the jumps. Then, writing explicitly the square, and separating the two contributions with identical ( $n_1 = n_2$ ) and

distinct ( $n_1 \neq n_2$ ) increments,

$$\begin{aligned}
\langle G_{q,m}^2 \rangle &= \\
&= \delta\gamma^{-2m} \left\langle \sum_{n_1, n_2=0}^{m-1} \binom{m-1}{n_1} \binom{m-1}{n_2} (-1)^{(n_1+n_2)} \Delta\Sigma_{n_1} \Delta\Sigma_{n_2} \right\rangle = \\
&= \delta\gamma^{-2m} \left\{ \sum_{n_1=0}^{m-1} \binom{m-1}{n_1}^2 \langle \Delta\Sigma_{n_1}^2 | \delta\gamma \rangle + \right. \\
&+ \left. \sum_{\substack{n_1, n_2=0 \\ n_1 \neq n_2}}^{m-1} \binom{m-1}{n_1} \binom{m-1}{n_2} (-1)^{(n_1+n_2)} \langle \Delta\Sigma_{n_1} | \delta\gamma \rangle \langle \Delta\Sigma_{n_2} | \delta\gamma \rangle \right\}. \quad (3.15)
\end{aligned}$$

We can neglect the second sum (that with  $n_1 \neq n_2$ ) because (3.5) implies that each term  $\langle \Delta\Sigma_{n_1} | \delta\gamma \rangle \langle \Delta\Sigma_{n_2} | \delta\gamma \rangle$  is of order  $\delta\gamma^2$ , while in the first sum each term  $\langle \Delta\Sigma_{n_1}^2 | \delta\gamma \rangle$  is of order  $\delta\gamma$ ; in the end,

$$\langle G_{q,m}^2 \rangle \sim \delta\gamma^{1-2m} \sum_{n_1=0}^{m-1} \binom{m-1}{n_1}^2 \sim \delta\gamma^{1-2m}; \quad (3.16)$$

this quantity diverges when  $\delta\gamma \rightarrow 0$ . Therefore we found that the variance of all quenched moduli diverges! Consequently, the annealed shear moduli are not a representative measure of the physical behavior of a single sample. This result follows directly from the fact that the stress-strain curve in the elastic regime behaves as a random walk, and we assumed that the jumps were independently distributed; the consequent result is then independent of the packing fraction of the system: the same divergence should be found either at jamming or in the surrounding marginal glass phase, where the system is always (in infinite dimensions, at least) described by a continuous replica symmetry breaking. Moreover, it has been proven in [Biroli and Urbani, 2016] that also at the Gardner transition introduced in Chapter 1 - *Systems of spheres and jamming*, where the system passes from a stable glass to the marginally stable phase with full replica symmetry breaking, the elastic response exhibits a singular behavior. At the transition they found that the averages of the shear modulus and of all the higher nonlinear moduli are finite; the variances, on the other hand, diverge in the thermodynamic limit, with the sole exception of the variance of the shear modulus  $G$ , whose fluctuations are subleading.

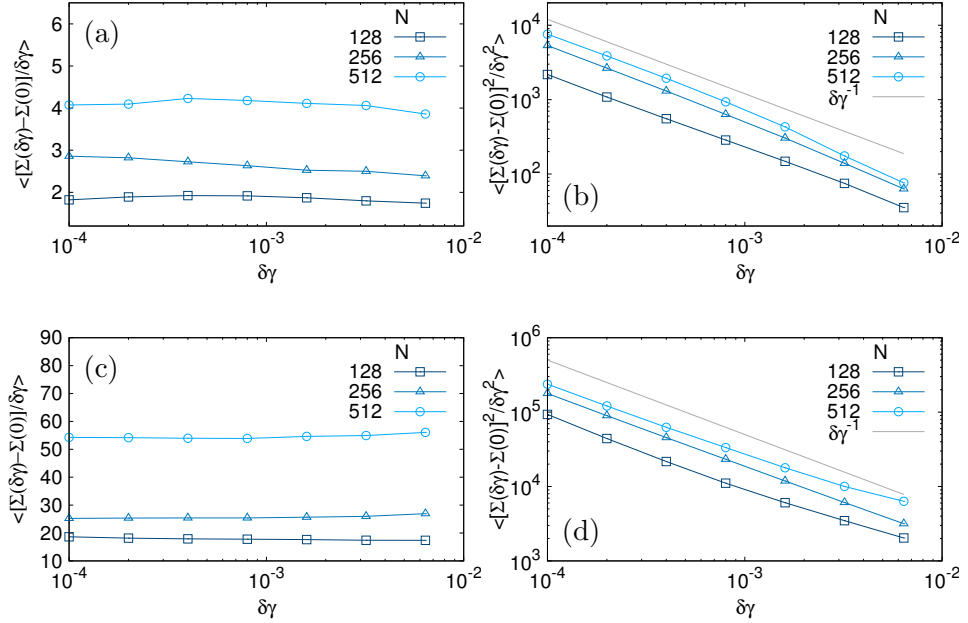


Figure 3.3: Behavior of the first two moments of the shear modulus  $G$  as a function of  $\delta\gamma$ , for different system sizes  $N = 128, 256, 512$ . The averages have been performed on the jumps of different samples found up to a maximum accumulated strain  $\gamma \approx 0.01$ . (a) and (c) show the average shear modulus (at jamming and at  $\phi = 0.75$ , respectively), that is finite in the  $\delta\gamma \rightarrow 0$  limit. (b) and (d) show the sample-to-sample variance of the shear modulus (again at jamming and at  $\phi = 0.75$ ); both diverge in the  $\delta\gamma \rightarrow 0$  limit as  $\delta\gamma^{-1}$ , as predicted. Log scale on the  $\delta\gamma$  axis in both figures; log scale on the vertical axis only in the pictures to the right.

### Numerical results

The theoretical predictions that we have shown here are, strictly speaking, only valid for infinite dimensional systems satisfying the assumption of stationarity in the elastic regime of the stress-strain curve, namely that consecutive jumps are independent and identically distributed. In order to test the validity of our results, we conclude this section with a comparison with some numerical simulations. The results are presented in Figure 3.3; in the picture we plotted both the average and the second moment of the quenched shear modulus  $G_q$ , namely  $\langle G_q \rangle$  and  $\langle G_q^2 \rangle$ , as a function of the finite strain step  $\delta\gamma$ ; comparing how these quantities scale with the step  $\delta\gamma$  allows us to extrapolate the limiting behavior. The numerical results show

that indeed the average values remain always finite even for small steps, and that the second moments diverge as  $\langle G_q^2 \rangle \sim \delta\gamma^{-1}$  in both phases, at jamming and in the UNSAT phase, as predicted.

### 3.3 Elastic moduli under different scalings

However, one has to be careful when interpreting these results. In order to properly study the elastic response of a system one should, in principle, first take the thermodynamic limit, computing the statistics of jumps at a fixed strain step  $\delta\gamma$ , and only in the end take the limit  $\delta\gamma \rightarrow 0$ . This is not what we do here; in the theoretical framework we need to assume that the perturbation is small, namely that  $\sqrt{N}\delta\gamma \ll 1$ : this assumption prevents us from taking the limit  $N \rightarrow \infty$  at a fixed strain step  $\delta\gamma$ . In the previous paragraphs we have analyzed what happens when the two limits are inverted, that is when the strain step becomes smaller and smaller while keeping constant the (finite) system size  $N$ . We can find some further insight by taking other (allowed) limits: in particular we have the instruments to study the behavior of the quenched shear moduli when both  $N \rightarrow \infty$  and  $\delta\gamma \rightarrow 0$  at the same time, with  $\sqrt{N}\delta\gamma \sim N^{-\alpha}$ ,  $\alpha \geq 0$ . We recall that we introduced this scaling in Chapter 2 - *Frequency of jumps*, when we studied the probability that the system does not jump when a strain  $\delta\gamma$  is applied. In particular, we found that the asymptotic behavior of the probability of not jumping depends on two exponents,  $\alpha$  and  $\alpha_c = \frac{1}{2}\beta(2\mu - 1)$ ;  $\mu$  is the usual exponent that governs the divergence of the Parisi function  $y(q)$ , and  $\beta$  is the tentative exponent that describes how this function scales with the system size  $N$  (its numerical value is not known). We have then argued that the probability of not jumping  $\mathcal{P}(\Delta E = 0)$  scales as

$$\mathcal{P}(\Delta E = 0) \approx e^{-\text{const} \cdot N^{\alpha_c - \alpha}}, \quad (3.17)$$

and in particular the system always jumps (in the thermodynamic limit) if  $\alpha < \alpha_c$  (“strong” perturbation), it never jumps if  $\alpha > \alpha_c$  (“weak” perturbation) and it has a finite probability non not jumping when  $\alpha = \alpha_c$ . The UNSAT case is somewhat marginal, since  $\mu = \frac{1}{2}$  and  $\alpha_c = 0$  lead to a logarithmic extra term:

$$\mathcal{P}(\Delta E = 0) \approx e^{-\text{const}_1 \cdot N^{-\alpha} \log(\text{const}_2 \cdot N)}. \quad (3.18)$$

In particular, if  $\alpha = 0$  too then  $\mathcal{P}(\Delta E = 0) \approx N^{-\text{const}}$ . (The constants appearing in the last equations depend on how the Parisi function scale with respect to  $N$  and on its behavior close to  $q = 1$ ). We will now assume that

the probability of not jumping with respect to the total energy is the same as for the shear stress:  $\mathcal{P}(\Delta E = 0) = \mathcal{P}(\Delta \Sigma = 0)$ ; this is true, because both probabilities arise from the very same term in equation (b.28) in Appendix b. The reason why we have recalled the scalings of the probability that the system does not jump is because now that  $\sqrt{N}\delta\gamma \sim N^{-\alpha}$ , the averages over jumps  $\Delta \Sigma$  should take into account a possibly large probability of not jumping; they should therefore be written as

$$\begin{aligned} \langle\langle f(\Delta \Sigma) | \delta\gamma \rangle\rangle &= \mathcal{P}(\Delta \Sigma = 0) \cdot f(0) + (1 - \mathcal{P}(\Delta \Sigma = 0)) \cdot \langle f(\Delta \Sigma) | \delta\gamma \rangle = \\ &= (1 - \mathcal{P}(\Delta \Sigma = 0)) \cdot \langle f(\Delta \Sigma) | \delta\gamma \rangle, \end{aligned} \quad (3.19)$$

where the expectations  $\langle f(\Delta \Sigma) | \delta\gamma \rangle$  is the average over the positive jumps only. We can now compute the average and second moment of the quenched linear shear modulus. Now that we are interested in the scalings with respect to the system size  $N$  we are going to define the ‘‘intensive modulus’’  $g_q$  as the shear modulus  $G_q$  normalized by  $N$ ; its first moments are

$$\langle\langle g_q \rangle\rangle \equiv N^{-1} \langle\langle G_q \rangle\rangle = \frac{\langle\langle \Delta \Sigma \rangle\rangle}{N\delta\gamma} = (1 - \mathcal{P}(\Delta \Sigma = 0)) \frac{\langle \Delta \Sigma \rangle}{N\delta\gamma}, \quad (3.20)$$

$$\langle\langle g_q^2 \rangle\rangle \equiv N^{-2} \langle\langle G_q^2 \rangle\rangle = \frac{\langle\langle \Delta \Sigma^2 \rangle\rangle}{N^2\delta\gamma^2} = (1 - \mathcal{P}(\Delta \Sigma = 0)) \frac{\langle \Delta \Sigma^2 \rangle}{N^2\delta\gamma^2}. \quad (3.21)$$

In order to get the right scalings with respect to  $N$  we also need to consider the  $N$  dependance that has been neglected in (3.5); explicitly (see equation (b.54)),

$$\langle \Delta \Sigma^k | \delta\gamma \rangle \sim N^{\frac{k+1}{2}} \delta\gamma \sim N^{\frac{k}{2}-\alpha}. \quad (3.22)$$

Plugging this scaling, the asymptotic behavior of the probability of not jumping, and the fact that  $\sqrt{N}\delta\gamma \sim N^{-\alpha}$  in equations (3.21) and (3.21) we find (for  $\alpha_c > 0$ )

$$\langle\langle g_q \rangle\rangle \sim \left(1 - e^{-\text{const} \cdot N^{\alpha_c - \alpha}}\right) \frac{N^{\frac{1}{2}-\alpha}}{N^{\frac{1}{2}-\alpha}} = 1 - e^{-\text{const} \cdot N^{\alpha_c - \alpha}}, \quad (3.23)$$

$$\langle\langle g_q^2 \rangle\rangle \sim \left(1 - e^{-\text{const} \cdot N^{\alpha_c - \alpha}}\right) \frac{N^{1-\alpha}}{N^{1-2\alpha}} = \left(1 - e^{-\text{const} \cdot N^{\alpha_c - \alpha}}\right) N^\alpha. \quad (3.24)$$

This means that when the applied perturbation is ‘‘strong’’ ( $\alpha < \alpha_c$ ), then  $\langle\langle g_q \rangle\rangle \sim 1$  is finite and the second moment  $\langle\langle g_q^2 \rangle\rangle \sim N^\alpha \rightarrow \infty$  diverges. If on the contrary the perturbation is ‘‘weak’’ ( $\alpha > \alpha_c$ ), then  $\langle\langle g_q \rangle\rangle \sim N^{\alpha_c - \alpha} \rightarrow 0$  and  $\langle\langle g_q^2 \rangle\rangle \sim N^{\alpha_c} \rightarrow \infty$ : therefore even though the system tends to jump less and less as its size increases, the second moment of the shear modulus diverges. The only case where the second moment is finite is for  $\alpha = 0$  (or equivalently when  $\delta\gamma \sim N^{-\frac{1}{2}}$ ), and then  $\langle\langle g_q \rangle\rangle \sim \langle\langle g_q^2 \rangle\rangle \sim 1$ . The only

dependence on the exponent  $\mu$  and therefore on the specific phase the system is in (namely, whether it is at jamming or in the UNSAT phase) comes from the exponent  $\alpha_c = \frac{1}{2}\beta(2\mu - 1)$ . In the UNSAT phase this exponent becomes particularly simple ( $\alpha_c = 0$ ) because  $\mu = \frac{1}{2}$ ; in this phase the probability of not jumping is described by a different asymptotic behavior, and the resulting moments for the linear shear modulus are

$$\langle\langle g_q \rangle\rangle \sim 1 - e^{-\text{const}_1 \cdot N^{-\alpha} \log(\text{const}_2 N)}, \quad (3.25)$$

$$\langle\langle g_q^2 \rangle\rangle \sim \left(1 - e^{-\text{const}_1 \cdot N^{-\alpha} \log(\text{const}_2 N)}\right) N^\alpha. \quad (3.26)$$

When  $\alpha > 0$  (that means for sufficiently small perturbations) we find that  $\langle\langle g_q \rangle\rangle \sim N^{-\alpha} \log(\text{const} \cdot N) \rightarrow 0$  and  $\langle\langle g_q^2 \rangle\rangle \sim \log(\text{const} \cdot N) \rightarrow \infty$ . When on the other hand  $\alpha = 0$  then  $\langle\langle g_q \rangle\rangle \sim \langle\langle g_q^2 \rangle\rangle \sim 1$ . All the results have been summarized in Table 3.1.

With these calculations we have shown that the elastic behavior of amorphous systems is not at all trivial in the marginal glass phase after the Gardner transition, at jamming and in the UNSAT phase. Apart from the case where  $\alpha = 0$  (regardless of  $\alpha_c$ ), the second moment of the shear modulus diverges, and therefore its mean is not representative of a typical samples' stress-strain curve. Of course all the scalings presented in Table 3.1 and derived from the mean-field theory should be studied numerically to see what is the extent of their validity. It would be extremely interesting also to see whether a finite size scaling of the response of these systems would allow the retrieval

	$\alpha < \alpha_c$	$\alpha = \alpha_c$	$\alpha > \alpha_c$
$\alpha_c > 0$	$\langle\langle g_q \rangle\rangle \sim 1$ $\langle\langle g_q^2 \rangle\rangle \sim N^\alpha$	$\langle\langle g_q \rangle\rangle \sim 1$ $\langle\langle g_q^2 \rangle\rangle \sim N^{\alpha_c}$	$\langle\langle g_q \rangle\rangle \sim N^{\alpha_c - \alpha}$ $\langle\langle g_q^2 \rangle\rangle \sim N^{\alpha_c}$
$\alpha_c = 0$	×	$\langle\langle g_q \rangle\rangle \sim 1$ $\langle\langle g_q^2 \rangle\rangle \sim 1$	$\langle\langle g_q \rangle\rangle \sim N^{-\alpha} \log(cN)$ $\langle\langle g_q^2 \rangle\rangle \sim \log(cN)$

Table 3.1: Scaling behavior for the first moments  $\langle\langle g_q \rangle\rangle$ ,  $\langle\langle g_q^2 \rangle\rangle$  of the quenched linear shear modulus, as a function of the two exponents  $\alpha, \alpha_c$ , when the system is sheared with a strain step that scales as  $\sqrt{N}\delta\gamma \sim N^{-\alpha}$ . The case  $\alpha_c = 0$  corresponds to the UNSAT phase where  $\mu = \frac{1}{2}$ , and the character  $c$  is just some constant — not necessarily equal in the two cases.

of the exponent  $\alpha_c$ , and thus of the exponent  $\beta$  that describes how the Edwards-Anderson parameter  $q_{EA}$  scales with  $N$ ,  $1 - q_{EA} \sim N^{-\beta}$ . Of course, one should compare all these results with the elastic response of system where the relevant limits have been taken in the proper order, namely  $N \rightarrow \infty$  first and then  $\delta\gamma \rightarrow 0$ .

# 4

## Reconstruction of the order parameter

Athermal mean-field disordered systems that can be described by a replica symmetry breaking ansatz are characterized by a functional order parameter, that is the Parisi function  $y(q)$ . In the previous chapters we have shown how this function governs the distribution of quasi-static avalanches at zero temperature induced by a class of perturbations, and in particular we have argued that if it diverges algebraically near  $q = 1$ , then the avalanche distribution develops a power-law behavior. This is for instance the case of infinite-dimensional dense systems of soft particles, either at jamming or in the denser UNSAT phase. The fact that the mean-field predictions are in good agreement with the finite-dimensional numerical simulations is not a general feature and it might be a peculiar property of these specific systems, that, as already suggested in previous works, seem to be mean-field-like even in low dimensions — at least at jamming. Scope of this chapter is to introduce a way to define and measure the function  $y(q)$  in numerical simulations, for an arbitrary system. Inverting the problem that we have treated in the previous sections, we will argue that it is possible to define the Parisi function via the avalanche distribution associated with a new perturbation. It is not clear to us, for the moment, whether this quantity might be meaningful for systems

that are not described within the replica symmetry breaking framework; nonetheless, this approach can be applied to any system, and the resulting tentative function  $y(q)$  might give some insights on the disordered nature of the energy landscape. In particular, we expect the result to be valid for dense systems of spheres, and an interesting application would be, for instance, to compute how the functional order parameter evolves as a function of the accumulated shear strain in a quasi-static perturbation; in particular, we would like to find the exponent  $\mu$  with which the Parisi function diverges near  $q = 1$ , for a system at or after the yielding point, that in Figure 3.2 is located approximately at  $\gamma \approx 0.02$ .

## 4.1 Mean-field framework

The zero-temperature Parisi function  $y(q)$  is defined as

$$\lim_{\beta \rightarrow \infty} \beta \int_0^q d\bar{q} \mathcal{P}(\bar{q}, \beta), \quad (4.1)$$

where  $\mathcal{P}(q, \beta)$  is the distribution of overlaps  $q$  between pairs of states: clearly, in systems with an exponentially large number of states we cannot even attempt at computing such a distribution by a direct enumeration of the energy minima. Furthermore, in finite-dimensional systems there are other complications that hinder the search for the states, such as the existence of many *metastable states* that do not exist in the mean-field counterpart. In principle, we can perturb a system in such a way that its response is described by the distribution of avalanches that we have already found; as we have shown, from such a distribution it is then possible to measure the exponent  $\mu$  that appears in the asymptotic behavior of the Parisi function close to  $q = 1$ , namely  $y'(q) \sim (1 - q)^{\mu-1}$ . In order to do so, the perturbation and the associated conjugate variable have to abide by the rules listed in Chapter 2 - *Mean-field analytical computation*: for instance, the conjugate variables have to be Gaussian distributed and independent from the energies of the states. A problem then arises when, for a generic system, it is not easy to find such a perturbation. Another issue is due to the fact that the distribution of avalanches found in (2.5)-(2.6) does not allow for a complete reconstruction of the full order parameter  $y(q)$ , but only of its exponent  $\mu$  (and only when the perturbation is small enough).

In [Franz and Parisi, 2000] the authors have found analytically the distribution of athermal, quasi-static avalanches in systems described by the replica symmetry breaking ansatz and subject to a perturbation that acts as a *repulsion* with respect to the the *ground state*: if the ground state configuration

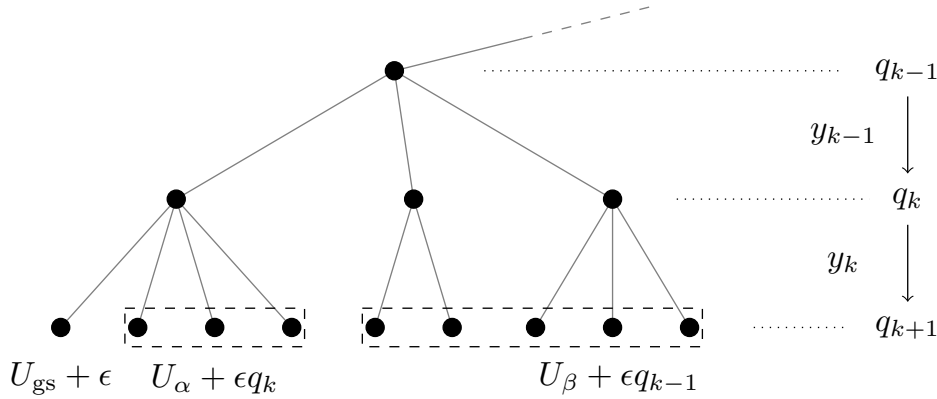


Figure 4.1: Representation of the perturbation on the ultrametric tree of the states of a system described by a replica symmetry breaking ansatz with  $k$  levels — as described in Chapter 1 - *Replica symmetry breaking* and in Appendix a, Appendix b. The leftmost leaf represents the ground state, at overlap  $q = 1$  with itself, whose perturbed energy is  $U_{\text{gs}} + \epsilon$ ,  $U_{\text{gs}}$  being its unperturbed energy. Each state  $\alpha$  in the first cluster (marked by the dashed lines) has overlap  $q_k$  with the ground state, and its energy is thus shifted by  $\epsilon q_k$ , which is smaller than  $\epsilon$ . The same holds for all the other clusters of states at a given overlap: for instance, in the next clusters, where all the states lie at overlap  $q_{k-1}$ , all the energies are shifted by  $\epsilon q_{k-1}$ . The terms  $\{y_i\}$  are the discretization of the Parisi function  $y(q)$  used to define the cascade of Poisson point processes for the distribution of the states, as in Appendix a.

is  $\underline{s}_0$ , the unperturbed energy  $\mathcal{H}(\underline{s})$  of a configuration  $\underline{s}$  is shifted by a term proportional to the overlap  $q(\underline{s}, \underline{s}_0)$  between  $\underline{s}$  and  $\underline{s}_0$ :

$$\mathcal{H}(\underline{s}) \rightarrow \mathcal{H}(\underline{s}) + \epsilon q(\underline{s}, \underline{s}_0). \quad (4.2)$$

This is a repulsion from the ground state, because the perturbation is maximum when  $q(\underline{s}, \underline{s}_0) = 1$ , which happens at  $\underline{s} = \underline{s}_0$ : therefore, the ground state is lifted by  $\epsilon$ ; all the other states, lying at a smaller overlap, are shifted by a smaller quantity (a graphical representation on the ultrametric tree is shown in Figure 4.1). To study the avalanches one has to find the new ground state when  $\epsilon \neq 0$ : equivalently, one has to find the state  $\alpha$  such that the total energy  $E_{\alpha} \equiv U_{\alpha} + \epsilon q_{\alpha}$  is minimal. With a calculation entirely based on elementary probabilistic methods, and assuming an ultrametric structure of states described by a functional order parameter  $y(q)$ , the authors have computed the probability distribution  $\mathcal{P}(\Delta E|\epsilon)$  for the difference of total

energy  $\Delta E$  between the new and unperturbed ground states. Its formula is<sup>1</sup>

$$\begin{aligned} \mathcal{P}(\Delta E|\epsilon) &= \\ &= \delta\left(\frac{\Delta E}{\epsilon} = 1\right) \epsilon^{-1} e^{-\epsilon\chi(1)} + \theta\left(\frac{\Delta E}{\epsilon} < 1\right) y\left(\frac{\Delta E}{\epsilon}\right) e^{-\epsilon\chi\left(\frac{\Delta E}{\epsilon}\right)}, \end{aligned} \quad (4.3)$$

where  $\chi(q) \equiv \int_0^q d\bar{q} y(\bar{q})$ . Let  $U_{\text{gs}}$  bet the energy of the unperturbed ground state,  $U'_{\text{gs}}$  that of the perturbed one, and let  $q$  be the overlap between them. Since  $U_{\text{gs}}$  is the ground-state energy, it is smaller than the energy of all the other states, and in particular  $U_{\text{gs}} < U'_{\text{gs}}$ . On the other hand,  $U'_{\text{gs}} + \epsilon q$  is, by definition, the total energy of the new ground state, and it is therefore smaller than the total energy of all the other states: therefore,  $U'_{\text{gs}} + \epsilon q < U_{\text{gs}} + \epsilon \times 1$ . These two inequalities imply that

$$0 < q < \frac{(U'_{\text{gs}} + \epsilon q) - (U_{\text{gs}} + 0 \times 1)}{\epsilon} \equiv \frac{\Delta E}{\epsilon} < 1, \quad (4.4)$$

where  $\Delta E \equiv U'_{\text{gs}} + \epsilon q - U_{\text{gs}}$  is the total energy difference between the two ground states. The bounds (4.4) state that  $\frac{\Delta E}{\epsilon}$  is a quantity similar to an overlap (between 0 and 1), and therefore there is no problem if it appears as an argument of the functions  $y(q)$  and  $\chi(q)$  in (4.3). The expression of the distribution simplifies a little if we define a scaling variable  $w = \frac{\Delta E}{\epsilon}$ :

$$\mathcal{P}(w|\epsilon) = \delta(w = 1) e^{-\epsilon\chi(1)} + \theta(w < 1) y(w) e^{-\epsilon\chi(w)}. \quad (4.5)$$

Notice some vague similarity with the avalanche distribution found in (2.5)-(2.6): the delta contribution corresponds to the probability that the system *does not jump* to a new ground state when the perturbation is turned on; the second term is the derivative of an exponential that depends on the functional order parameter  $y(q)$ . From (4.5) it is then possible to derive the cumulative distribution  $\mathcal{R}(w|\epsilon) \equiv \int_w^{1^+} d\bar{w} \mathcal{P}(\bar{w}|\epsilon) - 1^+$  in the extreme of integration stands to remind that we are integrating over the Dirac delta in  $w = 1$  too. This function corresponds to the function  $\mathcal{R}$  in (2.6), and its form is particularly simple:

$$\mathcal{R}(w|\epsilon) = e^{-\epsilon\chi(w)}. \quad (4.6)$$

Notice that this is the inverse cumulative function (that is, the probability that the variable is *larger* than  $w$ ): indeed,  $\mathcal{R}(0|\epsilon) = 1$ ,  $\mathcal{R}(1^-|\epsilon) \equiv \int_{1^-}^{1^+} d\bar{w} \mathcal{P}(\bar{w}|\epsilon) = e^{-\epsilon\chi(1)}$  and  $\mathcal{R}(1^+|\epsilon) \equiv \int_{1^+}^{1^+} d\bar{w} \mathcal{P}(\bar{w}|\epsilon) = 0$  — the difference

<sup>1</sup>For the sake of clarity, we are using again the notation  $\delta(A = B) \equiv \delta(A - B)$  and  $\theta(A < B) \equiv \theta(B - A)$ .

between the latter quantities being whether we include or not of the delta function in the integration.

Equation (4.6) allows us to infer the Parisi function, either from the cumulative distribution of avalanches  $\mathcal{R}(w|\epsilon)$  or from the probability distribution  $\mathcal{P}(w|\epsilon)$ ; recalling the definition of  $\chi(w)$  we have that

$$\int_0^w dq y(q) = -\frac{1}{\epsilon} \log \mathcal{R}(w|\epsilon), \quad (4.7)$$

$$y(q) = -\frac{1}{\epsilon} \partial_q \log \int_q^{1+} dw \mathcal{P}(w|\epsilon) = \frac{1}{\epsilon} \frac{\mathcal{P}(q|\epsilon)}{\int_q^{1+} dw \mathcal{P}(w|\epsilon)}. \quad (4.8)$$

Of course, the functions  $y(q)$  and  $\int_0^w dq y(q)$  in equations (4.7) and (4.8) do not depend on the value of the coupling  $\epsilon$ , even though the distributions  $\mathcal{P}(w|\epsilon)$  and  $\mathcal{R}(w|\epsilon)$  surely do.

## 4.2 Numerical simulations

The numerical simulation of this perturbation is not entirely straightforward, because computing the overlap between a given configuration and the unperturbed ground state is neither easy nor fast. In principle we would like to use the formula introduced in Chapter 1 - *Replica symmetry breaking*, namely

$$q(\underline{s}^1, \underline{s}^2) = N^{-1} \sum_{i,j=1}^N W(|\underline{s}_i^1 - \underline{s}_j^2|) \quad (4.9)$$

where  $\underline{s}^{1,2}$  are two configurations of  $N$  particles, and  $W(r)$  is a *window function* with  $W(0) = 1$  and such that it vanishes when the argument is large enough. This definition allows for a proper comparison between two configurations and, most importantly, is differentiable — if it were not differentiable, it would be much more difficult to minimize the total energy (4.2). Since its computation is quite slow, we tried using the fact that the overlap  $q$  between two configurations is approximately equal to  $1 - \Delta^2 \approx e^{-\Delta^2}$  ( $\Delta^2$  being the *mean squared displacement*) when  $q \approx 1$  and  $\Delta^2 \approx 0$ ; the computation of the mean squared displacement is much faster, therefore we used the following perturbation:

$$\mathcal{H}(\underline{s}) \rightarrow \mathcal{H}(\underline{s}) + \epsilon e^{-\Delta^2(\underline{s}, \underline{s}_0)}, \quad (4.10)$$

We then went on with the usual athermal quasi-static protocol, according to which the system is first initialized in its unperturbed ground state  $\underline{s}_0$ ,

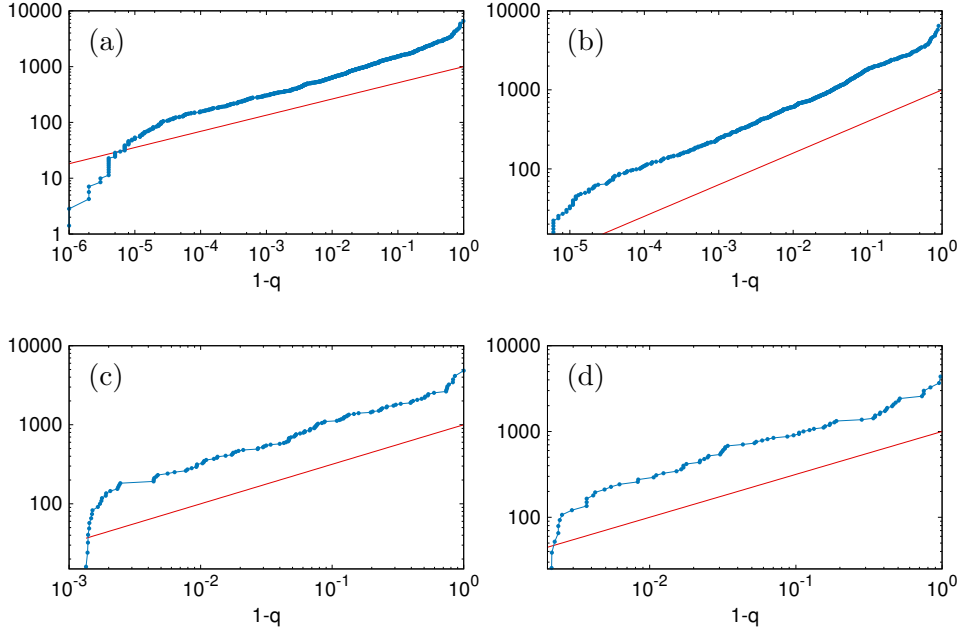


Figure 4.2: First numerical simulations for systems of  $N = 1024$  harmonic spheres at different packing fractions, with a coupling  $\epsilon = 10^{-3}$ . We plot  $-\frac{1}{\epsilon} \log [1 - \mathcal{R}(1 - q|\epsilon)] \sim q^{1-\mu}$ . The packing fractions and tentative power-law exponents are: (a)  $\phi = 0.65, \mu = 0.71$ ; (b)  $\phi = 0.65, \mu \approx 0.6$ , with an accumulated shear  $\gamma = 0.01$ , reached with steps  $\delta\gamma = 10^{-4}$ ; (c)  $\phi = 0.75, \mu = 0.5$ ; (d)  $\phi = 0.90, \mu = 0.5$ .

and then system's energy is minimized with a finite perturbation with  $\epsilon > 0$ , thus finding the new ground state.

The results of the simulations are presented in Figure 4.2, where we plot the quantity

$$\begin{aligned}
-\frac{1}{\epsilon} \log [1 - \mathcal{R}(1 - q|\epsilon)] &= -\frac{1}{\epsilon} \log \left[ 1 - \int_{1-q}^{1+} dw \mathcal{P}(w|\epsilon) \right] \approx \\
&\approx -\frac{1}{\epsilon} \log \left[ 1 - \text{const} \times \epsilon \int_{1-q}^{1+} dw y(w) \right] \approx \text{const} \times \int_{1-q}^{1+} dw y(w) \sim \\
&\sim q^{1-\mu}. \quad (4.11)
\end{aligned}$$

The first approximation comes from (4.8) for  $q \approx 1$ , since the denominator tends to  $e^{-\epsilon\chi(1)}$ ; the second one is valid for small  $\epsilon$  (we developed the logarithm in powers of  $\epsilon$ , and kept the first term only). This quantity

therefore is a measure of the integral  $\int_{1-q}^{1+} dw y(w)$ , or, alternatively, of the exponent  $\mu$ . Even with a low accuracy (due to the fact that, especially in the jammed UNSAT phase, we need many more samples, since big jumps are rare at small  $\epsilon$ ), we manage to find some agreement between the numerical results and the theoretical (mean-field) value of the exponent  $\mu$  found in previous works, namely  $\mu \approx 0.71$  at jamming and  $\mu = \frac{1}{2}$  at larger packing fractions. We find it also remarkable that systems at jamming, at an accumulated shear strain  $\gamma = 0.01$  — reached by small quasi-static steps with  $\delta\gamma = 10^{-4}$  — also display a power-law behavior in their response, with an exponent that is definitely different (it is approximately  $\mu \approx 0.6$ ). In the plots the power law does not continue down to  $q = 1$  — as it should. This could be ascribed to two different reasons (that have yet to be tested): one is a finite-size effect due to the coupling  $\epsilon$  (in (4.11) we took the limit  $\epsilon \rightarrow 0$ ); the other is the fact that the delta peak in  $q = 1$  in the cumulative distribution  $\mathcal{R}(q|\epsilon)$  is numerically smoothed out, and therefore the power-law behavior is only approximate in that region.

Unfortunately, the perturbation (4.10) does not induce the desired behavior: this is because  $q \approx e^{-\Delta^2}$  only when the mean squared displacement is small; the perturbation that we introduced destabilizes the initial ground state, and the dynamics tends to reach a configuration that has low intrinsic energy and that is furthest from it (that is, it tries maximizing the Euclidean distance between the two configurations).<sup>2</sup> The main problem lies in the fact that the proper overlap definition (4.9) is invariant under a permutation of the spheres (keeping all the positions fixed): if we compare a configuration  $\underline{s}_1$  with particles' coordinates  $(s_1, \dots, s_N)$  and another configuration  $\underline{s}_2$  whose coordinates are the same as  $\underline{s}_1$ , but shuffled, as in  $(s_{\pi(1)}, \dots, s_{\pi(N)})$  — where  $\pi$  is a permutation — then we find an overlap  $q(\underline{s}_1, \underline{s}_2) = 1$ . On the contrary, the mean squared displacement in (4.10) is not invariant under shuffling of the particles' labels, because it is computed as the sum of squared distances between corresponding particles in the two configurations: if two particles  $i$  and  $j$  are exchanged in one of the two, the Euclidean distance changes. The difference between the dynamics induced by (4.10) and by (4.2) can be understood with a one-dimensional example (see Figure 4.3). The first row in the picture shows the initial ground state of a dense packing (the red dots represent the position of the particles): in one dimension this is a regular

---

<sup>2</sup>Moreover, we simulate the spheres in a unit box with *periodic* boundary conditions, and this results in a discontinuity at the borders of the box (it is possible to avoid this issue by adding a cut-off to the term  $e^{-\Delta^2}$ , such that it decays to zero sufficiently fast when  $\Delta^2$  increases).

lattice. The former dynamics would simply translate the system, in such a way to minimize the extra term  $e^{-\Delta^2}$  and therefore maximizing the mean squared displacement  $\Delta^2$  with the initial configuration (the energy term  $\mathcal{H}(\underline{s})$  is already minimized, because the initial configuration is the ground state). Conversely, the true dynamics (4.2) does not allow such behavior. Let us assume that the initial configuration is  $\underline{s}_0$  and that  $\underline{s} \equiv \underline{s}_0 + \delta\underline{s}$  is a shifted configuration, where each particle is translated by the same amount  $\delta s_i \equiv \delta s$ ; then, the overlap  $q(\underline{s}, \underline{s}_0)$  is a periodic function of the displacement  $\delta s$ , with period the particles' diameter. The periodicity comes from the fact that the overlap does not depend on the specific order of the particles: it simply measures the amount of *similarity* between the two packings; when the displacement is equal to a particle's diameter, the two configurations end up being identical, apart from a relabeling of the particles' indices.

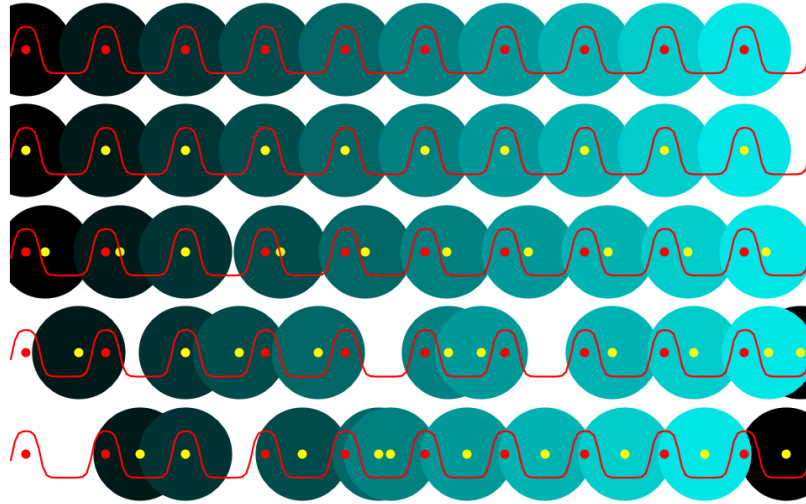


Figure 4.3: Repulsion from the ground state in one dimension. The red curve is a representation of the overlap  $q$  between the initial ground state and an identical configuration that is shifted horizontally, with a window function  $W(r) = \frac{1}{2} + \frac{1}{2} \tanh(K(a_0 - r))$ ; we have chosen  $K = 10/R$  and  $a_0 = 0.3R$ ,  $R$  being the spheres' radius. Red dots represent the initial ground state — drawn in the first row. Each of the lower rows show the new ground state (yellow dots), for different values of the coupling  $\epsilon = 10^{-2}, 1, 10^2, 10^4$ . The system is at a packing fraction  $\phi = 1.17$ .

In Figure 4.3 the red curve represent the overlap  $q(\underline{s}, \underline{s}_0)$  as a function of the displacement  $\delta s$ , for a specific choice of the window function  $W(r)$ . Each row corresponds to a different value of the coupling  $\epsilon$  (that increases from the top to the bottom), and the yellow dots are the positions of the particles in the perturbed ground state, that can be compared easily with the initial positions, marked with the red dots. In all the different samples, one of the particles (the third one, in the picture) has been quenched: this way it is simpler to observe how a configuration evolves with different perturbations. When  $\epsilon$  is small (as in the second row, where  $\epsilon = 10^{-2}$ ), the system barely moves, because the harmonic repulsion between neighboring spheres is much stronger; as  $\epsilon$  is increased the particles find new equilibrium positions. When the perturbation is strong enough to overcome the harmonic contact forces, the particles tend to “fall” into the basins defined by the potential  $\epsilon q(\underline{s}, \underline{s}_0)$ , that are the valleys of the red curve in the picture.

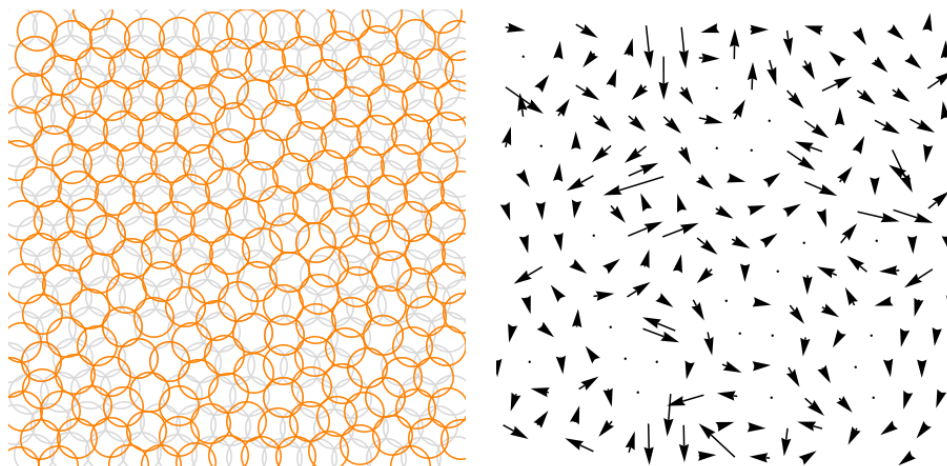


Figure 4.4: Repulsion from the ground state in two dimensions. Even though The overlap — not shown here — is still a periodic function, the particles can move in a higher dimensional space that allows for more complex displacements. The gray circles are the initial configuration, and the orange ones are the new ground state when the coupling is  $\epsilon = 10^2$ . On the right we show the displacement field between the two configurations; of course, the quenched particles did not move. The system is at a packing fraction  $\phi = 1.17$ .

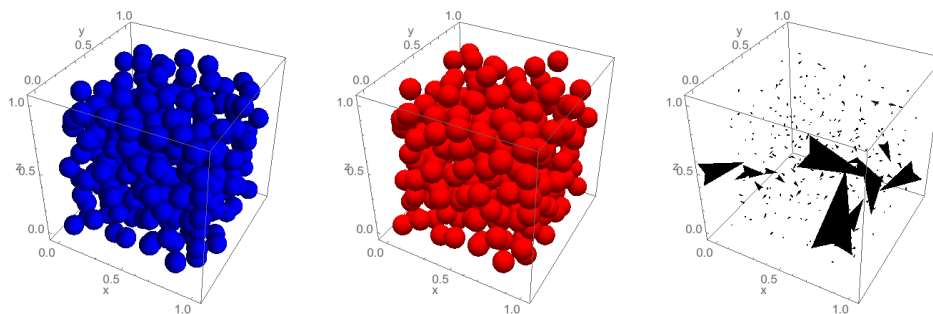


Figure 4.5: Repulsion from the ground state in three dimensions. The blue and red spheres are the initial configuration and the perturbed ground state, respectively. On the right, we show the displacement field, where the arrow size is proportional to the magnitude of the displacement.

Of course the one-dimensional example does not capture the complete nature of the jammed packings, since it is ordered. In Figure 4.4 and Figure 4.5 we present a comparison between the initial and the perturbed ground states in two- and three-dimensional systems, and we also draw the displacement field between the two configurations. In order to compute reliably the overlap between two configurations, we followed the prescription presented in [Karmakar and Parisi, 2013] according to which about 9% of the particles are quenched in space — in the two-dimensional example shown in Figure 4.4 it is easy to spot the frozen particles: they are those that did not move. The main reason to quench some particles is that otherwise the system would be invariant to translations and rotations (and not only to a relabeling of the particles' indices). Therefore, two configurations  $\underline{s}_1$  and  $\underline{s}_2$  linked by a combination of such transformations should be regarded as identical, and in particular their overlap should be  $q(\underline{s}_1, \underline{s}_2) = 1$ . The overlap (4.9), though, is not invariant, as can be deduced from the red curve in Figure 4.3. However, quenching some particles solves this issue, because it breaks the rotational and translational invariance of the system.

We still do not have enough statistics from the results of the numerical simulations for the repulsion from the ground state with quenched particles and the correct definition of the overlap (4.9). In any case, we expect to recover results similar to those presented in Figure 4.2 — perhaps with some improvements. What strikes the most in the previous simulations, where there is evidence suggesting that the perturbation did not perform as expected, is that we still managed to recover the exponents  $\mu$  predicted by the (mean-field) theory of infinite-dimensional spheres. A possible justification would be that the Parisi function  $y(q)$  is strictly related to the distribution of the states at overlap  $q$  with respect to the ground state (actually, with respect to any state), and in the systems that we studied we already know that this function diverges near  $q = 1$ . This suggests that there is a humongous number of states that are close to the initial minimum, and we might expect that numerical simulations find the closest “acceptable minimum”, whatever (non-pathological) perturbation is applied. It seems reasonable then that the distribution of such a minimum is somehow influenced by the function  $y(q)$  in a much more general setting, and when the applied perturbation is weak we can expect to be able to see some trace of its divergence.



# Conclusions

In this thesis we have re-examined the problem of avalanches in glassy disordered systems described within the framework of replica symmetry breaking. We have computed the avalanche distribution for systems perturbed by a class of perturbations that includes, for instance, the spin glass (the Sherrington-Kirkpatrick model) in a magnetic field and dense systems of soft spheres under a shear strain. We have shown how such a distribution, within the hypothesis on the external forces, depends on the specific system only through the functional order parameter that describes the replica symmetry breaking, namely the Parisi function  $y(q)$ . In particular, systems of soft spheres at jamming and in the UNSAT phase (at larger packing fractions) are characterized by different functions  $y(q)$ , and in both phases they diverge at  $q = 1$  as  $y(q) \sim (1 - q)^\mu$ , with different exponents  $\mu$ ; this divergence turns out to be governing the response of the system to a small quasi-static external driving, and for this reason the corresponding avalanche distribution develops a power-law behavior, that is therefore described by two different exponents according to the packing fraction of the system. We have then compared the infinite-dimensional predictions with three-dimensional numerical simulations of harmonic soft spheres. Rather interestingly we have found that the results are in agreement with the mean-field predictions, that is that the response displays a power-law region when the external perturbation is sufficiently small and that such a power law has different exponents when the system is at jamming or in the denser phase, where the exponent is remarkably constant. As a consequence of the properties of the avalanche distribution we have also shown that the elastic properties of these granular systems (in the linear regime) are critical at jamming and in the UNSAT phase, in the sense that all the elastic moduli have a divergent variance, and thus the average behavior of a sample is not, in general, the typical one.

The last chapter of this thesis has been devoted to the discussion of our ongoing work, where we argue that it is possible to compute the Parisi

function  $y(q)$  by measuring the avalanche statistics induced by a specific perturbation that acts as a repulsion of the states from the ground state. Ideally we would like to use this approach to compute how the Parisi function evolves when we increase the accumulated shear strain in a sheared system: in this way we could find, for instance, what is its exponent  $\mu$  at the yielding point, or even after that, in the so-called elasto-plastic phase, where the response of the system becomes stationary. This would allow us to compare our results on the avalanches with all the works that have been published in the field, for example [Maloney and Lemaitre, 2004; Fiocco et al., 2013; Arévalo and Ciamarra, 2014; Regev et al., 2015; Lin et al., 2015; Puosi et al., 2016; Leishangthem et al., 2016; Jaiswal et al., 2016].

# Appendices



# a

## Derrida-Ruelle cascades

In this appendix we describe the picture of the ergodicity breaking that emerges from the solution of mean-field disordered models described by replica symmetry breaking. At sufficiently low temperature the Gibbs measure of these systems is split in sample-dependent ergodic components, known as *pure states*. To describe the organization of the states in the phase-space we first introduce the notion of *overlap*  $q(\underline{s}^1, \underline{s}^2)$  between two configurations  $\underline{s}^1, \underline{s}^2$ : this is a *co-distance* that measures the similarity between two configurations; its absolute value is normalized between 1 and 0 (for identical and maximally different configurations, respectively). Different definitions are used for different systems: for instance, for a spin glass with  $N$  spins (e.g. the Sherrington-Kirkpatrick model) it can be defined as  $q(\underline{s}^1, \underline{s}^2) = N^{-1} \underline{s}^1 \cdot \underline{s}^2$ ; for  $N$  spheres,  $q(\underline{s}^1, \underline{s}^2) = N^{-1} \sum_{i,j=1}^N W(|\underline{s}_i^1 - \underline{s}_j^2|)$ , where  $\underline{s}_i^{1,2}$  is the position of the  $i$ -th particle in the two configurations and  $W(r)$  is a *window* function that vanishes when  $r$  is larger than some threshold and such that  $w(0) = 1$ . The specific choice is irrelevant for what follows, since proper definitions are *equivalent* [Parisi, 1998; Franz et al., 1999; Parisi and Ricci-Tersenghi, 2000; Parisi, 2002]. Then, after defining the overlap between configurations, we define the overlap between two states  $\alpha, \beta$  as the average of the overlap between configurations belonging to the two states,

$q_{\alpha\beta} = \sum_{\underline{s}^1 \in \alpha, \underline{s}^2 \in \beta} w(\underline{s}^1; \beta) w(\underline{s}^2; \beta) q(\underline{s}^1, \underline{s}^2)$ ; here  $w(\underline{s}; \beta)$  is the Boltzmann weight  $Z_J^{-1} \exp(-\beta \mathcal{H}(\underline{s}; J))$  at inverse temperature  $\beta$ , and we consider a configuration  $\underline{s}$  belonging to a state  $\alpha$  if it lies in its basin (or, operatively, if a zero temperature steepest descent dynamics brings the configuration to the minimum of the basin, called the state's *inherent structure*). A good choice as order parameter for replica symmetry breaking turns out to be the sample-averaged probability distribution of the overlap between pairs of states,  $\mathcal{P}(q, \beta) = \overline{\sum_{\alpha, \gamma} w_\alpha(\beta) w_\gamma(\beta) \delta(q - q_{\alpha\gamma})}$  [Mézard et al., 2008], where  $w_\alpha(\beta) = \frac{e^{-\beta F_\alpha}}{\sum_\gamma e^{-\beta F_\gamma}}$  is the Boltzmann weight of the state  $\alpha$ , and  $\{F_\alpha\}$  are the states' free energies; equivalently, we can consider the *Parisi function*  $\beta x(q, \beta) = \int_0^q dq \mathcal{P}(q, \beta)$ . The free energies  $\{F_\alpha\}$  of the states are in full generality the sum of an extensive, sample-independent part  $F_0$ , a subleading sample-dependent part  $\tilde{F}_0$  (that is the same for each state in a given sample) and an  $\mathcal{O}(N^0)$  state-dependent term  $f_\alpha$ . The latter are random variables whose distribution is almost universal, in the sense that it depends on the specific system only through its Parisi function  $\beta x(q, \beta)$ , and it can be defined as the suitable limit of a *hierarchical* sequence of Poisson point processes. The induced probability distribution for the normalized weights  $\{w_\alpha(\beta)\}$  is then called *Derrida-Ruelle cascade* [Mézard and Virasoro, 1985; Mézard et al., 1985, 1984b, 2008, 1984c; Ruelle, 1987; Aizenman et al., 2006; Arguin, 2007].

Before introducing the hierarchical construction, we will briefly describe the continuous Poisson point processes, restricted to the scope of our interest, with the aim of fixing a clear notation. The Poisson point process [Streit, 2010] is a probability distribution associated with a set of points  $\{f_1, \dots, f_n\}$  belonging to a suitable space, that we will assume to be the set  $\mathbb{R}$  of real numbers; an *event* is then defined as the object  $\xi = (\{f_1, \dots, f_n\}, n) \equiv (f_1, \dots, f_n; n)$ , where the  $n$  points  $\{f_i\}$  are considered unordered. The probability distribution  $\mathcal{P}(\xi)$  of a Poisson point process is parametrized by an *intensity function*  $\lambda(f)$  defined on the same space that the points  $\{f_i\}$  belong to, i.e. the reals. Then, the distribution of any event is decomposed into the product of the probability of the number  $n$  of points (that is a Poisson variable), and the conditional probability of those points:

$$\mathcal{P}_N(n) = \frac{1}{n!} \left( \int_{\mathbb{R}} df \lambda(f) \right)^n e^{-\int_{\mathbb{R}} df \lambda(f)}, \quad (\text{a.1})$$

$$\mathcal{P}_{f|N}(f_1, \dots, f_n | n) = \prod_{i=1}^n \frac{\lambda(f_i)}{\int_{\mathbb{R}} df \lambda(f)}, \quad (\text{a.2})$$

$$\begin{aligned} \mathcal{P}[\xi = (f_1, \dots, f_n; n)] &= \mathcal{P}_N(n) \mathcal{P}_{f|N}(f_1, \dots, f_n|n) = \\ &= \frac{e^{-\int_{\mathbb{R}} df \lambda(f)}}{n!} \prod_{i=1}^n \lambda(f_i). \quad (\text{a.3}) \end{aligned}$$

$\mathcal{P}_N(n)$  is the Poisson distribution for the number of points, with mean and variance  $\Lambda \equiv \int_{\mathbb{R}} df \lambda(f)$ , and  $\mathcal{P}_{f|N}(f_1, \dots, f_n|n)$  is a product of conditionally independent distributions for the value of each point. One simple calculation that will be useful in the next appendix is to compute the distribution of the minimum value  $f$  generated by a Poisson point process; this is the probability that some point has value  $f$  and that all the other points have larger values, namely<sup>1</sup>

$$\begin{aligned} \mathcal{P}_{\min}(f) &\equiv \mathbb{E} \sum_i \delta(f - f_i) \prod_{j \neq i}^{1,n} \theta(f_j > f) = \\ &= e^{-\Lambda} \sum_{n \geq 0} \frac{1}{n!} \sum_i \lambda(f) \prod_{j \neq i}^{1,n} \int_f^{\infty} df_j \lambda(f_j) = \\ &= \lambda(f) e^{-\Lambda} \sum_{n \geq 1} \frac{\left[ \int_f^{\infty} df' \lambda(f') \right]^{n-1}}{(n-1)!} = \lambda(f) e^{-\int_{-\infty}^f df' \lambda(f')}. \quad (\text{a.4}) \end{aligned}$$

Notice that  $\int_{\mathbb{R}} df \mathcal{P}_{\min}(f) = 1 - e^{-\Lambda} < 1$  if  $\Lambda < \infty$ , because with probability  $e^{-\Lambda}$  there are no points. On the other hand, there is no problem in defining a Poisson point process with  $\Lambda = \infty$ : this simply means that on average there is an infinite number of points in each realization of the process, scattered all over the space ( $\mathbb{R}$ ); indeed, this happens for the distributions of free energies in systems with replica symmetry breaking, since they have an infinite number of states. Keep in mind that if  $\Lambda = \infty$  then the integrals in (a.1)-(a.3) should be regularized in order to be finite and one can take the suitable limits after performing the calculations, for instance in (a.4). Formally, this can be done by substituting  $\lambda(f)$  with a truncated  $\tilde{\lambda}(f; c)$ , such that  $\tilde{\Lambda}(c) \equiv \int_{\mathbb{R}} df \tilde{\lambda}(f; c)$  is finite when  $c < \infty$ , and  $\lim_{c \rightarrow \infty} \tilde{\lambda}(f; c) = \lambda(f)$ , but the specific calculations need not be performed.

We are also going to need a straightforward generalization of Poisson point processes, namely *marked* Poisson point processes, that are defined by associating a random object (i.e. a *mark*, or random labels) to each point

<sup>1</sup>Throughout this book, for the sake of clarity, we use the notation  $\theta(A > B) \equiv \theta(A - B)$  and  $\theta(A < B) \equiv \theta(B - A)$ ,  $\theta(\cdot)$  being the step function.

of the underlying process. Let  $d\mu(\sigma)$  be a probability density defined on  $\mathbb{R}$ , and  $(\{f_1, \dots, f_n\}, n)$  a realization of a Poisson point process with intensity  $\lambda(f)$ ; then, we mark this realization with  $n$   $\mu$ -distributed points

$$\begin{aligned} (\{f_1, \dots, f_n\}, n) &\rightarrow (\{(f_1, \sigma_1), \dots, (f_n, \sigma_n)\}, n) \equiv \\ &\equiv (f_1, \sigma_1, \dots, f_n, \sigma_n; n). \end{aligned} \quad (\text{a.5})$$

Its probability is simply

$$\begin{aligned} \mathcal{P}[\xi = (f_1, \sigma_1, \dots, f_n, \sigma_n; n)] &= \\ &= \mathcal{P}_N(n) \mathcal{P}_{f|N}(f_1, \dots, f_n|n) \mathcal{P}_{\sigma|N}(\sigma_1, \dots, \sigma_n|n) = \\ &= \frac{e^{-\Lambda}}{n!} \prod_{i=1}^n \lambda(f_i) \mu(\sigma_i). \end{aligned} \quad (\text{a.6})$$

Noting that  $\Lambda = \int_{\mathbb{R}} df \lambda(f) = \int_{\mathbb{R}^2} df d\sigma \lambda(f) \mu(\sigma)$  ( $\mu$  is a normalized distribution), it is easy to observe that this marked Poisson point process is just a Poisson point process defined on the Cartesian product  $\mathbb{R}^2$  of the pairs  $(f, \sigma)$ , with intensity function  $\tilde{\lambda}(f, \sigma) \equiv \lambda(f) \mu(\sigma)$  (this is the essence of the *marking theorem*). We can find the distribution of the “minimum” of such a marked process, too, provided we define an order for the pairs  $(f_1, \sigma_1) < (f_2, \sigma_2)$  according to  $f_1 - \gamma\sigma_1 < f_2 - \gamma\sigma_2$  (anticipating that the  $f$ ’s are going to be the free energies and the  $\sigma$ ’s the stresses of the states, with  $\gamma$  being a shear strain). Thanks to the marking theorem, we need not redo the calculations:

$$\begin{aligned} \mathcal{P}_{\min}(f, \sigma|\gamma) &\equiv \mathcal{P}_{\min}[(f, \sigma)] = \\ &= \tilde{\lambda}(f, \sigma) e^{-\int_{\mathbb{R}^2} df' d\sigma' \theta[(f', \sigma') < (f, \sigma)] \tilde{\lambda}(f', \sigma')} \equiv \\ &\equiv \lambda(f) \mu(\sigma) e^{-\int_{\mathbb{R}^2} df' d\sigma' \theta(f' - \gamma\sigma' < f - \gamma\sigma) \lambda(f') \mu(\sigma')}. \end{aligned} \quad (\text{a.7})$$

This is the distribution of the free energy  $f$  and stress  $\sigma$  of the point  $(f, \sigma)$  that minimizes the “total energy”  $f - \gamma\sigma$ .

We will now describe the hierarchical structure of the states and the distribution of their free energies and stresses. The free energies can be generated via a stochastic branching process starting from a root reference node. It is usually described considering first a tree of finite depth  $k$ , and then taking the suitable limit for  $k \rightarrow \infty$ : the process is fully characterized by  $2k + 1$  parameters  $q_1 < \dots < q_{k+1}$ ,  $\beta x_1 < \dots < \beta x_k$  that can be thought of as a step-wise function  $\beta x(q, \beta) = y_i$  in  $(q_i, q_{i+1})$ ; the function  $y(q, \beta)$  is the Parisi function  $\beta x(q, \beta)$ , and in the limit  $k \rightarrow \infty$  it becomes continuous. For the systems that we are dealing with, the function  $\beta x(q, \beta)$  is known from

previous analytical works [Kurchan et al., 2012, 2013; Charbonneau et al., 2014a; Franz et al., 2017], and is defined as the solution to a variational problem; for large inverse temperature  $\beta$ ,  $\beta x(q, \beta) \sim y(q) + \mathcal{O}(\beta^{-1})$  where  $y(q)$  is the zero-temperature limit of  $\beta x(q, \beta)$ , which will be needed later to study the zero-temperature distribution of the states.

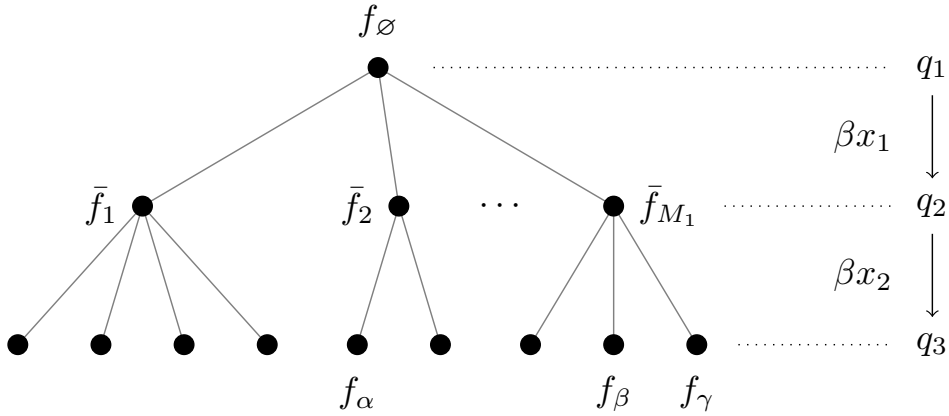


Figure a.1: A realization of the cascade of Poisson point processes for a  $k = 2$  tree; three generic states  $\alpha, \beta, \gamma$  are explicitly shown.

In order to describe the branching process, we start with an example of a system with  $k = 2$  levels of replica symmetry breaking, as in Figure a.1. We start from a reference free energy  $\bar{f}_\emptyset$ :  $\bar{f}_\emptyset$  in principle might be absorbed in the subextensive, sample dependent part of the free energy  $\tilde{F}_\alpha$ , but we prefer to keep it here as a reminder that all this distribution concerns the states of a single sample. The first level of the tree is extracted from a Poisson point process with intensity function

$$\lambda_1(\bar{f}) \equiv \lambda_1(\bar{f}_\emptyset \rightarrow \bar{f}) \equiv e^{\beta x_1(\bar{f} - \bar{f}_\emptyset)}, \quad (\text{a.8})$$

and it defines the  $M_1$  branches  $\bar{f}_\emptyset \rightarrow (\bar{f}_1, \dots, \bar{f}_{M_1}; M_1)$ . Keep in mind that this function is such that  $\Lambda_1 \equiv \int_{-\infty}^{\infty} d\bar{f} \lambda_1(\bar{f}) = \infty$ : indeed, the expected number of nodes generated at each step is infinite. Then, for each node  $\alpha_i = 1, \dots, M_1$  at the first level, we generate its sub-branch according to another Poisson point process with intensity

$$\lambda_2(\bar{f}) \equiv \lambda_2(\bar{f}_{\alpha_i} \rightarrow \bar{f}) \equiv e^{\beta x_2(\bar{f} - \bar{f}_{\alpha_i})}. \quad (\text{a.9})$$

This branch is made of the nodes  $(\bar{f}_{\alpha_i,1}, \dots, \bar{f}_{\alpha_i, M_{\alpha_i}}; M_{\alpha_i})$ ; joining all the sub-branches corresponding to different nodes  $\alpha_i$  at the first level, we have

generated the free energies  $\{\bar{f}_{\alpha_1\alpha_2}\} \equiv \{f_\alpha\}$  of all the states. We can also associate each overlap  $q_i$  to the  $i$ -th level, as shown in the figure: then, the overlap between two states (i.e. leaves) is simply the value  $q_i$  at the level of the closest common ancestor node; for instance, for the states  $\alpha, \beta, \gamma$  in Figure a.1,  $q_{\alpha\beta} = q_{\gamma\alpha} = q_1$  and  $q_{\beta\gamma} = q_2$ , while the self-overlaps are all identical to  $q_{\alpha\alpha} = q_3$  ( $q_3 \equiv q_{\text{EA}}$  is known as the Edwards-Anderson order parameter in spin glasses, and at zero temperature it becomes 1). At this point the *ultrametric* structure is manifest: it states that for any choice of the states  $\{\alpha, \beta, \gamma\}$ , the two smallest overlaps between them are equal; alternatively, one can say that the triangle with sides  $\{q_{\alpha\beta}, q_{\beta\gamma}, q_{\gamma\alpha}\}$  is always isosceles.

The general process for a tree with  $k$  levels is a straightforward iteration of the Poisson point process for all  $k$  levels; for each node  $\alpha_1 \cdots \alpha_{i-1}$  at the  $i$ -th level, with free energy  $\bar{f}_{\alpha_1 \cdots \alpha_{i-1}}$ , its sub-branch is a realization of a Poisson point process with intensity

$$\lambda_i(\bar{f}) \equiv \lambda_i(\bar{f}_{\alpha_1 \cdots \alpha_{i-1}} \rightarrow \bar{f}) \equiv e^{\beta x_i (\bar{f} - \bar{f}_{\alpha_1 \cdots \alpha_{i-1}})}. \quad (\text{a.10})$$

We label the  $M_{\alpha_1 \cdots \alpha_{i-1}}$  elements of the realization  $\alpha_1 \cdots \alpha_{i-1} \alpha_i$  (with  $\alpha_i = 1, \dots, M_{\alpha_1 \cdots \alpha_{i-1}}$ ). In the end, i.e. after generating all the nodes  $\alpha_1 \cdots \alpha_k$ , the free-energies of the states  $\{f_\alpha\} \equiv \{\bar{f}_{\alpha_1 \cdots \alpha_k}\}$  are generated as the leaves of the tree.

In the literature [Mézard et al., 1985; Mézard and Parisi, 2001; Mézard et al., 2008] this ultrametric tree is often generated via a different process. Starting from a node  $\bar{f}_\emptyset = 0$  (in order to simplify the notation), it is possible to generate  $M$  points  $\{\bar{f}_1, \dots, \bar{f}_M$  that are independent and identically distributed, with probability  $\mathcal{P}(\bar{f}) = \beta x_1 e^{\beta x_1 (\bar{f} - \bar{f}_c)} \theta(\bar{f}_c - \bar{f})$ , where  $\bar{f}_c$  is a cutoff. In the end the true distribution is found in the limit  $\bar{f}_c \rightarrow \infty$ ,  $M \rightarrow \infty$ ,  $M e^{-\beta x_1 \bar{f}_c} \rightarrow \text{const.}$  The two approaches are equivalent [Ruelle, 1987]. After defining the distribution of all the free energies  $\{f_\alpha\}$ , we can write down the distribution for the corresponding normalized Boltzmann weights,  $w_\alpha = \frac{e^{-\beta f_\alpha}}{\sum_\gamma e^{-\beta f_\gamma}}$ ; for a  $k = 1$  RSB system, the resulting distribution is a *Poisson-Dirichlet* process, and the generalization for any  $k$  is called Derrida-Ruelle probability cascade. In the literature (e.g. in [Ruelle, 1987; Panchenko and Talagrand, 2007]) it is possible to find a more detailed study of the properties of such processes; notice that often it is customary to change variables, from free-energy-like variables  $f$  to  $x = e^f$ .

When we apply a small perturbation to a system, we are introducing an additional term in the energy. If we shear a system of spheres, the free

energy of a single state is shifted as  $f_\alpha \rightarrow f_\alpha - \gamma\sigma_\alpha$ , where  $\gamma$  is the shear strain and  $\sigma_\alpha$  is an intrinsic state-dependent shear stress. The situation for a magnetic system (e.g. the Sherrington-Kirkpatrick model) in a magnetic field is similar: the magnetic field plays the role of the shear and the magnetizations correspond to the stresses. Both the Sherrington-Kirkpatrick model and the systems of spheres share the property that these conjugate variables (the stresses and magnetizations) are uncorrelated [Yoshino and Mézard, 2010] with the energy, and it can be shown [Mézard and Virasoro, 1985] that they are correlated Gaussian variables, the correlation between two different states being related to their mutual overlap only. It is possible to generate the stresses with the following *diffusion process* on the same ultrametric tree generated by the previous branching process (a.8)-(a.10): we start from some reference stress  $\bar{\Sigma}_\emptyset$  related to the sample — just like for the free energy; then, the stress  $\bar{\Sigma}_{\alpha_1 \dots \alpha_i}$  of each node  $\alpha_1 \dots \alpha_i$  in the tree is Gaussian distributed with average the stress  $\bar{\Sigma}_{\alpha_1 \dots \alpha_{i-1}}$  of its parent node and variance proportional to  $q_i - q_{i-1}$ ; its distribution is thus

$$\mu(\bar{\Sigma}_{\alpha_1 \dots \alpha_i} | \bar{\Sigma}_{\alpha_1 \dots \alpha_{i-1}}) = \frac{e^{-\frac{(\bar{\Sigma}_{\alpha_1 \dots \alpha_i} - \bar{\Sigma}_{\alpha_1 \dots \alpha_{i-1}})^2}{2N(q_i - q_{i-1})}}}{\sqrt{2\pi N(q_i - q_{i-1})}}. \quad (\text{a.11})$$

Again, we continue the process until we reach the states, located on the leaves of the tree. Notice that, since we are attaching a random variable (the stress) to each point of a realization of some Poisson point process, we can also think that the process of all the energies and stresses  $\{f_\alpha, \Sigma_\alpha\}$  in the states is a cascade of marked Poisson point processes.

In the end we, we are interested in systems with full replica symmetry breaking; to study the structure of their states we have to take the continuous limit  $k \rightarrow \infty$ . Without loss of generality we can set  $q_i = i \delta q$ , such that in the limit  $k \rightarrow \infty$  we have  $\delta q \rightarrow 0$ ,  $k\delta q \rightarrow 1$ , and  $\beta x_i \equiv \beta x(q_i) \rightarrow \beta x(q, \beta)$ .



# b

## Distribution of athermal avalanches

In this Appendix we show how to compute the exact distribution of static avalanches, via an approach based entirely on elementary probabilistic methods. Our goal is to study the static avalanches in systems of spheres under shear strain, and therefore we are going to consider only systems whose structure is given by the Derrida-Ruelle construction presented in Appendix a, namely systems with replica symmetry breaking whose response to the external perturbation is described by Gaussian distributed conjugate variables (that in the case of spheres are the states' stresses and, for instance, in the Sherrington-Kirkpatrick model in a magnetic field are the states' magnetizations).

Suppose that the system is in its unperturbed ground state. When the perturbation is turned on and set to some small value  $\gamma$ , we expect the structure of the states not to change a lot, in the sense that there are no minima that disappear and that no new minimum is created; the only effect of such a perturbation is to shift the energies by some random amount. For spheres under a shear strain  $\gamma$ , the total free energies of the states are  $F_\alpha - \gamma\Sigma_\alpha$ , with  $F_\alpha$  and  $\Sigma_\alpha$  being the free energy and stress distributed according to the processes described in Appendix a. In particular the free

energies  $\{F_\alpha\}$  of a system of  $N$  spheres are the sum of some higher order terms (that in the thermodynamic limit tend to the extensive contribution to the free energy of the system and are the same for all the states) and  $\mathcal{O}(1)$  terms  $\{f_\alpha\}$  that are in general different for each state. In this appendix we want to study the distribution of the instantaneous ground state as a function of the external field  $\gamma$ ; when comparing the total energy of two states we are only concerned with their *energy difference*: for this reason, we are going to keep only the terms  $\{f_\alpha\}$ , since  $F_\alpha - F_\beta = f_\alpha - f_\beta$  when the two states  $\alpha, \beta$  belong to the *same sample*. In order to further simplify the notation, we are going to rescale the stresses as  $\Sigma_\alpha \equiv \sqrt{N} \sigma_\alpha$ , so that the stresses' variance is independent of the system size; the dependence on  $N$  can then be absorbed into the shear strain  $\gamma$ , calling  $\tilde{\gamma} \equiv \sqrt{N} \gamma$ . Keep in mind that, in general, we might want  $\gamma$  to scale with  $N$  in the thermodynamic limit, and different scalings will give rise to different behaviors (see Chapter 2 - *Asymptotic behavior - Frequency of jumps*).

The goal of this Appendix is to compute the probability distribution of the new ground state, that is the state  $\alpha$  that minimizes the total energy  $e_\alpha \equiv u_\alpha - \tilde{\gamma} \sigma_\alpha$  among all the possible states ( $u_\alpha$  being the energy of the state, i.e. the zero-temperature free energy  $f_\alpha$ ), that are random realizations of the process described in Appendix a, taken at  $\beta \rightarrow \infty$  and thus governed by the Parisi function  $\beta x(q, \beta) \rightarrow y(q)$ . The object that we are interested in is the joint probability distribution  $\mathcal{P}_{\min}(\Delta u, \Delta \sigma, q | \tilde{\gamma})$  that the perturbed ground state (at a shear  $\tilde{\gamma}$ ) has energy  $u_{\text{gs}} + \Delta u$  and stress  $\sigma_{\text{gs}} + \Delta \sigma$ , relative to the unperturbed ground state with energy and stress  $u_{\text{gs}}, \sigma_{\text{gs}}$ , and that the overlap between the two ground states is  $q$ . We would like to compute this distribution as an average over the possible states  $\alpha$  that minimize the total energy<sup>1</sup>:

$$\begin{aligned} \mathcal{P}_{\min}(\Delta u, \Delta \sigma, q | \tilde{\gamma}) = \mathbb{E} \sum_{\alpha} \delta(u_\alpha = u_{\text{gs}} + \Delta u) \delta(\sigma_\alpha = \sigma_{\text{gs}} + \Delta \sigma) \times \\ \times \delta(q_{\alpha, \text{gs}} = q) \prod_{\beta \neq \alpha} \theta(u_\beta - \tilde{\gamma} \sigma_\beta > u_\alpha - \tilde{\gamma} \sigma_\alpha), \quad (\text{b.1}) \end{aligned}$$

In this formula  $q_{\alpha, \text{gs}}$  stands for the overlap between the state  $\alpha$  and the unperturbed ground state “gs”. The expectation is taken over the whole ultrametric tree, marked with the stresses' Gaussian process, conditional on the unperturbed ground state. The computation of this distribution is not straightforward when we want to deal with the case of arbitrary number  $k$

---

<sup>1</sup>Here we are using the following notations:  $\delta(A = B) \equiv \delta(A - B)$  and  $\theta(A > B) \equiv \theta(A - B)$ .

of RSB levels, but it is nonetheless possible to perform the calculations by exploiting the ultrametric, tree-like structure of the states.

### Introducing clusters and their joint probability

Even though in the end we want to describe systems with a continuous replica symmetry breaking, it is easier to deal with a finite number  $k$  of levels of replica symmetry breaking, and to take only in the end the limit  $k \rightarrow \infty$ . The structure of the states is then completely described by a discretized Parisi function  $y(q)$ , defined by the discrete points  $q_1, \dots, q_{k+1}$  and  $y_i \equiv y(q_i)$ . We can then partition the leaves of the ultrametric tree (that are identified with the states) into *clusters*  $\mathcal{C}_i$ , with  $i = 1, \dots, k+1$ : each cluster  $\mathcal{C}_i$  is the set of states at overlap  $q_i$  with the unperturbed ground state; by definition, the cluster  $\mathcal{C}_{k+1}$  contains only the ground state, because  $q_{k+1}$  is the overlap of a state with itself, at for  $\beta \rightarrow \infty, k \rightarrow \infty$  we will have, in the end,  $q_{k+1} \rightarrow 1$ .

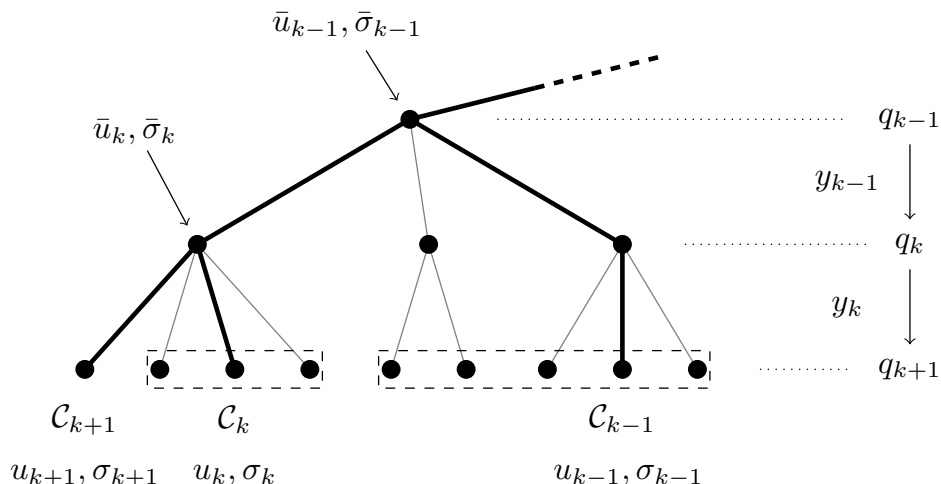


Figure b.1: A portion of an ultrametric tree for a  $k$ -RSB system. The dashed boxes enclose the  $\mathcal{C}_k$  and  $\mathcal{C}_{k-1}$  clusters; the cluster  $\mathcal{C}_{k+1}$  contains the unperturbed ground state only. The minima in each cluster are also shown, and the corresponding states can be tracked along the tree following the thick lines.

In Figure b.1 it is shown a portion of an ultrametric tree with  $k$  levels, with the first clusters explicitly shown. The original, unperturbed ground state has been put arbitrarily to the left of the picture: it is the only node in the first cluster,  $\mathcal{C}_{k+1}$ . Each cluster  $\mathcal{C}_i$  can be easily visualized as the set of nodes whose closest common ancestor node  $(\bar{u}_i, \bar{\sigma}_i)$  with the ground state lies at

overlap  $q_i$ . In this way, we can climb the ultrametric tree starting from the ground state, and for each ancestor node there will be an associated cluster spawning from it. The idea to compute the distribution (b.1) is to, first, find the conditional distribution of the *minima inside each cluster*: namely, the energies and stresses  $\{u_i, \sigma_i\}$ , such that  $u_i - \tilde{\gamma}\sigma_i$  is the minimum total energy found among the nodes in  $\mathcal{C}_i$ , conditional on the ancestor node  $(\bar{u}_i, \bar{\sigma}_i)$  of the whole cluster, at the scale  $q_i$ . In Figure b.1, for instance, the conditional ancestor nodes for the clusters  $\mathcal{C}_k$  and  $\mathcal{C}_{k-1}$  are the ones marked with  $(\bar{u}_k, \bar{\sigma}_k)$  and  $(\bar{u}_{k-1}, \bar{\sigma}_{k-1})$ , respectively. Let us call these conditional distributions for each cluster's minimum  $p_i(u_i, \sigma_i | \bar{u}_i, \bar{\sigma}_i; \tilde{\gamma})$ . Introducing these quantities, we are effectively integrating out all the nodes that are not minima inside their clusters, and in the end we are left with the *factor graph* shown in Figure b.2, where there is a single node per cluster, and a backbone of the tree that can be thought of as the thick lines in Figure b.1. We call it a factor graph because, when integrated over the intermediate (ancestor) nodes  $\{\bar{u}_i, \bar{\sigma}_i\}$ , it represents the joint distribution  $\mathcal{P}_{\text{cluster}}[\{\underline{u}, \underline{\sigma}\} | \tilde{\gamma}]$  of the minima in all the clusters. Indeed:

$$\begin{aligned} \mathcal{P}_{\text{cluster}}[\{\underline{u}, \underline{\sigma}\} | \tilde{\gamma}; \bar{u}_\emptyset, \bar{\sigma}_\emptyset] &= \int \left[ \prod_{i=2}^{k+1} d\bar{u}_i d\bar{\sigma}_i \right] \times \\ &\times \left[ \prod_{i=1}^k \tilde{\lambda}_i[(\bar{u}_i, \bar{\sigma}_i) \rightarrow (\bar{u}_{i+1}, \bar{\sigma}_{i+1})] \right] \left[ \prod_{i=1}^{k+1} p_i(u_i, \sigma_i | \bar{u}_i, \bar{\sigma}_i; \tilde{\gamma}) \right], \quad (\text{b.2}) \end{aligned}$$

Notice that the the first product starts from  $i = 2$ , because the ancestor node  $(\bar{u}_1, \bar{\sigma}_1)$  is the reference root node of the tree (see Appendix a): it depends on the specific sample, but it is not, in principle, Poisson distributed. In the following, when it will be important to distinguish this term from the other ancestor variables over which we are integrating, we will call its variables  $\bar{u}_\emptyset$  and  $\bar{\sigma}_\emptyset$  for the sake of clarity. Of course, this means that the whole probability distribution  $\mathcal{P}_{\text{cluster}}$  depends on such variables, and this is why we have written the explicit dependence in  $\mathcal{P}_{\text{cluster}}[\{\underline{u}, \underline{\sigma}\} | \tilde{\gamma}; \bar{u}_\emptyset, \bar{\sigma}_\emptyset]$ .

The functions  $\tilde{\lambda}_i$  that appear in (b.2) are the intensity functions that completely define the *marked* Poisson point processes for the branching at each level. The intensity  $\tilde{\lambda}_i[(\bar{u}_i, \bar{\sigma}_i) \rightarrow (\bar{u}_{i+1}, \bar{\sigma}_{i+1})]$  can also be interpreted as exactly the probability that, among the points of the Poisson point process, there is at least one branch going from the ancestor node  $(\bar{u}_i, \bar{\sigma}_i)$  to the

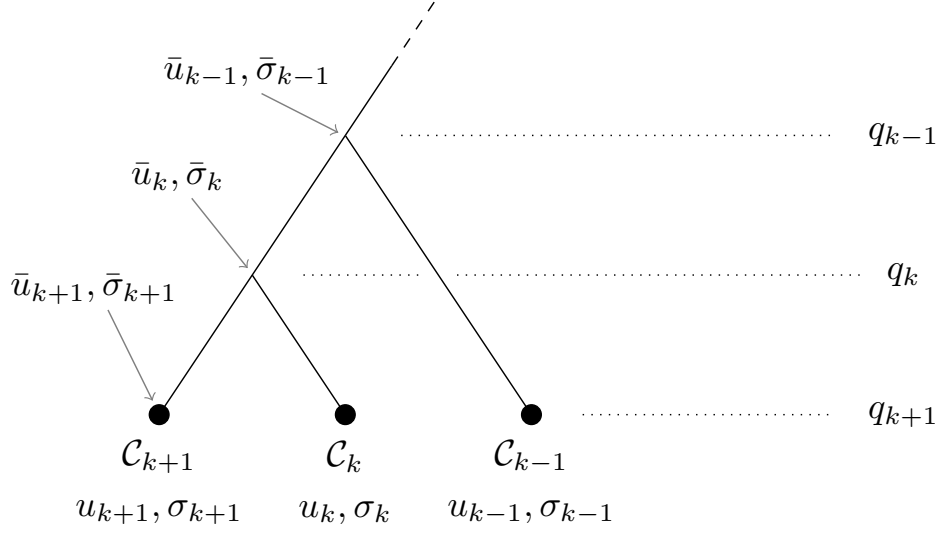


Figure b.2: The tree after the integration of the states that are not minima of any cluster, leaving only the relevant branches (thick ones in Figure b.1 left); this tree can be thought of as the factor graph of the joint probability  $\mathcal{P}_{\text{cluster}}[\{\underline{u}, \underline{\sigma}\} | \tilde{\gamma}]$  of the minima in each cluster.

ancestor node  $(\bar{u}_{i+1}, \bar{\sigma}_{i+1})$ :

$$\begin{aligned} \tilde{\lambda}_i [(\bar{u}_i, \bar{\sigma}_i) \rightarrow (\bar{u}_{i+1}, \bar{\sigma}_{i+1})] &\equiv \lambda_i(\bar{u}_i \rightarrow \bar{u}_{i+1}) \mu(\bar{\sigma}_i \rightarrow \bar{\sigma}_{i+1}) = \\ &= e^{y_i(\bar{u}_{i+1} - \bar{u}_i)} \frac{e^{-\frac{(\bar{\sigma}_{i+1} - \bar{\sigma}_i)^2}{2\Delta q}}}{\sqrt{2\pi\Delta q}}. \end{aligned} \quad (\text{b.3})$$

(Without loss of generality, we have chosen  $q_{i+1} - q_i \equiv \Delta q$  for all levels; compare this formula with (a.10)-(a.11)).

### Distribution of the minimum in a cluster

Let us assume that all the backbone in Figure b.2 has been generated, sampling from the product of the distributions  $\tilde{\lambda}_i$  in (b.2). At this point we have to find an expression for the distributions  $p_i$ , conditional on the ancestor nodes in the backbone. The probability of the minimum inside  $\mathcal{C}_{k+1}$  is trivial, since such a cluster contains only one state:

$$p_{k+1}(u_i, \sigma_i | \bar{u}_i, \bar{\sigma}_i; \tilde{\gamma}) = \delta(u_i - \bar{u}_i) \delta(\sigma_i - \bar{\sigma}_i). \quad (\text{b.4})$$

In Figure b.1 we see that the clusters are somehow self-similar, in the sense that a cluster  $\mathcal{C}_i$  is the union of several (infinite, actually) subclusters that

are statistically equivalent to the cluster  $\mathcal{C}_{i+1}$ .<sup>2</sup>

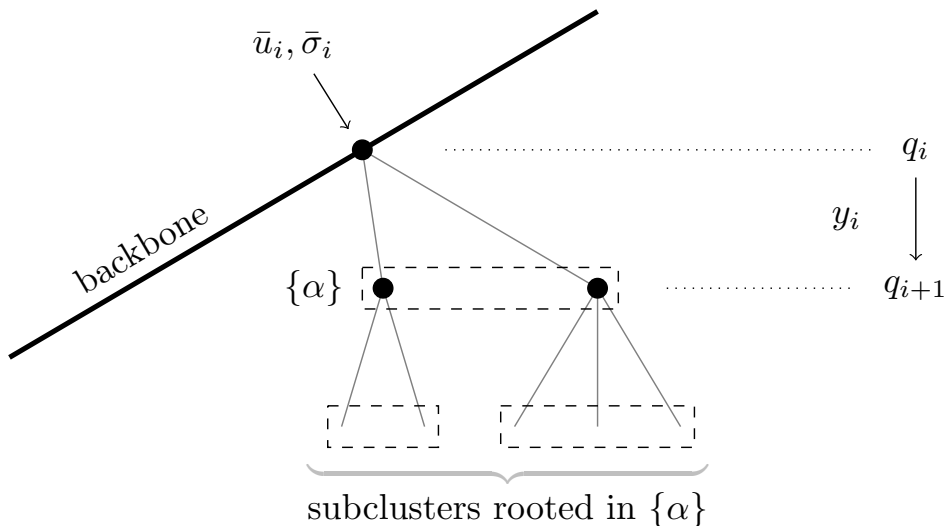


Figure b.3: The initial (near  $q_i$ ) part of cluster  $\mathcal{C}_i$ . The first level generated from the associated Poisson point process with intensity function  $\lambda_i$  is the set of nodes  $\{\alpha\}$ , and from each node  $\alpha$  there is a subcluster that is statistically equivalent to the cluster  $\mathcal{C}_{i+1}$ .

Let us consider the cluster  $\mathcal{C}_i$ , shown in some detail in Figure b.3, sprouting from the backbone of the factor graph. The first level of its descendent nodes, called  $\{\alpha\}$  in what follows, has been generated with a Poisson point process with intensity function  $\tilde{\lambda}_i [(\bar{u}_i, \bar{\sigma}_i) \rightarrow (\bar{u}_\alpha, \bar{\sigma}_\alpha)]$ . The subclusters rooted in each node  $\alpha$  are statistically equivalent to the cluster  $\mathcal{C}_{i+1}$ , since the corresponding cascades of Poisson point processes have the same intensities at each level. For this reason we can proceed recursively, the main idea being that the minimum of  $\mathcal{C}_i$  has to be the minimum of one of the smaller subclusters equivalent to  $\mathcal{C}_{i+1}$ . Given the distribution  $p_{i+1}$  of the minimum in  $\mathcal{C}_{i+1}$ , we can write

<sup>2</sup>Strictly speaking, the statistical equivalence only holds if the average number of branches sprouting from a node is infinite, which is the case here since  $\int du \lambda_i(u) = \infty$  — see Appendix a. If the number of child nodes were finite, than one would need be more careful, because one of the branches of the cluster  $\mathcal{C}_i$  belongs to the backbone in Figure b.1 and in Figure b.3.

$$\begin{aligned}
p_i(u, \sigma | \bar{u}_i, \bar{\sigma}_i; \tilde{\gamma}; \{\bar{u}_\alpha, \bar{\sigma}_\alpha\}, M) &= \sum_{\alpha=1}^M p_{i+1}(u, \sigma | \bar{u}_\alpha, \bar{\sigma}_\alpha; \tilde{\gamma}) \times \\
&\times \prod_{\substack{\beta=1 \\ \beta \neq \alpha}}^M \int du' d\sigma' p_{i+1}(u', \sigma' | \bar{u}_\beta, \bar{\sigma}_\beta; \tilde{\gamma}) \theta(u' - \tilde{\gamma}\sigma' > u - \tilde{\gamma}\sigma). \quad (\text{b.5})
\end{aligned}$$

The meaning of this formula is that we are looking for the probability that  $(u, \sigma)$  is the minimum of a subcluster rooted in some node  $\alpha$  (this is what  $p_{i+1}$  is there for), with the constraint that the minimum in any other subcluster has larger total energy. The distribution is conditional on the realization  $(\{\bar{u}_\alpha, \bar{\sigma}_\alpha\}, M)$  of the first Poisson point process spawned from  $(\bar{u}_i, \bar{\sigma}_i)$  ( $M$  stands for the number of points in the set). Next, we take the expectation over such a marked branching process:

$$p_i(u, \sigma | \bar{u}_i, \bar{\sigma}_i; \tilde{\gamma}) \equiv \mathbb{E}_{\{\bar{u}_\alpha, \bar{\sigma}_\alpha\}, M} p_i(u, \sigma | \bar{u}_i, \bar{\sigma}_i; \tilde{\gamma}; \{\bar{u}_\alpha, \bar{\sigma}_\alpha\}, M). \quad (\text{b.6})$$

Using equation (a.3) we can easily show that equation (b.5) can be cast as

$$\begin{aligned}
p_i(u, \sigma | \bar{u}_i, \bar{\sigma}_i; \tilde{\gamma}) &= \hat{p}_i(u, \sigma | \bar{u}_i, \bar{\sigma}_i; \tilde{\gamma}) \times \\
&\times \exp \left[ - \int du' d\sigma' \hat{p}_i(u', \sigma' | \bar{u}_i, \bar{\sigma}_i; \tilde{\gamma}) \theta(u' - \tilde{\gamma}\sigma' < u - \tilde{\gamma}\sigma) \right], \quad (\text{b.7})
\end{aligned}$$

where

$$\begin{aligned}
\hat{p}_i(u, \sigma | \bar{u}_i, \bar{\sigma}_i; \tilde{\gamma}) &= \\
&\int d\bar{u}_{i+1} d\bar{\sigma}_{i+1} \tilde{\lambda}_i [(\bar{u}_i, \bar{\sigma}_i) \rightarrow (\bar{u}_{i+1}, \bar{\sigma}_{i+1})] p_{i+1}(u, \sigma | \bar{u}_{i+1}, \bar{\sigma}_{i+1}). \quad (\text{b.8})
\end{aligned}$$

Compare these formulae with (a.7) in Appendix a: the distribution of the minimum in the cluster has the same form, but in this case the corresponding intensity function, instead of being  $\tilde{\lambda}_i = \lambda_i \mu_i$ , is the average of  $\tilde{\lambda}_i$  weighted with  $p_{i+1}$ .

Luckily, this recursion on the distributions  $\{p, \hat{p}\}$  can be solved exactly, because the functions  $\lambda, \mu$  are simple exponentials and Gaussian distributions. The following results can be proven by induction starting from  $p_{k+1}$  (defined in (b.4)):

$$\begin{aligned}
p_i(u_i, \sigma_i | \bar{u}_i, \bar{\sigma}_i; \tilde{\gamma}) &= \\
&= \hat{p}_i(u_i, \sigma_i | \bar{u}_i, \bar{\sigma}_i; \tilde{\gamma}) \exp \left[ - \frac{c_i}{y_i} e^{y_i(u_i - \bar{u}_i - \tilde{\gamma}(\sigma_i - \bar{\sigma}_i))} \right], \quad (\text{b.9})
\end{aligned}$$

and

$$\begin{aligned} \hat{p}_i(u_i, \sigma_i | \bar{u}_i, \bar{\sigma}_i; \tilde{\gamma}) &= \\ &= c_i \exp \left[ y_i(u_i - \bar{u}_i) - \frac{(\sigma_i - \bar{\sigma}_i)^2}{2(k+1-i)\Delta q} + \tilde{\gamma} f_i(\sigma_i - \bar{\sigma}_i) \right]. \end{aligned} \quad (\text{b.10})$$

Where we have defined  $\Delta y_i \equiv y_i - y_{i-1}$ ,  $f_i \equiv \frac{\sum_{j=i}^k y_j}{k+1-i} - y_i$ , and

$$c_i \equiv c_{i+1} \left( \frac{c_{i+1}}{y_{i+1}} \right)^{1 - \frac{\Delta y_{i+1}}{y_{i+1}}} \Gamma \left( \frac{\Delta y_{i+1}}{y_{i+1}} \right), \quad (\text{b.11})$$

with  $c_k \equiv 1$ . In the computation we have neglected quadratic terms in  $\tilde{\gamma}^2$ , because we are only interested in the leading behavior for small  $\tilde{\gamma}$ . We have written the value of the constants  $c_i$  for completeness, but in the end they will not be relevant). Notice that all these functions depend only on  $u_i - \bar{u}_i$ ,  $\sigma - \bar{\sigma}_i$  (since this property was shared by all the processes involved).

### From clusters' minima to global ground states

Once we have the joint probability for the minima in all the clusters we can compute the distribution of the *jumps* in all the relevant observables between the unperturbed ground state and the perturbed one. We can rewrite equation (b.1) as

$$\begin{aligned} \mathcal{P}_{\min}(\Delta u, \Delta \sigma, q_j | \tilde{\gamma}; \bar{u}_\emptyset, \bar{\sigma}_\emptyset) &= \\ &= \int du_{\text{gs}} du'_{\text{gs}} d\sigma_{\text{gs}} d\sigma'_{\text{gs}} \mathcal{P}_{\text{gs}}(u_{\text{gs}}, \sigma_{\text{gs}}, k+1; u'_{\text{gs}}, \sigma'_{\text{gs}}, j | \tilde{\gamma}; \bar{u}_\emptyset, \bar{\sigma}_\emptyset) \times \\ &\quad \times \delta(u'_{\text{gs}} - u_{\text{gs}} = \Delta u) \delta(\sigma'_{\text{gs}} - \sigma_{\text{gs}} = \Delta \sigma). \end{aligned} \quad (\text{b.12})$$

In this formula we are integrating over all possible energies and stresses of the unperturbed ground state ( $u_{\text{gs}}$  and  $\sigma_{\text{gs}}$ ) and of the perturbed one ( $u'_{\text{gs}}$  and  $\sigma'_{\text{gs}}$ ) with a constraint on their differences. We want to find also the distribution of the overlap between the two states. In order to do so, we recall that the unperturbed minimum has been put arbitrarily and without loss of generality in the first cluster  $\mathcal{C}_{k+1}$  — this is just a labeling of the leaves of the ultrametric tree; constraining the new ground state to lie in the cluster  $\mathcal{C}_j$  is equivalent to demand that the overlap between the two minima is the corresponding overlap scale  $q_j$  (see Figure b.1).  $\mathcal{P}_{\text{gs}}(u_{\text{gs}}, \sigma_{\text{gs}}, k+1; u'_{\text{gs}}, \sigma'_{\text{gs}}, j | \tilde{\gamma}; \bar{u}_\emptyset, \bar{\sigma}_\emptyset)$  is then the joint probability that among all the states of the system, the minimum at  $\tilde{\gamma} = 0$  is found in the cluster  $\mathcal{C}_{k+1}$  and takes the values  $(u_{\text{gs}}, \sigma_{\text{gs}})$ ,

and that the minimum at  $\tilde{\gamma} > 0$  is found in the cluster  $\mathcal{C}_j$ , with energy  $u'_{\text{gs}}$  and stress  $\sigma'_{\text{gs}}$ ; explicitly, it can be written as

$$\begin{aligned}
\mathcal{P}_{\text{gs}}(u_{\text{gs}}, \sigma_{\text{gs}}, k+1; u'_{\text{gs}}, \sigma'_{\text{gs}}, j | \tilde{\gamma}; \bar{u}_{\emptyset}, \bar{\sigma}_{\emptyset}) &= \\
&= \int du_1 \cdots du_{k+1} d\sigma_1 \cdots d\sigma_{k+1} \mathcal{P}_{\text{cluster}}[\{\underline{u}, \underline{\sigma}\} | \tilde{\gamma}; \bar{u}_{\emptyset}, \bar{\sigma}_{\emptyset}] \times \\
&\quad \times \delta(u_{k+1} = u_{\text{gs}}) \delta(\sigma_{k+1} = \sigma_{\text{gs}}) \delta(u_j = u'_{\text{gs}}) \delta(\sigma_j = \sigma'_{\text{gs}}) \times \\
&\quad \times \prod_{\substack{i=1 \\ i \neq k+1}}^{k+1} \theta(u_i > u_{\text{gs}}) \prod_{\substack{i=1 \\ i \neq j}}^{k+1} \theta(u_i - \tilde{\gamma}\sigma_i > u'_{\text{gs}} - \tilde{\gamma}\sigma'_{\text{gs}}). \quad (\text{b.13})
\end{aligned}$$

In this equation we have integrated out all the clusters' minima, constrained in such a way that the minima in  $\mathcal{C}_{k+1}$  and  $\mathcal{C}_j$  assume the desired values; the last products are the conditions for the two states being global minima, at different values of the perturbation  $\tilde{\gamma}$ : the first asserts that the unperturbed ground state has the lowest internal energy  $u_{\text{gs}}$ ; the second asserts that at  $\tilde{\gamma}$  the total energy  $u'_{\text{gs}} - \tilde{\gamma}\sigma'_{\text{gs}}$  is minimum.

Plugging this formula into the former one and integrating the delta functions when possible we find

$$\begin{aligned}
\mathcal{P}_{\text{min}}(\Delta u, \Delta \sigma, q_j | \tilde{\gamma}; \bar{u}_{\emptyset}, \bar{\sigma}_{\emptyset}) &= \\
&= \int du_1 \cdots du_{k+1} d\sigma_1 \cdots d\sigma_{k+1} \mathcal{P}_{\text{cluster}}[\{\underline{u}, \underline{\sigma}\} | \tilde{\gamma}; \bar{u}_{\emptyset}, \bar{\sigma}_{\emptyset}] \times \\
&\quad \times \delta(u_j - u_{k+1} = \Delta u) \delta(\sigma_j - \sigma_{k+1} = \Delta \sigma) \times \\
&\quad \times \prod_{\substack{i=1 \\ i \neq k+1}}^{k+1} \theta(u_i > u_{k+1}) \prod_{\substack{i=1 \\ i \neq j}}^{k+1} \theta(u_i - \tilde{\gamma}\sigma_i > u_j - \tilde{\gamma}\sigma_j). \quad (\text{b.14})
\end{aligned}$$

We can simplify this expression a little by changing integration variables, writing each variable relatively to the unperturbed ground state in  $\mathcal{C}_{k+1}$ :  $u_i \rightarrow u_{k+1} + \Delta u_i$ ,  $\sigma_i \rightarrow \sigma_{k+1} + \Delta \sigma_i$ . Of course the variables  $u_{k+1}$  and  $\sigma_{k+1}$  are not shifted, but we introduce nonetheless the variables  $\Delta u_{k+1}$  and  $\Delta \sigma_{k+1}$ ; in this way, the set of all energies and stresses  $\{\underline{u}, \underline{\sigma}\}$  can be written as  $\{u_{k+1} + \underline{\Delta u}, \sigma_{k+1} + \underline{\Delta \sigma}\}$ . At this point we use equation (b.2) to show that

$$\begin{aligned}
\mathcal{P}_{\text{cluster}} [\{u_{k+1} + \underline{\Delta u}, \sigma_{k+1} + \underline{\Delta \sigma}\} | \tilde{\gamma}; \bar{u}_\emptyset, \bar{\sigma}_\emptyset] &= \\
&= \int d\bar{u}_2 \cdots d\bar{u}_{k+1} d\bar{\sigma}_2 \cdots d\bar{\sigma}_{k+1} \left[ \prod_{i=1}^k \tilde{\lambda}_i [(\bar{u}_i, \bar{\sigma}_i) \rightarrow (\bar{u}_{i+1}, \bar{\sigma}_{i+1})] \right] \times \\
&\quad \times \left[ \prod_{i=1}^{k+1} p_i(u_{k+1} + \Delta u_i, \sigma_{k+1} + \Delta \sigma_i | \bar{u}_i, \bar{\sigma}_i; \tilde{\gamma}) \right] = \\
&= \int d\bar{u}_2 \cdots d\bar{u}_{k+1} d\bar{\sigma}_2 \cdots d\bar{\sigma}_{k+1} \tilde{\lambda}_1(\bar{u}_2 - \bar{u}_\emptyset, \bar{\sigma}_2 - \bar{\sigma}_\emptyset) \times \\
&\times \left[ \prod_{i=2}^k \tilde{\lambda}_i(\bar{u}_{i+1} - \bar{u}_i, \bar{\sigma}_{i+1} - \bar{\sigma}_i) \right] p_1(u_{k+1} + \Delta u_1 - \bar{u}_\emptyset, \sigma_{k+1} + \Delta \sigma_1 - \bar{\sigma}_\emptyset) \times \\
&\quad \times \left[ \prod_{i=2}^{k+1} p_i(u_{k+1} + \Delta u_i - \bar{u}_i, \sigma_{k+1} + \Delta \sigma_i - \bar{\sigma}_i) \right] = \\
&= \int d\hat{u}_2 \cdots d\hat{u}_{k+1} d\hat{\sigma}_2 \cdots d\hat{\sigma}_{k+1} \tilde{\lambda}_1(\hat{u}_2 - \bar{u}_\emptyset + u_{k+1}, \hat{\sigma}_2 - \bar{\sigma}_\emptyset + \sigma_{k_1}) \times \\
&\times \left[ \prod_{i=2}^k \tilde{\lambda}_i(\hat{u}_{i+1} - \hat{u}_i, \hat{\sigma}_{i+1} - \hat{\sigma}_i) \right] p_1(\Delta u_1 - \bar{u}_\emptyset + u_{k+1}, \Delta \sigma_1 - \bar{\sigma}_\emptyset + \sigma_{k+1}) \times \\
&\quad \times \left[ \prod_{i=2}^{k+1} p_i(\Delta u_i - \hat{u}_i, \Delta \sigma_i - \hat{\sigma}_i) \right] = \\
&= \mathcal{P}_{\text{cluster}} [\{\underline{\Delta u}, \underline{\Delta \sigma}\} | \tilde{\gamma}; \bar{u}_\emptyset - u_{k+1}, \bar{\sigma}_\emptyset - \sigma_{k+1}]. \quad (\text{b.15})
\end{aligned}$$

(At first, we have shown the dependence of  $\tilde{\lambda}_1$  and  $p_1$  on the root variables  $\bar{u}_\emptyset, \bar{\sigma}_\emptyset$ , and we have explicitly shown the fact that all the functions depend on the variables' differences; then, we have shifted all the integration variables). In practice equation (b.15) says that we can set the ground state energy and stress to zero by shifting the root energy and stress, which will turn out to be irrelevant for the scope of our calculations.

Performing the change of variables  $u_i \rightarrow u_{k+1} + \Delta u_i$ ,  $\sigma_i \rightarrow \sigma_{k+1} + \Delta \sigma_i$ , introducing  $\delta(\Delta u_{k+1})$  and  $\delta(\Delta \sigma_{k+1})$ , and using equation (b.15), the distribution (b.14) becomes

$$\begin{aligned}
\mathcal{P}_{\min}(\Delta u, \Delta \sigma, q_j | \tilde{\gamma}; \bar{u}_\emptyset, \bar{\sigma}_\emptyset) &= \int d\Delta u_1 \cdots d\Delta u_{k+1} d\Delta \sigma_1 \cdots d\Delta \sigma_{k+1} \times \\
&\times \int du_{k+1} d\sigma_{k+1} \mathcal{P}_{\text{cluster}} [\{\underline{\Delta u}, \underline{\Delta \sigma}\} | \tilde{\gamma}; \bar{u}_\emptyset - u_{k+1}, \bar{\sigma}_\emptyset - \sigma_{k+1}] \times \\
&\times \delta(\Delta u_{k+1}) \delta(\Delta \sigma_{k+1}) \delta(\Delta u_j - \Delta u) \delta(\Delta \sigma_j - \Delta \sigma) \times \\
&\times \prod_{\substack{i=1 \\ i \neq k+1}}^{k+1} \theta(\Delta u_i > 0) \prod_{\substack{i=1 \\ i \neq j}}^{k+1} \theta(\Delta u_i - \tilde{\gamma} \Delta \sigma_i > \Delta u - \tilde{\gamma} \Delta \sigma). \quad (\text{b.16})
\end{aligned}$$

That, in the end, can be written as

$$\begin{aligned}
\mathcal{P}_{\min}(\Delta u, \Delta \sigma, q_j | \tilde{\gamma}) &= \\
&= \int d\Delta u_1 \cdots d\Delta u_{k+1} d\Delta \sigma_1 \cdots d\Delta \sigma_{k+1} \delta(\Delta u_{k+1}) \delta(\Delta \sigma_{k+1}) \times \\
&\times \delta(\Delta u_j - \Delta u) \delta(\Delta \sigma_j - \Delta \sigma) \prod_{\substack{i=1 \\ i \neq j}}^{k+1} \theta(\Delta u_i - \tilde{\gamma} \Delta \sigma_i > \Delta u - \tilde{\gamma} \Delta \sigma) \times \\
&\times \mathcal{P}_{\text{cluster}} [\{\underline{\Delta u}, \underline{\Delta \sigma}\} | \tilde{\gamma}], \quad (\text{b.17})
\end{aligned}$$

where we have defined

$$\begin{aligned}
\mathcal{P}_{\text{cluster}} [\{\underline{\Delta u}, \underline{\Delta \sigma}\} | \tilde{\gamma}] &\equiv \\
&\equiv \int du_{k+1} d\sigma_{k+1} \mathcal{P}_{\text{cluster}} [\{\underline{\Delta u}, \underline{\Delta \sigma}\} | \tilde{\gamma}; -u_{k+1}, -\sigma_{k+1}] \quad (\text{b.18})
\end{aligned}$$

Deriving equation (b.17) we have proven what was already fairly intuitive; it roughly says that the new ground state is the minimum among all the clusters' minima. Notice that the distribution (b.17) does no longer depend on the root variables  $\bar{u}_\emptyset, \bar{\sigma}_\emptyset$ , that vanish when integrating over  $u_{k+1}, \sigma_{k+1}$  in (b.18), since in (b.15) they only appeared in the differences  $\bar{u}_\emptyset - u_{k+1}, \bar{\sigma}_\emptyset - \sigma_{k+1}$ . In (b.17) we have not written any of the functions  $\theta(\Delta u_i > 0)$  that appeared in (b.16): this is because, to lighten the notation, from now on we are going to assume that the variables  $\{\Delta u_i\}$  are always positive — they are indeed the energy gaps *above* the unperturbed ground state.

### Computation of the cluster probability

We can now compute  $\mathcal{P}_{\text{cluster}} [\{\underline{\Delta u}, \underline{\Delta \sigma}\} | \tilde{\gamma}]$  explicitly, starting from (b.2) and (b.18); in the following computation we rename the integration variables

$u_{k+1}, \sigma_{k+1}$  to  $u_{\text{gs}}, \sigma_{\text{gs}}$ , to avoid confusion with the other indices:

$$\begin{aligned} \mathcal{P}_{\text{cluster}} [\{\underline{\Delta u}, \underline{\Delta \sigma}\} | \tilde{\gamma}] &= \int du_{\text{gs}} d\sigma_{\text{gs}} \int d\bar{u}_2 \cdots d\bar{u}_{k+1} d\bar{\sigma}_2 \cdots d\bar{\sigma}_{k+1} \times \\ &\times \left[ \prod_{i=2}^k \tilde{\lambda}_i(\bar{u}_{i+1} - \bar{u}_i, \bar{\sigma}_{i+1} - \bar{\sigma}_i) \right] \left[ \prod_{i=2}^{k+1} p_i(\Delta u_i - \bar{u}_i, \Delta \sigma_i - \bar{\sigma}_i) \right] \times \\ &\times \tilde{\lambda}_1(\bar{u}_2 + u_{\text{gs}}, \bar{\sigma}_2 + \sigma_{\text{gs}}) p_1(\Delta u_1 + u_{\text{gs}}, \Delta \sigma_1 + \sigma_{\text{gs}}). \end{aligned} \quad (\text{b.19})$$

We can write explicitly  $p_{k+1}$  as a product of two delta functions, as in (b.4). If we rename  $u_{\text{gs}} \rightarrow -\bar{u}_1$  and  $\sigma_{\text{gs}} \rightarrow -\bar{\sigma}_1$ , we can absorb the corresponding terms inside the previous products of  $\tilde{\lambda}$ 's and  $p$ 's:

$$\begin{aligned} \mathcal{P}_{\text{cluster}} [\{\underline{\Delta u}, \underline{\Delta \sigma}\} | \tilde{\gamma}] &= \int d\bar{u}_1 \cdots d\bar{u}_{k+1} d\bar{\sigma}_1 \cdots d\bar{\sigma}_{k+1} \times \\ &\times \left[ \prod_{i=1}^k \tilde{\lambda}_i(\bar{u}_{i+1} - \bar{u}_i, \bar{\sigma}_{i+1} - \bar{\sigma}_i) \right] \left[ \prod_{i=1}^k p_i(\Delta u_i - \bar{u}_i, \Delta \sigma_i - \bar{\sigma}_i) \right] \times \\ &\times \delta(\Delta u_{k+1} - \bar{u}_{k+1}) \delta(\Delta \sigma_{k+1} - \bar{\sigma}_{k+1}). \end{aligned} \quad (\text{b.20})$$

Keeping in mind that our goal is to compute equation (b.17), where everything is multiplied by the two delta functions  $\delta(\Delta u_{k+1})\delta(\Delta \sigma_{k+1})$ , we can simplify (b.20) and set those variables to 0; then we can integrate also the term  $\delta(\Delta u_{k+1} - \bar{u}_{k+1}) \delta(\Delta \sigma_{k+1} - \bar{\sigma}_{k+1}) = \delta(0 - \bar{u}_{k+1}) \delta(0 - \bar{\sigma}_{k+1})$ , whose only effect is to set to 0 the variables  $\bar{u}_{k+1}, \bar{\sigma}_{k+1}$  that appear in the intensity  $\tilde{\lambda}_k$ :

$$\begin{aligned} \mathcal{P}_{\text{cluster}} [\{\underline{\Delta u}, \underline{\Delta \sigma}\} | \tilde{\gamma}] &= \int d\bar{u}_1 \cdots d\bar{u}_k d\bar{\sigma}_1 \cdots d\bar{\sigma}_k \times \\ &\times \left[ \prod_{i=1}^k \tilde{\lambda}_i(\bar{u}_{i+1} - \bar{u}_i, \bar{\sigma}_{i+1} - \bar{\sigma}_i) \right] \left[ \prod_{i=1}^k p_i(\Delta u_i - \bar{u}_i, \Delta \sigma_i - \bar{\sigma}_i) \right]. \end{aligned} \quad (\text{b.21})$$

(The terms  $\bar{u}_{k+1}, \bar{\sigma}_{k+1}$  inside  $\lambda_k$  are both 0 and are kept just for ease of notation).

It is easier to deal with this integral if we manage to decouple energies and stresses. To achieve this we will split each function  $\tilde{\lambda}_i$  into its exponential, energy dependent intensity  $\lambda_i$  and its Gaussian, stress dependent component  $\mu$ , as in (b.3). The functions  $\{p_i\}$  can also be decomposed; from (b.9) we can define

$$p_i(u, \sigma) = \lambda_i(u) \mu_i(\sigma) e^{\tilde{\gamma} f_i \sigma} \xi_i(u - \tilde{\gamma} \sigma), \quad (\text{b.22})$$

where  $\lambda_i$  is the usual exponential intensity,  $\mu_i(\sigma)$  is a zero-mean Gaussian distribution with variance  $(k+1-i)\Delta q \approx 1 - q_i$  (in the large  $k$  limit), and

$\xi_i(x) = c_i \exp\left[-\frac{c_i}{y_i} e^{y_i x}\right]$ . Consequently, the joint probability for the clusters' minima becomes

$$\begin{aligned} \mathcal{P}_{\text{cluster}}[\{\underline{\Delta u}, \underline{\Delta \sigma}\} | \tilde{\gamma}] &\propto \\ &\propto \int \left[ \prod_{i=1}^k d\bar{\sigma}_i \right] \left[ \prod_{i=1}^k \mu(\bar{\sigma}_{i+1} - \bar{\sigma}_i) e^{\tilde{\gamma} f_i(\Delta\sigma_i - \bar{\sigma}_i)} \mu_i(\Delta\sigma_i - \bar{\sigma}_i) \right] \times \\ &\times \int \left[ \prod_{i=1}^k d\bar{u}_i \right] \left[ \prod_{i=1}^k \lambda_i(\bar{u}_{i+1} - \bar{u}_i) \lambda_i(\Delta u_i - \bar{u}_i) \xi_i(\Delta u_i - \bar{u}_i - \tilde{\gamma} \Delta\sigma_i + \tilde{\gamma} \bar{\sigma}_i) \right], \end{aligned} \quad (\text{b.23})$$

and, writing explicitly the exponential intensities  $\lambda_i$ :

$$\begin{aligned} \mathcal{P}_{\text{cluster}}[\{\underline{\Delta u}, \underline{\Delta \sigma}\} | \tilde{\gamma}] &\propto \int \mathcal{D}^k \bar{\sigma} \left[ \prod_{i=1}^k e^{\tilde{\gamma} f_i(\Delta\sigma_i - \bar{\sigma}_i)} \mu_i(\Delta\sigma_i - \bar{\sigma}_i) \right] \times \\ &\times \prod_{i=1}^k e^{y_i \Delta u_i} \int d\bar{u}_i e^{-(2y_i - y_{i-1})\bar{u}_i} \xi_i(\Delta u_i - \bar{u}_i - \tilde{\gamma} \Delta\sigma_i + \tilde{\gamma} \bar{\sigma}_i), \end{aligned} \quad (\text{b.24})$$

where we have introduced a shorthand for the Gaussian integration,  $\int \mathcal{D}^k \bar{\sigma} \equiv \int \left[ \prod_{i=1}^k d\bar{\sigma}_i \right] \left[ \prod_{i=1}^k \mu(\bar{\sigma}_{i+1} - \bar{\sigma}_i) \right]$ , and we have defined  $y_0 \equiv 0$ . Now the integrals containing the functions  $\xi_i$  can be evaluated exactly, yielding

$$\begin{aligned} \mathcal{P}_{\text{cluster}}[\{\underline{\Delta u}, \underline{\Delta \sigma}\} | \tilde{\gamma}] &\propto \left[ \prod_{i=1}^k e^{-(y_i - y_{i-1})\Delta u_i} \right] \times \\ &\times \int \mathcal{D}^k \bar{\sigma} \left[ \prod_{i=1}^k \mu_i(\bar{\sigma}_i - \Delta\sigma_i) e^{-\tilde{\gamma}(2y_i - y_{i-1} + f_i)(\bar{\sigma}_i - \Delta\sigma_i)} \right] \propto \\ &\propto \left[ \prod_{i=1}^k e^{-(y_i - y_{i-1})\Delta u_i} \right] \times \\ &\times \int \mathcal{D}^k \bar{\sigma} \left[ \prod_{i=1}^k \mu_i(\bar{\sigma}_i - \Delta\sigma_i + \tilde{\gamma}(2y_i - y_{i-1} + f_i)(k+1-i)\Delta q) \right]. \end{aligned} \quad (\text{b.25})$$

Let us call  $z_i \equiv (2y_i - y_{i-1} + f_i)(k+1-i)\Delta q$ ; plugging in the definition of  $f_i$  (b.9), we have that

$$z_i = (k+1-i)(y_i - y_{i-1})\Delta q + \Delta q \sum_{j=i}^k y_j \approx (1-q_i) \Delta y_i + Y(q_i), \quad (\text{b.26})$$

where we have defined  $Y(q) \equiv \int_q^1 dq' y(q')$  (we recall that  $\Delta y_i = y_i - y_{i-1}$ ,  $y_0 \equiv 0$ ). This formula of course is valid for large  $k$ .

Therefore the normalized joint distribution is

$$\mathcal{P}_{\text{cluster}} [\{\underline{\Delta u}, \underline{\Delta \sigma}\}|\tilde{\gamma}] = \int \mathcal{D}^k \bar{\sigma} \prod_{i=1}^k \Delta y_i e^{\Delta y_i \Delta u_i} \mu_i(\bar{\sigma}_i - \Delta \sigma_i + \tilde{\gamma} z_i). \quad (\text{b.27})$$

### Avalanche distribution for the total energy

After computing  $\mathcal{P}_{\text{cluster}}$  we want to go on with the calculation of the distribution  $\mathcal{P}_{\text{min}}$  of finding the new ground state at overlap  $q_i$  with the unperturbed one, and with a difference in energy and stress equal to  $\Delta u$  and  $\Delta \sigma$ , respectively. We can now integrate (b.17), finding

$$\begin{aligned} \mathcal{P}_{\text{min}}(\Delta u, \Delta \sigma, q_i|\tilde{\gamma}) &\equiv \\ &\equiv \int \left[ \prod_{j=1, j \neq i}^{k+1} d\Delta u_j d\Delta \sigma_j \theta(\Delta u_j - \tilde{\gamma} \Delta \sigma_j > \Delta u - \tilde{\gamma} \Delta \sigma) \right] \times \\ &\quad \times \delta(\Delta u_{k+1}) \delta(\Delta \sigma_{k+1}) \mathcal{P}_{\text{cluster}} [\{\underline{\Delta u}, \underline{\Delta \sigma}\}|\tilde{\gamma}] = \\ &= \delta_{i,k+1} \delta(\Delta u) \delta(\Delta \sigma) \int \mathcal{D}^k \bar{\sigma} \prod_{j=1}^k \chi_j(0; \bar{\sigma}_j) + (1 - \delta_{i,k+1}) \theta(\Delta u - \tilde{\gamma} \Delta \sigma < 0) \times \\ &\quad \times \int \mathcal{D}^k \bar{\sigma} \Delta y_i e^{-\Delta y_i \Delta u} \mu_i(\bar{\sigma}_i - \Delta \sigma + \tilde{\gamma} z_i) \prod_{j=1, j \neq i}^k \chi_j(\Delta u - \tilde{\gamma} \Delta \sigma; \bar{\sigma}_j), \quad (\text{b.28}) \end{aligned}$$

where  $\delta_{i,k+1}$  is the Kronecker delta. Notice that contrary to (b.17) we have not written the delta functions fixing  $\Delta u_j = \Delta u$  and  $\Delta \sigma_j = \Delta \sigma$ : this is implicitly done when we skip the integration over  $\Delta u_j, \Delta \sigma_j$  in (b.28). The auxiliary functions  $\chi_i(s; \bar{\sigma}_i)$  are defined as (after neglecting  $\mathcal{O}(\tilde{\gamma}^2)$  terms)

$$\begin{aligned} \chi_i(s; \bar{\sigma}_i) &\equiv \\ &\equiv \int_0^\infty d\Delta u \int_{-\infty}^\infty d\Delta \sigma \theta(\Delta u - \tilde{\gamma} \Delta \sigma > s) \Delta y_i e^{-\Delta y_i \Delta u} \mu_i(\bar{\sigma}_i - \Delta \sigma + \tilde{\gamma} z_i) = \\ &= \mathbb{H} \left( -|\tilde{\gamma}| \Delta y_i \sqrt{1 - q_i} - \frac{s/|\tilde{\gamma}| + \bar{\sigma}_i \cdot \text{sign}(\tilde{\gamma}) + |\tilde{\gamma}| Y(q_i)}{\sqrt{1 - q_i}} \right) + \\ &\quad + \mathbb{H} \left( \frac{s/|\tilde{\gamma}| + \bar{\sigma}_i \cdot \text{sign}(\tilde{\gamma}) + |\tilde{\gamma}| Y(q_i)}{\sqrt{1 - q_i}} \right) e^{-|\tilde{\gamma}| \Delta y_i [s/|\tilde{\gamma}| + \bar{\sigma}_i \cdot \text{sign}(\tilde{\gamma}) + |\tilde{\gamma}| Y(q_i)]}. \quad (\text{b.29}) \end{aligned}$$

We define the function  $\mathbb{H}(x)$  as the complementary error function

$$\mathbb{H}(x) \equiv \frac{1}{2} \text{erfc} \left( -\frac{x}{\sqrt{2}} \right) \equiv \int_{-\infty}^x \frac{dt}{\sqrt{2\pi}} e^{-\frac{t^2}{2}}. \quad (\text{b.30})$$

It is important that these functions  $\chi_i$  essentially do not depend on the sign of the perturbation  $\tilde{\gamma}$ . The only terms where the sign of  $\tilde{\gamma}$  ( $\text{sign}(\tilde{\gamma})$ ) appears are those that multiply  $\bar{\sigma}_i$ , but since the integral  $\int \mathcal{D}^k \bar{\sigma}$  is invariant if we invert the signs of all the  $\{\bar{\sigma}_i\}$  we can absorb  $\text{sign}(\tilde{\gamma})$  and regard the  $\chi_i$  as even functions of the perturbation.

From this object we can extract the distributions of jumps in the total energy, as the distribution of  $\Delta e \equiv \Delta u - \tilde{\gamma} \Delta \sigma$ ; this distribution is

$$\begin{aligned}
\mathcal{P}(\Delta e|\tilde{\gamma}) &\equiv \\
&\equiv \sum_{i=1}^{k+1} \int_0^\infty d\Delta u \int_{-\infty}^\infty d\Delta \sigma \delta(\Delta u - \tilde{\gamma} \Delta \sigma - \Delta e) \mathcal{P}_{\min}(\Delta u, \Delta \sigma, q_i|\tilde{\gamma}) \equiv \\
&\equiv \delta(\Delta e) \int \mathcal{D}^k \bar{\sigma} \prod_{j=1}^k \chi_j(0; \bar{\sigma}_j) + \theta(\Delta e < 0) \int \mathcal{D}^k \bar{\sigma} \sum_i \prod_{j=1, j \neq i}^k \chi_j(\Delta e; \bar{\sigma}_j) \times \\
&\times \int_0^\infty d\Delta u \int_{-\infty}^\infty d\Delta \sigma \delta(\Delta u - \tilde{\gamma} \Delta \sigma - \Delta e) \Delta y_i e^{-\Delta y_i \Delta u} \mu_i(\bar{\sigma}_i - \Delta \sigma + \tilde{\gamma} z_i).
\end{aligned} \tag{b.31}$$

Since the last integral is exactly  $-\partial_{\Delta e} \chi_i(\Delta e; \sigma_i)$  we can write the distribution of the jump  $\Delta e$  between the new ground state and the unperturbed one as

$$\mathcal{P}(\Delta e|\tilde{\gamma}) \equiv \delta(\Delta e) \mathcal{R}(0|\tilde{\gamma}) - \theta(\Delta e < 0) \partial_{\Delta e} \mathcal{R}(\Delta e|\tilde{\gamma}), \tag{b.32}$$

The function  $\mathcal{R}$  is defined as

$$\begin{aligned}
\mathcal{R}(\Delta e|\tilde{\gamma}) &\equiv \lim_{\substack{k \rightarrow \infty \\ k \Delta q \rightarrow 1}} \int \mathcal{D}^k \bar{\sigma} \prod_{i=1}^k \chi_j(\Delta e; \bar{\sigma}_i) \equiv \\
&\equiv \lim \int \mathcal{D}^k \bar{\sigma} \left\{ 1 - |\tilde{\gamma}| \Delta q \sum_i y'(q_i) \sqrt{1 - q_i} \tilde{\rho} \left( \frac{\Delta e / |\tilde{\gamma}| + \bar{\sigma}_i + |\tilde{\gamma}| Y(q_i)}{\sqrt{1 - q_i}} \right) \right\}.
\end{aligned} \tag{b.33}$$

The last expression is found setting  $\Delta y_i \equiv y'(q_i) \Delta q$  in the functions  $\chi_i$ , and then expanding them for small  $\Delta q$ . We have also defined  $\tilde{\rho}(x) \equiv (2\pi)^{-\frac{1}{2}} e^{-\frac{x^2}{2}} + x \mathbf{H}(x)$ . We want to stress that the whole probability distribution (b.32) does not depend on the sign of the shear strain  $\tilde{\gamma}$  (this property is inherited from the functions  $\chi_i$  through  $\mathcal{R}$ ); for this reason, in general there will be a cusp at  $\tilde{\gamma} = 0$ . Since we are interested in the case  $|\tilde{\gamma}| \ll 1$

(and  $|\Delta e| \sim \mathcal{O}(|\tilde{\gamma}|)$  or smaller) we can write

$$\begin{aligned} \mathcal{R}(\Delta e|\tilde{\gamma}) &= \\ &= \lim \left\{ 1 - |\tilde{\gamma}| \Delta q \sum_i y'(q_i) \sqrt{1 - q_i} \int \mathcal{D}^k \bar{\sigma} \tilde{\rho} \left( \frac{\Delta e/|\tilde{\gamma}| + \bar{\sigma}_i + |\tilde{\gamma}| Y(q_i)}{\sqrt{1 - q_i}} \right) \right\} \equiv \\ &\equiv \exp \left\{ -|\tilde{\gamma}| \int dq y'(q) \sqrt{1 - q} \rho \left( \frac{\Delta e/|\tilde{\gamma}| + |\tilde{\gamma}| Y(q)}{\sqrt{1 - q}} \right) \right\}. \quad (\text{b.34}) \end{aligned}$$

The function  $\rho(x)$  is the average of  $\tilde{\rho}(x)$  over the Gaussian process introduced in (b.24):

$$\begin{aligned} \rho(x) &\equiv \int d\bar{\sigma}_k \cdots d\bar{\sigma}_1 \mu(\bar{\sigma}_k) \mu(\bar{\sigma}_k - \bar{\sigma}_{k-1}) \cdots \mu(\bar{\sigma}_{i+1} - \bar{\sigma}_i) \times \\ &\quad \times \tilde{\rho} \left( x + \frac{\bar{\sigma}_i}{\sqrt{1 - q_i}} \right) \mu(\bar{\sigma}_i - \bar{\sigma}_{i-1}) \cdots \mu(\bar{\sigma}_2 - \bar{\sigma}_1) = \\ &= \int d\bar{\sigma}_k \cdots d\bar{\sigma}_i \mu(\bar{\sigma}_k) \mu(\bar{\sigma}_k - \bar{\sigma}_{k-1}) \cdots \mu(\bar{\sigma}_{i+1} - \bar{\sigma}_i) \tilde{\rho} \left( x + \frac{\bar{\sigma}_i}{\sqrt{1 - q_i}} \right) = \\ &= \int d\bar{\sigma}_i \frac{e^{-\frac{\bar{\sigma}_i^2}{2(1 - q_i)}}}{\sqrt{2\pi(1 - q_i)}} \tilde{\rho} \left( x + \frac{\bar{\sigma}_i}{\sqrt{1 - q_i}} \right) = \int d\sigma \frac{e^{-\frac{\sigma^2}{2}}}{\sqrt{2\pi}} \tilde{\rho}(x + \sigma). \quad (\text{b.35}) \end{aligned}$$

The last equality is due to the integration over  $k + 1 - i$  Gaussians with the same variance  $\Delta q$ , resulting in a Gaussian with variance  $(k + 1 - i)\Delta q \equiv 1 - q_i$ . Since  $\partial_x \rho(x) = (2\pi)^{-\frac{1}{2}} \int d\sigma e^{-\frac{1}{2}\sigma^2} \partial_x \tilde{\rho}(x + \sigma)$  and  $\partial_x \tilde{\rho}(x) = \mathbb{H}(x)$  one can show that  $\rho(x) = 2(4\pi)^{-\frac{1}{2}} e^{-\frac{1}{4}x^2} + x \mathbb{H}\left(\frac{x}{\sqrt{2}}\right)$  (see [Ng and Geller, 1969], paragraph 4.3, equation (13)).

### Asymptotic behavior

We have computed the distribution of total energy jumps when a small shear strain  $\tilde{\gamma}$  is applied to the system. The probability of *not jumping* (i.e. the probability that the original ground state is still the global minimum in the total energy landscape) is given by

$$\mathcal{P}(\Delta e = 0|\tilde{\gamma}) = \mathcal{R}(0|\tilde{\gamma}) \equiv \exp \left\{ -|\tilde{\gamma}| \int dq y'(q) \sqrt{1 - q} \rho \left( \frac{|\tilde{\gamma}| Y(q)}{\sqrt{1 - q}} \right) \right\}, \quad (\text{b.36})$$

and since the function  $\rho(x)$  is positive and increasing and  $\frac{|\tilde{\gamma}| Y(q)}{\sqrt{1 - q}}$  is positive for any  $q$ ,

$$\mathcal{P}(\Delta e = 0|\tilde{\gamma}) < \exp \left\{ -|\tilde{\gamma}| \rho(0) \int dq y'(q) \sqrt{1 - q} \right\}. \quad (\text{b.37})$$

This implies that whenever the exponent in the right hand side diverges, the system *always jumps*. For a more detailed discussion on the probability of not jumping, see *Asymptotic behavior* in Chapter 2.

When the function  $y(q)$  diverges as  $(1 - q)^{-\mu}$  near  $q = 1$  (with  $\mu \geq \frac{1}{2}$ ), the jump distribution becomes critical. The probability of a jump is

$$\mathcal{P}(\Delta e|\tilde{\gamma}) = -\partial_{\Delta e} e^{\log \mathcal{R}(\Delta e|\tilde{\gamma})} = -\partial_{\Delta e} \log \mathcal{R}(\Delta e|\tilde{\gamma}) \cdot \mathcal{R}(\Delta e|\tilde{\gamma}), \quad (\text{b.38})$$

and

$$\begin{aligned} -\partial_{\Delta e} \log \mathcal{R}(\Delta e|\tilde{\gamma}) &= \int dq y'(q) \rho' \left( \frac{\Delta e/|\tilde{\gamma}| + |\tilde{\gamma}| Y(q)}{\sqrt{1-q}} \right) \approx \\ &\underset{|\tilde{\gamma}| \ll 1}{\approx} \int dq y'(q) \rho' \left( \frac{\Delta e}{|\tilde{\gamma}| \sqrt{1-q}} \right). \end{aligned} \quad (\text{b.39})$$

This integral is dominated by the divergence in  $q = 1$  of the function  $y'(q)\sqrt{1-q}$ ; the convergence is guaranteed by

$$\rho' \left( \frac{\Delta e/|\tilde{\gamma}|}{\sqrt{1-q}} \right) = \int \frac{d\sigma}{\sqrt{2\pi}} e^{-\frac{\sigma^2}{2}} \mathbb{H} \left( \sigma + \frac{\Delta e}{|\tilde{\gamma}| \sqrt{1-q}} \right) \equiv \mathbb{H} \left( \frac{\Delta e}{\sqrt{2} |\tilde{\gamma}| \sqrt{1-q}} \right). \quad (\text{b.40})$$

The last equality can be proven using formula (13) in [Ng and Geller, 1969], paragraph 4.3. This term is exponentially small when  $q \approx 1$  because  $\Delta e < 0$  and  $\mathbb{H}(x) \rightarrow 0$  as  $x \rightarrow -\infty$ . As  $|\Delta e/\tilde{\gamma}|$  gets smaller, the integrand develops an increasing peak close to  $q = 1$ ; the leading behavior in  $\Delta e/\tilde{\gamma}$  can be extracted as follows:

$$\begin{aligned} -\partial_{\Delta e} \log \mathcal{R}(\Delta e|\tilde{\gamma}) &\sim \int dq (1-q)^{-\mu} \mathbb{H} \left( -\frac{|\Delta e|}{\sqrt{2} |\tilde{\gamma}| \sqrt{1-q}} \right) \sim \\ &\sim \left| \frac{\Delta e}{\tilde{\gamma}} \right|^{-2\mu} \int_{|\Delta e/\tilde{\gamma}|}^{\infty} d\xi \xi^{2\mu-1} \mathbb{H} \left( -\frac{\xi}{\sqrt{2}} \right) \sim \left| \frac{\Delta e}{\tilde{\gamma}} \right|^{-2\mu}. \end{aligned} \quad (\text{b.41})$$

Then, upon integration we find the asymptotic behavior of  $\mathcal{R}(\Delta e|\tilde{\gamma})$  and, finally, of the whole distribution

$$\begin{aligned} \mathcal{P}(\Delta e|\tilde{\gamma}) &= -\partial_{\Delta e} \log \mathcal{R}(\Delta e|\tilde{\gamma}) \cdot \mathcal{R}(\Delta e|\tilde{\gamma}) \sim \\ &\sim \begin{cases} \left| \frac{\Delta e}{\tilde{\gamma}} \right|^{-2\mu} \exp \left\{ -\text{const} \cdot |\tilde{\gamma}| \left| \frac{\Delta e}{\tilde{\gamma}} \right|^{-2\mu+1} \right\}, & \mu > \frac{1}{2}, \\ \left| \frac{\Delta e}{\tilde{\gamma}} \right|^{-2\mu+\text{const} \cdot |\tilde{\gamma}|} = \left| \frac{\Delta e}{\tilde{\gamma}} \right|^{-1+\text{const} \cdot |\tilde{\gamma}|}, & \mu = \frac{1}{2}. \end{cases} \end{aligned} \quad (\text{b.42})$$

The distribution is different in the two cases  $\mu = \frac{1}{2}$  and  $\mu > \frac{1}{2}$  because in the former the integration of  $\log \mathcal{R}(\Delta e|\tilde{\gamma})$  gives rise to logarithmic corrections, that in the end result in a linear contribution  $\mathcal{O}(\tilde{\gamma})$  in the power-law exponent  $-2\mu \equiv -1$ . Thanks to this correction, the power-law is integrable near  $\Delta e = 0$ . For  $\mu > \frac{1}{2}$  the distribution is integrable in the origin as well, because the exponential term suppresses the divergent power when  $|\Delta e| \ll |\tilde{\gamma}|^{1+\frac{1}{2\mu-1}}$ .

We have thus proven that the distribution of jumps in the total energy  $\Delta e < 0$  is a power law  $\mathcal{P}(\Delta e|\tilde{\gamma}) \sim \left|\frac{\Delta e}{\tilde{\gamma}}\right|^{-2\mu}$  when  $|\tilde{\gamma}|^{1+\frac{1}{2\mu-1}} \ll |\Delta e| \ll |\tilde{\gamma}| \ll 1$ .

In the main text we have written these last formulae with the substitution  $\tilde{\gamma} \rightarrow \sqrt{N}\gamma$ .

### Distribution of other observables

Starting from (b.28) it is possible to compute the leading behavior of the distribution of the jumps in the stress  $\Delta\sigma$ , in the energy  $\Delta u$  and in the overlap  $q$ . We cannot compute these quantities exactly, but we can write the Taylor expansion for small  $\tilde{\gamma}$ ; in general the Taylor expansion will not be valid for small jumps. For instance, Taylor expanding the distribution (b.42) (say, for  $\mu > \frac{1}{2}$ ), we find that  $\mathcal{P}(\Delta e|\tilde{\gamma}) \approx \left|\frac{\Delta e}{\tilde{\gamma}}\right|^{-2\mu}$ , yielding the correct power law exponent, but losing the information regarding the lower cutoff. This happens because in the point  $\Delta e = 0$  the distribution has an essential singularity and it is not analytic.

Working only with the probability density of finite jumps (that is, neglecting the delta contribution of not jumping) in (b.28), and for small  $\tilde{\gamma}$ , we can write

$$\begin{aligned} \mathcal{P}(\Delta u, \Delta\sigma, q) &= \theta(\Delta u - \tilde{\gamma}\Delta\sigma < 0)y'(q) \times \\ &\times \int \mathcal{D}^k \bar{\sigma} \mu(\bar{\sigma}_q - \Sigma; 1 - q) \mathcal{R}(\Delta u - \tilde{\gamma}\Delta\Sigma; \{\bar{\sigma}\}). \end{aligned} \quad (\text{b.43})$$

Integrating out the energy and the stress, and keeping only the first order in

$\tilde{\gamma}$ , we find the leading behavior of the distribution of stress jumps:

$$\begin{aligned}
\mathcal{P}(\Delta\sigma) &= \int dq y'(q) \int \mathcal{D}^k \bar{\sigma} \mu(\bar{\sigma}_q - \Delta\sigma; 1-q) \int_{-\gamma\Delta\sigma}^0 dx \mathcal{R}(x; \{\bar{\sigma}\}) \approx \\
&\approx \tilde{\gamma}\theta(\Delta\sigma)\Delta\sigma \int dq y'(q) \mu(\Delta\sigma; 2(1-q)) \sim \\
&\sim \tilde{\gamma}\theta(\Delta\sigma)\Delta\sigma \int dq (1-q)^{-\mu-1} \frac{e^{-\frac{\Delta\sigma^2}{4(1-q)}}}{\sqrt{4\pi(1-q)}} = \\
&= \tilde{\gamma}\theta(\Delta\sigma)\Delta\sigma^{-2\mu} \int_{\Delta\sigma^2}^{\infty} dt e^{-t} t^{\mu-\frac{1}{2}} \sim \tilde{\gamma}\Delta\sigma^{-2\mu}. \quad (\text{b.44})
\end{aligned}$$

With a similar reasoning we find the distribution of the energy jumps  $\Delta u$ :

$$\begin{aligned}
\mathcal{P}(\Delta u) &= \int dq y'(q) \int \mathcal{D}^k \bar{\sigma} \int_0^{\infty} dx \mu(x + \bar{\sigma}_q - \Delta u/\tilde{\gamma}; 1-q) \mathcal{R}(\tilde{\gamma}x; \{\bar{\sigma}\}) \approx \\
&\approx \int dq y'(q) \int \mathcal{D}^k \underline{\sigma} \int_0^{\infty} dx \mu(x + \bar{\sigma}_q - \Delta u/\tilde{\gamma}; 1-q) = \\
&= \int dq y'(q) \int_0^{\infty} dx \mu(x - \Delta u/\tilde{\gamma}; 2(1-q)) \equiv \int dq y'(q) \mathbb{H}\left(-\frac{\Delta u}{\tilde{\gamma}\sqrt{1-q}}\right) \sim \\
&= \left|\frac{\Delta u}{\tilde{\gamma}}\right|^2 \int_{(\Delta u/\tilde{\gamma})^2}^1 dt t^{\mu-1} \mathbb{H}(-\sqrt{t}) \sim \left|\frac{\Delta u}{\tilde{\gamma}}\right|^{-2\mu}. \quad (\text{b.45})
\end{aligned}$$

Finally, the leading behavior of the distribution of overlaps between the unperturbed ground state and the new one is

$$\begin{aligned}
\mathcal{P}(\Delta u) &= y'(q) \int \mathcal{D}^k \bar{\sigma} \int_0^{\infty} d\Delta\sigma \mu(\bar{\sigma}_q - \Delta\sigma; 1-q) \int_{-\tilde{\gamma}\Delta\sigma}^0 dx \mathcal{R}(x; \{\bar{\sigma}\}) \approx \\
&\approx \tilde{\gamma}y'(q) \int_0^{\infty} d\Delta\sigma \mu(\Delta\sigma; 2(1-q)) = \tilde{\gamma}y'(q) \sqrt{\frac{1-q}{\pi}}. \quad (\text{b.46})
\end{aligned}$$

We can also compute the order of the moments — with respect to  $\tilde{\gamma}$  — of the jumps in all the observables. Starting from the formula (b.28) we can easily write (for  $n > 0$ )

$$\begin{aligned}
\langle |\Delta e|^n \rangle &= \tilde{\gamma}^{n+1} \int \mathcal{D}^k \bar{\sigma} \int dq y'(q) \times \\
&\times \int_0^{\infty} d\Delta\sigma \mu(\bar{\sigma}_q - \Delta\sigma; 1-q) \int_{-\Delta\sigma}^0 dx (-x)^n R(\tilde{\gamma}x; \{\bar{\sigma}\}), \quad (\text{b.47})
\end{aligned}$$

$$\begin{aligned} \langle \Delta\sigma^n \rangle &= \tilde{\gamma} \int \mathcal{D}^k \bar{\sigma} \int dq y'(q) \times \\ &\times \int_0^\infty d\Delta\sigma \Delta\sigma^n \mu(\bar{\sigma}_q - \Delta\sigma; 1 - q) \int_{-\Delta\sigma}^0 dx R(\tilde{\gamma}x; \{\bar{\sigma}\}), \end{aligned} \quad (\text{b.48})$$

$$\begin{aligned} \langle q^n \rangle &= \tilde{\gamma} \int \mathcal{D}^k \bar{\sigma} \int dq y'(q) q^n \times \\ &\times \int_0^\infty d\Delta\sigma \mu(\bar{\sigma}_q - \Delta\sigma; 1 - q) \int_{-\Delta\sigma}^0 dx R(\tilde{\gamma}x; \{\bar{\sigma}\}). \end{aligned} \quad (\text{b.49})$$

Recalling equation (b.33), we see that in the end

$$\langle |\Delta e|^n \rangle \sim \mathcal{O}(\tilde{\gamma}^{n+1}), \quad (\text{b.50})$$

$$\langle \Delta\sigma^n \rangle \sim \mathcal{O}(\tilde{\gamma}), \quad (\text{b.51})$$

$$\langle q^n \rangle \sim \mathcal{O}(\tilde{\gamma}). \quad (\text{b.52})$$

We can also write the moments of the observables with the correct factors  $N$ , i.e. with  $\tilde{\gamma} = \gamma\sqrt{N}$ ,  $\Delta u = \Delta U$  (the extensive term does not contribute to the jump),  $\Delta\sigma = N^{-\frac{1}{2}}\Delta\Sigma$  and  $\Delta e = \Delta u - \tilde{\gamma}\Delta\sigma = \Delta U - \gamma\Delta\Sigma = \Delta E$ :

$$\langle |\Delta E|^k \rangle \sim \mathcal{O}(N^{\frac{k+1}{2}} \gamma^{k+1}), \quad (\text{b.53})$$

$$\langle \Delta\Sigma^k \rangle \sim \mathcal{O}(N^{\frac{k+1}{2}} \gamma), \quad (\text{b.54})$$

$$\langle q^k \rangle \sim \mathcal{O}(\sqrt{N}\gamma). \quad (\text{b.55})$$

# Bibliography



- Aizenman, M., Sims, R., and Starr, S. L. (2006). Mean-field spin glass models from the cavity–rost perspective. *arXiv preprint math-ph/0607060*.
- Altieri, A., Franz, S., and Parisi, G. (2016). The jamming transition in high dimension: an analytical study of the tap equations and the effective thermodynamic potential. *Journal of Statistical Mechanics: Theory and Experiment*, 2016(9):093301.
- Angell, C. A. et al. (1995). Formation of glasses from liquids and biopolymers. *Science*, 267(5206):1924–1935.
- Arévalo, R. and Ciamarra, M. P. (2014). Size and density avalanche scaling near jamming. *Soft Matter*, 10(16):2728–2732.
- Arguin, L.-P. (2007). Spin glass computations and ruelle’s probability cascades. *Journal of Statistical Physics*, 126(4-5):951–976.
- Atkinson, S., Stillinger, F. H., and Torquato, S. (2013). Detailed characterization of rattlers in exactly isostatic, strictly jammed sphere packings. *Physical Review E*, 88(6):062208.
- Berthier, L. and Biroli, G. (2011). Theoretical perspective on the glass transition and amorphous materials. *Reviews of Modern Physics*, 83(2):587.
- Biroli, G. (2007). Jamming: A new kind of phase transition? *Nature Physics*, 3(4):222–223.
- Biroli, G. and Urbani, P. (2016). Breakdown of elasticity in amorphous solids. *Nature physics*, 12:11301133.
- Bitzek, E., Koskinen, P., Gähler, F., Moseler, M., and Gumbsch, P. (2006). Structural relaxation made simple. *Physical review letters*, 97(17):170201.
- Castellani, T. and Cavagna, A. (2005). Spin-glass theory for pedestrians. *Journal of Statistical Mechanics: Theory and Experiment*, 2005(05):P05012.
- Cavagna, A. (2009). Supercooled liquids for pedestrians. *Physics Reports*, 476(4):51–124.
- Charbonneau, P., Corwin, E. I., Parisi, G., Poncet, A., and Zamponi, F. (2016). Universal non-debye scaling in the density of states of amorphous solids. *Physical review letters*, 117(4):045503.
- Charbonneau, P., Corwin, E. I., Parisi, G., and Zamponi, F. (2012). Universal microstructure and mechanical stability of jammed packings. *Physical review letters*, 109(20):205501.

- Charbonneau, P., Corwin, E. I., Parisi, G., and Zamponi, F. (2015). Jamming criticality revealed by removing localized buckling excitations. *Phys. Rev. Lett.*, 114:125504.
- Charbonneau, P., Kurchan, J., Parisi, G., Urbani, P., and Zamponi, F. (2014a). Exact theory of dense amorphous hard spheres in high dimension. iii. the full replica symmetry breaking solution. *Journal of Statistical Mechanics: Theory and Experiment*, 2014(10):P10009.
- Charbonneau, P., Kurchan, J., Parisi, G., Urbani, P., and Zamponi, F. (2014b). Fractal free energy landscapes in structural glasses. *Nature communications*, 5:3725.
- Combe, G. and Roux, J. (2000). Strain versus stress in a model granular material: a devil's staircase. *Physical Review Letters*, 85(17):3628.
- De Dominicis, C. and Giardinà, I. (2006). *Random fields and spin glasses: a field theory approach*. Cambridge University Press.
- Debenedetti, P. G. and Stillinger, F. H. (2001). Supercooled liquids and the glass transition. *Nature*, 410(6825):259.
- DeGiuli, E., Lerner, E., Brito, C., and Wyart, M. (2014). The distribution of forces affects vibrational properties in hard sphere glasses. *arXiv preprint arXiv:1402.3834*.
- Derrida, B. (1980). Random-energy model: Limit of a family of disordered models. *Physical Review Letters*, 45(2):79.
- Derrida, B. (1981). Random-energy model: An exactly solvable model of disordered systems. *Physical Review B*, 24(5):2613.
- Dubey, A. K., Procaccia, I., Shor, C. A. B. Z., and Singh, M. (2016). Elasticity in amorphous solids: nonlinear or piecewise linear? *Physical review letters*, 116(8):085502.
- Fiocco, D., Foffi, G., and Sastry, S. (2013). Oscillatory athermal quasistatic deformation of a model glass. *Physical Review E*, 88(2):020301.
- Franz, S., Gradenigo, G., and Spigler, S. (2016). Random-diluted triangular plaquette model: Study of phase transitions in a kinetically constrained model. *Physical Review E*, 93(3):032601.
- Franz, S., Mezard, M., Parisi, G., and Peliti, L. (1999). The response of glassy systems to random perturbations: A bridge between equilibrium and off-equilibrium. *Journal of statistical physics*, 97(3):459–488.

- Franz, S. and Parisi, G. (2000). Non trivial overlap distributions at zero temperature. *The European Physical Journal B-Condensed Matter and Complex Systems*, 18(3):485–491.
- Franz, S. and Parisi, G. (2016). The simplest model of jamming. *Journal of Physics A: Mathematical and Theoretical*, 49(14):145001.
- Franz, S., Parisi, G., Sevelev, M., Urbani, P., and Zamponi, F. (2017). Universality of the sat-unsat (jamming) threshold in non-convex continuous constraint satisfaction problems. *arXiv preprint arXiv:1702.06919*.
- Franz, S., Parisi, G., Urbani, P., and Zamponi, F. (2015). Universal spectrum of normal modes in low-temperature glasses. *Proceedings of the National Academy of Sciences*, 112(47):14539–14544.
- Gardner, E. (1985). Spin glasses with p-spin interactions. *Nuclear Physics B*, 257:747–765.
- Hentschel, H., Karmakar, S., Lerner, E., and Procaccia, I. (2011). Do athermal amorphous solids exist? *Physical Review E*, 83(6):061101.
- Jaiswal, P. K., Procaccia, I., Rainone, C., and Singh, M. (2016). Mechanical yield in amorphous solids: a first-order phase transition. *Physical review letters*, 116(8):085501.
- Jesi, M. B. (2015). Criticality and energy landscapes in spin glasses.
- Karmakar, S. and Parisi, G. (2013). Random pinning glass model. *Proceedings of the National Academy of Sciences*, 110(8):2752–2757.
- Kirkpatrick, T. and Thirumalai, D. (1987a). Dynamics of the structural glass transition and the p-spininteraction spin-glass model. *Physical review letters*, 58(20):2091.
- Kirkpatrick, T. and Thirumalai, D. (1987b). p-spin-interaction spin-glass models: Connections with the structural glass problem. *Physical Review B*, 36(10):5388.
- Kirkpatrick, T. and Thirumalai, D. (2012). Random first-order phase transition theory of the structural glass transition. *Structural Glasses and Supercooled Liquids: Theory, Experiment, and Applications*, page 223.
- Kirkpatrick, T. and Thirumalai, D. (2014). Universal aspects of the random first order phase transition theory of the structural glass transition. *arXiv preprint arXiv:1401.2024*.

- Kirkpatrick, T., Thirumalai, D., and Wolynes, P. G. (1989). Scaling concepts for the dynamics of viscous liquids near an ideal glassy state. *Physical Review A*, 40(2):1045.
- Kirkpatrick, T. and Wolynes, P. (1987). Connections between some kinetic and equilibrium theories of the glass transition. *Physical Review A*, 35(7):3072.
- Kobayashi, H. and Yamamoto, R. (2011). Implementation of lees-edwards periodic boundary conditions for direct numerical simulations of particle dispersions under shear flow. *The Journal of chemical physics*, 134(6):064110.
- Krzakala, F. and Martin, O. C. (2002). Chaotic temperature dependence in a model of spin glasses. *The European Physical Journal B*, 28(2):199–208.
- Kurchan, J., Parisi, G., Urbani, P., and Zamponi, F. (2013). Exact theory of dense amorphous hard spheres in high dimension. ii. the high density regime and the gardner transition. *J. Phys. Chem. B*, 117(42):pp 1297912994.
- Kurchan, J., Parisi, G., and Zamponi, F. (2012). Exact theory of dense amorphous hard spheres in high dimension i. the free energy. *Journal of Statistical Mechanics: Theory and Experiment*, 2012(10):P10012.
- Le Doussal, P., Müller, M., and Wiese, K. J. (2012). Equilibrium avalanches in spin glasses. *Phys. Rev. B*, 85(21):214402.
- Le Doussal, P. and Wiese, K. (2009). Size distributions of shocks and static avalanches from the functional renormalization group. *Physical Review E*, 79(5):051106.
- Lees, A. and Edwards, S. (1972). The computer study of transport processes under extreme conditions. *Journal of Physics C: Solid State Physics*, 5(15):1921.
- Leishangthem, P., Parmar, A., and Sastry, S. (2016). The yielding transition in amorphous solids under oscillatory shear deformation. *arXiv preprint arXiv:1612.02629*.
- Lerner, E., Düring, G., and Wyart, M. (2013). Low-energy non-linear excitations in sphere packings. *Soft Matter*, 9(34):8252–8263.
- Lin, J., Gueudré, T., Rosso, A., and Wyart, M. (2015). Criticality in the approach to failure in amorphous solids. *Physical review letters*, 115(16):168001.

- Lin, J., Lerner, E., Rosso, A., and Wyart, M. (2014). Scaling description of the yielding transition in soft amorphous solids at zero temperature. *Proceedings of the National Academy of Sciences*, 111(40):14382–14387.
- Liu, A. J. and Nagel, S. R. (1998). Nonlinear dynamics: Jamming is not just cool any more. *Nature*, 396(6706):21–22.
- Liu, A. J. and Nagel, S. R. (2010). The jamming transition and the marginally jammed solid. *Annu. Rev. Condens. Matter Phys.*, 1(1):347–369.
- Liu, A. J., Nagel, S. R., Van Saarloos, W., and Wyart, M. (2011). *The jamming scenario—an introduction and outlook*. Oxford University Press.
- Liu, C., Ferrero, E. E., Puosi, F., Barrat, J. L., and Martens, K. (2016). Driving rate dependence of avalanche statistics and shapes at the yielding transition. *Physical review letters*, 116(6):065501.
- Liu, Y. and Dahmen, K. A. (2009). Random-field ising model in and out of equilibrium. *EPL (Europhysics Letters)*, 86(5):56003.
- Maloney, C. and Lemaitre, A. (2004). Subextensive scaling in the athermal, quasistatic limit of amorphous matter in plastic shear flow. *Physical review letters*, 93(1):016001.
- Mézard, M. and Parisi, G. (2001). The bethe lattice spin glass revisited. *The European Physical Journal B-Condensed Matter and Complex Systems*, 20(2):217–233.
- Mézard, M., Parisi, G., Sourlas, N., Toulouse, G., and Virasoro, M. (1984a). Nature of the spin-glass phase. *Physical review letters*, 52(13):1156.
- Mézard, M., Parisi, G., Sourlas, N., Toulouse, G., and Virasoro, M. (1984b). Replica symmetry breaking and the nature of the spin glass phase. *Journal de Physique*, 45(5):843–854.
- Mézard, M., Parisi, G., Sourlas, N., Toulouse, G., and Virasoro, M. (1984c). Replica symmetry breaking and the nature of the spin glass phase. *Journal de Physique*, 45(5):pp.843–854.
- Mézard, M., Parisi, G., and Virasoro, M. A. (1985). Random free energies in spin glasses. *Journal de Physique Lettres*, 46(6):217–222.
- Mézard, M., Parisi, G., Virasoro, M. A., and Thouless, D. J. (2008). Spin glass theory and beyond. *Physics Today*, 41(12):109–110.

- Mézard, M. and Virasoro, M. (1985). The microstructure of ultrametricity. *Journal de Physique*, 46:pp. 1293–1307.
- Milne-Thomson, L. M. (2000). *The calculus of finite differences*. American Mathematical Soc.
- Müller, M. and Wyart, M. (2015). Marginal stability in structural, spin, and electron glasses. *Annual Review of Condensed Matter Physics*, 6(1):177–200.
- Newman, M. and Moore, C. (1999). Glassy dynamics and aging in an exactly solvable spin model. *Physical Review E*, 60(5):5068.
- Ng, E. W. and Geller, M. (1969). A table of integrals of the error functions. *Journal of Research of the National Bureau of Standards B*, 73(1):1–20.
- Nishimori, H. (2001). *Statistical physics of spin glasses and information processing: an introduction*, volume 111. Clarendon Press.
- O’Hern, C. S., Langer, S. A., Liu, A. J., and Nagel, S. R. (2002). Random packings of frictionless particles. *Physical Review Letters*, 88(7):075507.
- O’Hern, C. S., Silbert, L. E., Liu, A. J., and Nagel, S. R. (2003). Jamming at zero temperature and zero applied stress: The epitome of disorder. *Phys. Rev. E*, 68:011306.
- Panchenko, D. and Talagrand, M. (2007). Guerra’s interpolation using derrida-ruelle cascades. *arXiv preprint arXiv:0708.3641*.
- Parisi, G. (1979). Infinite number of order parameters for spin-glasses. *Physical Review Letters*, 43(23):1754.
- Parisi, G. (1980). A sequence of approximated solutions to the sk model for spin glasses. *Journal of Physics A: Mathematical and General*, 13(4):L115.
- Parisi, G. (1983). Order parameter for spin-glasses. *Physical Review Letters*, 50(24):1946.
- Parisi, G. (1998). On the probabilistic formulation of the replica approach to spin glasses. *arXiv preprint cond-mat/9801081*.
- Parisi, G. (2002). The physical meaning of replica symmetry breaking. *arXiv preprint cond-mat/0205387*.
- Parisi, G. and Ricci-Tersenghi, F. (2000). On the origin of ultrametricity. *Journal of Physics A: Mathematical and General*, 33(1):113.

- Parisi, G. and Zamponi, F. (2010). Mean-field theory of hard sphere glasses and jamming. *Reviews of Modern Physics*, 82(1):789.
- Puosi, F., Rottler, J., and Barrat, J.-L. (2016). Plastic response and correlations in athermally sheared amorphous solids. *arXiv preprint arXiv:1606.08745*.
- Regev, I., Weber, J., Reichhardt, C., Dahmen, K. A., and Lookman, T. (2015). Reversibility and criticality in amorphous solids. *Nature communications*, 6.
- Rizzo, T. and Yoshino, H. (2006). Chaos in glassy systems from a Thouless-Anderson-Palmer perspective. *Phys. Rev. B*, 73(6):064416.
- Rosso, A., Le Doussal, P., and Wiese, K. J. (2009). Avalanche-size distribution at the depinning transition: A numerical test of the theory. *Physical Review B*, 80(14):144204.
- Ruelle, D. (1987). A mathematical reformulation of derrida’s REM and GREM. *Communications in Mathematical Physics*, 108(2):225–239.
- Sethna, J. P., Dahmen, K. A., and Myers, C. R. (2001). Crackling noise. *Nature*, 410(6825):242–250.
- Spigler, S. (2014). Plaquette models for glasses.
- Streit, R. L. (2010). *Poisson point processes: imaging, tracking, and sensing*. Springer Science & Business Media.
- Talagrand, M. (2003). The generalized parisi formula. *Comptes Rendus Mathematique*, 337(2):111–114.
- Van Hecke, M. (2009). Jamming of soft particles: geometry, mechanics, scaling and isostaticity. *Journal of Physics: Condensed Matter*, 22(3):033101.
- Verlet, L. (1967). Computer” experiments” on classical fluids. i. thermodynamical properties of lennard-jones molecules. *Physical review*, 159(1):98.
- Wyart, M. (2012). Marginal stability constrains force and pair distributions at random close packing. *Physical review letters*, 109(12):125502.
- Wyart, M., Silbert, L. E., Nagel, S. R., and Witten, T. A. (2005). Effects of compression on the vibrational modes of marginally jammed solids. *Physical Review E*, 72(5):051306.

- Yan, L., Baity-Jesi, M., Müller, M., and Wyart, M. (2015). Dynamics and correlations among soft excitations in marginally stable glasses. *Physical review letters*, 114(24):247208.
- Yoshino, H. and Mézard, M. (2010). Emergence of rigidity at the structural glass transition: A first-principles computation. *Phys. Rev. Letters*, 105(1):015504.
- Yoshino, H. and Rizzo, T. (2008). Stepwise responses in mesoscopic glassy systems: A mean-field approach. *Phys. Rev. B*, 77(10):104429.
- Yoshino, H. and Zamponi, F. (2014). Shear modulus of glasses: Results from the full replica-symmetry-breaking solution. *Phys. Rev. E*, 90(2):022302.
- Young, A. P., Bray, A. J., and Moore, M. A. (1984). Lack of self-averaging in spin glasses. *J. Phys. C*, 17(5):L149.
- Young, A. P. and Kirkpatrick, S. (1982). Low-temperature behavior of the infinite-range ising spin-glass: Exact statistical mechanics for small samples. *Phys. Rev. B*, 25(1):440.
- Zamponi, F. (2010). Mean field theory of spin glasses. *J. Phys. A*.



## Résumé

Beaucoup de systèmes qui ont un certain degré de désordre ont des similarités dans leur structure: le paysage énergétique est aléatoire et il a plusieurs minima locaux de l'énergie. Quand on ajoute une petite perturbation externe au système à basse température, il est raisonnable d'attendre que la dynamique conduira le système d'un minimum à l'autre, et ça donne lieu à une réponse aléatoire et saccadée. Les sautes discontinues que l'on observe sont appelés avalanches, et l'intérêt de ce travail est le calcul de leur distribution. Un des résultats est en effet le développement d'un cadre pour calculer cette distribution dans des systèmes en dimension infinie qui peuvent être décrits avec le replica symmetry breaking. Nous appliquons les résultats à l'un des modèles les plus simples des verres structuraux, c'est à dire les empilements denses de sphères molles avec répulsion harmonique, avec une déformation (shear strain) du volume comme perturbation. Nous soutenons que, quand la déformation est suffisamment petite, une portion de la distribution des avalanches devient une loi de puissance, dont l'exposant peut être directement lié au paramètre d'ordre de la brisure de symétrie de replica. Cet exposant est également lié à la distribution des forces de contact (au moins entre certaines sphères), dont le comportement asymptotique on sait que ne dépend pas fortement de la dimension spatiale; pour cette raison nous comparons les prédictions de champ moyen en dimension infinie avec des simulation du même système en dimension trois et, remarquablement, on trouve un bon accord. Dans le reste de la thèse nous discutons aussi les similarités avec des travaux précédents et quelques conséquences que la distribution des avalanches donne sur les propriétés élastiques de la matière granulaire dense.

## Mots Clés

Distribution des avalanches, jamming, sphères molles, réponse élastique, shear stress

## Abstract

Many systems that are somehow characterized by a degree of disorder share a similar structure: the energy landscape has many sample-dependent local energy minima. When a small external perturbation is applied to the system at low temperature, it is reasonable to expect that the dynamics will lead the system from a minimum to another, thus displaying a random and jerky response. The discontinuous jumps that one observes are called avalanches, and the focus of this work is the computation of their distribution. One of the results is indeed the development of a framework that allows the computation of this distribution in infinite-dimensional systems that can be described within a replica symmetry breaking ansatz. We apply the results to one of the simplest models of structural glasses, namely dense packings of (harmonic) soft spheres, either at jamming or at larger densities, subject to a shear transformation that induces jumps both in the total energy and in the shear stress of the system. We argue that, when the shear strain is small enough, the avalanche distribution develops a power-law behavior, whose exponent can be directly related to the functional order parameter of the replica symmetry breaking solution. This exponent is also related to the distribution of contact forces (or at least of the contact forces between some of the spheres), whose asymptotic behavior is known not to depend strongly on the spatial dimension; for this reason, we compare the infinite-dimensional prediction with three-dimensional simulations of the same systems and, remarkably, we find a good agreement. In the rest of the thesis we compare our results with previous works, and we also discuss some of the consequences that the avalanche distribution leads to, concerning the statistical elastic properties of dense granular media.

## Keywords

Avalanche distribution, jamming, soft spheres, elastic response, shear stress